EPA/600/R-25/232
July 2026
www.epa.gov/isa

Integrated Science Assessment for Oxides of Nitrogen – Health Criteria

Chapter 1: Atmospheric Chemistry and Ambient Concentrations

External Review Draft

July 2026

U.S. Environmental Protection Agency

Disclaimer

This document is an external review draft for peer review purposes only. This information is distributed solely for the purpose of pre-dissemination peer review under applicable information quality guidelines. It has not been formally disseminated by the U.S. Environmental Protection Agency. It does not represent and should not be construed to represent any agency determination or policy. Mention of trade names or commercial products does not constitute endorsement or recommendation for use.

Document Guide

This Document Guide is intended to orient readers to the organization of the Oxides of Nitrogen Integrated Science Assessment (ISA) in its entirety and to the sub-section of the ISA at hand (indicated in bold). The ISA consists of the Front Matter (list of authors, contributors, reviewers, and acronyms), Executive Summary, Integrated Synthesis, and 14 chapters, which can all be found at https://www.epa.gov/isa/integrated-science-assessment-isa-oxides-nitrogen-health-criteria.

Front Matter

Executive Summary

Integrated Synthesis

Chapter 1. Atmospheric Chemistry and Ambient Concentrations

Chapter 2. Exposure and Dosimetry of Inhaled Oxides of Nitrogen

Chapter 3. Respiratory Effects – Short-Term Exposure

Chapter 4. Respiratory Effects – Long-Term Exposure

Chapter 5. Cardiovascular Effects – Short-Term Exposure

Chapter 6. Cardiovascular Effects – Long-Term Exposure

Chapter 7. Reproductive and Developmental Effects

Chapter 8. Metabolic Syndrome and Diabetes

Chapter 9. Nervous System Effects

Chapter 10. Total Mortality – Short-Term Exposure

Chapter 11. Total Mortality – Long-Term Exposure

Chapter 12. Cancer

Chapter 13. Health Effects with Limited Evidence

Chapter 14. Process for Developing the Integrated Science Assessment for Oxides of Nitrogen – Health Criteria

Appendix A. Appendix Tables

Table of Contents

Disclaimer ii
Document Guide iii
Table of Contents iv
List of Tables vi
List of Figures vii
Acronyms and Abbreviation viii
Atmospheric Chemistry and Ambient Concentrations 1
1.1 Introduction 1
1.2 Sources 2
1.2.1 Emissions Estimation 2
1.2.2 Emissions Trends 6
1.2.3 Highway Vehicles 9
1.2.4 Non-road Mobile Sources 12
1.2.5 Fuel Combustion and Utilities 15
1.2.6 Industrial Sources 16
1.2.7 Other Sources 17
1.2.8 COVID-19 Changes to NO_X Emissions 23
1.2.9 Emissions Summary 24
1.3 Atmospheric Chemistry and Fate 24
1.3.1 Formation, Reactions, and Sinks 25
1.3.2 Chemistry in Wildfire Smoke 30
1.4 Measurement and Modeling Methods 31
1.4.1 Federal Reference and Equivalent Methods 31
1.4.2 Ambient Monitoring Networks 35
1.4.3 Other Methods for Measuring NO_X 37
1.4.4 Low-Cost Sensors 38
1.4.5 Satellite Remote Sensing 38
1.4.6 Modeling 45
1.5 Ambient Concentrations of NO_X and Copollutants 49
1.5.1 Current National Scale Trends 49
1.5.2 Urban Scale Spatial Trends 55
1.5.3 Near-road Trends 56
1.5.4 National and Regional Temporal Trends 60
1.5.5 Seasonal, Diurnal, Weekday, and Weekend Temporal Trends 64

1.5.6 Copollutant Associations 66
1.6 Conclusions 70
1.7 References 71

List of Tables

Table 1-1 STEM statement to define the criteria and framework for identifying relevant oxides of nitrogen atmospheric studies 2

Table 1-2 Oxides of nitrogen emissions per amount of fuel used for various types of non-road mobile sources, as reported in the literature 14

Table 1-3 Selected satellite platforms for atmospheric NO_2 measurement 40

Table 1-4 Summary statistics based on two daily NO_2 NAAQS metrics: the daily maximum 1-hour metric and the daily 24-hour average metric for 2021 to 2023 52

Table 1-5 Comparison of two-year average NO_2 concentrations at near-road and non-near-road monitoring stations 57

Table 1-6 Regional trends in annual 98^{th} percentile of daily max 1-hour average NO_2 concentrations at United States monitoring network stations 63

Table 1-7 National distribution of NO_2 concentrations by season for data reported to Air Quality Systems from 2021 to 2023 65

Table 1-8 Association between maximum daily 1-hour average NO_2 concentrations and maximum daily average 8-hour O_3, July 2022 to June 2023 68

List of Figures

Figure 1-1	Source distribution of United States NO_X emissions.	4
Figure 1-2	United States county-level NO_X emissions density estimates in tons/year/mi^2.	5
Figure 1-3	United States anthropogenic NO_X emissions trends from 2002 to 2023.	7
Figure 1-4	Historical Chicago, IL, U.S., area real-world fleet emissions for carbon monoxide, hydrocarbons, and nitric oxide measured at an urban interstate on-ramp.	11
Figure 1-5	Non-road mobile NO_X emissions quantified from the 2020 NEI.	13
Figure 1-6	Estimated mean soil NO_X emissions from GEOS-Chem for July 2013.	18
Figure 1-7	Simplified schematic diagram of the cycle of reactive oxidized nitrogen species in the atmosphere.	26
Figure 1-8	Schematic diagram of the cycle of oxidized nitrogen species in the atmosphere, showing the complexity of relationships among inorganic and organic products that are simplified in Figure 1-7.	27
Figure 1-9	Map of United States NO_X monitoring stations reporting data to EPA, 2021 to 2023.	37
Figure 1-10	Annual average NO_2 design values, based on data from 2023.	50
Figure 1-11	Three-year averages of the annual 98th percentile daily maximum 1-hour average NO_2 design values for the 2021 to 2023 period.	51
Figure 1-12	TROPOMI NO_2 tropospheric vertical column density (molecules/cm^2) sampled to 0.01° × 0.01° spatial resolution from May 1, 2018 to December 31, 2019.	54
Figure 1-13	2006 mean annual NO_2 concentration versus distance from Minneapolis, MN, U.S., city center.	55
Figure 1-14	NO_2 and NO_X concentration trends at near-road monitors in Anaheim, CA, U.S., and Houston, TX, U.S.	59
Figure 1-15	Station-level trends in annual average NO_2 concentrations based on data from 2000 to 2023.	61
Figure 1-16	Station-level trends in three-year averages of the annual 98th percentile daily maximum 1-hour average NO_2 concentrations from 2000 to 2023.	62

Acronyms and Abbreviation

ADMS	Atmospheric Dispersion Modeling System
AERMOD	American Meteorological Society and EPA Regulatory Model
AMF	air mass factor
AQAST	Air Quality Applied Sciences Team
AQS	Air Quality System
avg	average
β	beta
ρ	Correlation coefficient, rho
CAIRSENSE	Community Air Sensor Network
CAMS	Copernicus Atmospheric Monitoring Service
CAMx	Comprehensive Air Quality Model with Extensions
CAPS	cavity attenuated phase shift
CEMS	continuous emissions monitoring system
Cl	chlorine
$ClNO_2$	nitryl chloride
CMAQ	Community Multiscale Air Quality
CO	carbon monoxide
CRACMM	Community Regional Atmospheric Chemistry Multiphase Mechanism
CTM	chemical transport modeling
d	day(s)
DA24	daily 24 h average
DESID	Detailed Emissions Scaling, Isolation, and Diagnostic
DOAS	differential optical absorption spectroscopy
EGU	Electric Generating Units
e.g.	exempli gratia (for example)
ENVISAT	Environmental Satellite
EQUATES	Air QUAlity TimE Series
ERS-2	European Remote Sensing Satellite-2
ESA	European Space Agency
etc.	et cetera
EUMETSAT	European Organization for the Exploitation of Meteorological Satellites
EPA	Environmental Protection Agency
FEMs	Federal Equivalent Methods
FIVE	Fuel-based Inventory of Vehicle Emissions
FRM	Federal Reference Method
g	gram(s)
GCAS	Airborne Simulator
GEO-CAPE	GEOstationary Coastal and Air Pollution Events
GEOS-Chem	Goddard Earth Observing System-Chemistry
GeoTASO	Geostationary Trace Gas and Aerosol Sensor Optimization
GOME	Global Ozone Monitoring Experiment
HAQAST	Health and Air Quality Applied Systems Team
HC	hydrocarbons
HCl	Hydrogen chloride
HNO_3	nitric acid
HONO	nitrous acid
hr	hour(s)
IS40e	Intelsat 40e
ISA	Integrated Science Assessment
JPSS	Joint Polar Satellite Systems
L	liter(s)
LIF	laser-induced fluorescence
LOPAP	long path absorption photometry
LUR	Land use regression
MACC	Monitoring Atmospheric Composition and Climate
Max	maximum
MAX-DOAS	Maximum differential optical absorption spectroscopy
Min	minimum
m	meter(s)
MDA1	daily maximum 1 h average
µg	microgram
µmol	micromole
min	minute(s)
mL	milliliter
mo	month(s)
mpp	multiphase process
MoOx	molybdenum oxide
MOVES	Motor Vehicle Emissions Simulator
n	sample size
N	nitrogen
N.obs	number of observations
N.stations	number of stations
N_2	dinitrogen

NAAQS	National Ambient Air Quality Standard
NASA	National Aeronautics and Space Administration
NCore	National Core
NEI	National Emissions Inventory
NO	nitric oxide
NO_2	nitrogen dioxide
NO_3	nitrate radical
N_2O	nitrous oxide
N_2O_5	dinitrogen pentoxide
NO_X	the sum of NO_2 + NO
NO_Y	the sum of all oxides of nitrogen
NO_Z	the sum of all oxides of nitrogen except NO_X
NOAA	National Oceanic and Atmospheric Administration
O_2	oxygen
O_3	ozone
Obs	observed
OH	hydroxyl radical
OMI	Ozone Monitoring Instrument
OMPS	Ozone Mapping and Profiler Suite
PAMS	Photochemical Assessment Monitoring Stations
PAN	peroxyacetic nitric anhydride or peroxyacetyl nitrate
PGN	Pandonia Global Network
PM	particulate matter
P.M.	post meridiem
PM_{10}	particulate matter with a nominal mean aerodynamic diameter less than or equal to 10 µm
$PM_{2.5}$	particulate matter with a nominal mean aerodynamic diameter less than or equal to 2.5 µm
pNO_3^-	particulate nitrate
ppb	parts per billion
ppbv	parts per billion by volume
ppm	parts per million
QA	quality assurance
QC-TILDAS	quantum cascade-tunable infrared laser differential absorption spectrometer
R	Organic radical
R1	reaction 1
R2	reaction 2
RLINE	Research Line Source
$RONO_2$	organic nitrates
RO_2NO_2	peroxy nitrates
SCIAMACHY	Scanning Imaging Absorption Spectrometer for Atmospheric Chartography
SD	standard deviation
SLAMS	State and Local Air Monitoring Stations
SO_2	sulfur dioxide
SPMs	Special Purpose Monitors
STEM	sources, transport and transformation, extent (concentration), and measurement and modeling
TEMPO	Tropospheric Emissions: Monitoring Pollution
TD-CAPS	Thermal dissociation cavity attenuated phase shift
TROPOMI	Tropospheric Monitoring Instrument
UFP	ultra fine particles
U.K.	United Kingdom
U.S.	United States
UV	ultraviolet
VOCs	volatile organic compounds
vs.	versus
WRF-Chem	Weather Research and Forecasting model coupled with Chemistry
wk	week(s)
yr	year(s)
ΣANs	alkyl nitrates, $RONO_2$
ΣPNs	peroxy nitrates, RO_2NO_2

CHAPTER 1 Atmospheric Chemistry and Ambient Concentrations

1.1 Introduction

This chapter presents concepts and findings relating to emissions sources, atmospheric chemistry and fate, measurement and modeling techniques, and spatial and temporal concentration patterns for oxides of nitrogen. It is intended as a prologue for detailed discussions on the evidence for human exposure to, and health effects of, oxides of nitrogen that follow in subsequent chapters and as a source of information to help interpret those effects in the context of data about atmospheric concentrations.

In this Integrated Science Assessment (ISA), the term "oxides of nitrogen" refers to all forms of oxidized, reactive nitrogen (N) compounds, including nitric oxide (NO), nitrogen dioxide (NO_2), and all other oxidized N-containing compounds. Nitrous oxide (N_2O) is present in the troposphere but is unreactive on timescales relevant to this ISA and is therefore not discussed (U.S. EPA, 1971). Throughout much of this ISA, the abbreviation NO_X is used. NO_X refers specifically to the sum of NO and NO_2, the dominant forms emitted by all major sources. Another abbreviation, NO_Y, refers to all forms of oxidized nitrogen, including NO, NO_2, and other forms resulting from secondary reactions. Oxides of nitrogen is the criteria air pollutant (U.S. EPA, 1971) while NO_2 is the current indicator for the National Ambient Air Quality Standard (NAAQS) for oxides of nitrogen. The NAAQS indicator is one of four basic elements that make up the NAAQS in addition to its form, averaging time (see Section 1.5), and level (U.S. EPA, 2017).

This chapter describes the origins, distribution, and fate of gaseous oxides of nitrogen. NO and NO_2 are also important precursors in the formation of other of other air pollutants such as ozone (O_3) and particulate matter (PM) (such as particulate nitrate [pNO_3^-]), which are addressed in the ISAs for Ozone and Related Photochemical Oxidants (U.S. EPA, 2020a) and PM (U.S. EPA, 2019), respectively. Material cited in this chapter was selected using discipline-specific scoping statements to identify potentially relevant atmospheric science studies. Application of scoping statements that consider pollutant sources, transport and transformation, extent (concentration), and measurement and modeling (STEM) is consistent with current best practices for reporting or evaluating health science data as recommended by the National Academy of Sciences, Engineering, and Medicine (NASEM, 2022). The STEM statement for the Atmospheric Science Chapter of the ISA shown in Table 1-1 has been informed by the body of evidence from the previous ISAs, Air Quality Criteria Documents, and expert knowledge of the relevant scientific literature. It defines the objectives of the Atmospheric Science Chapter and establishes criteria to be met for published studies to be considered in the ISA. A study meeting any of the four aspects of the STEM statement was considered for inclusion. To provide the most current emissions and concentration data from the NO_2 monitoring network, a selection of annually updated graphics drawn from a separate document, "Overview of Nitrogen Dioxide (NO_2) Air Quality in the United States," are included in this chapter (U.S. EPA, 2023d).

Table 1-11 STEM statement to define the criteria and framework for identifying relevant oxides of nitrogen atmospheric studies

Statement	Description
Source (S)	Studies reporting quantitative emissions estimates of oxides of nitrogen or observations of physical and chemical characteristics that add to our understanding of pollutant sources and emissions of oxides of nitrogen.
Transport and Transformation (T)	Studies investigating atmospheric fate and transport, transformation, or deposition processes involving oxides of nitrogen, including transport of air pollutants at various scales (i.e., global, national, regional, urban, neighborhood), atmospheric chemical transformations in the atmosphere, or estimates of atmospheric deposition that add to our understanding of atmospheric processes.
Exposure/Extent (E)	Studies reporting observations and estimates of ambient air concentrations or their trends for oxides of nitrogen, including spatial variability on various scales (i.e., global, national, regional, urban, neighborhood); temporal trends such as diurnal, weekday/weekend, seasonal, and long-term trends; or characteristics, such as composition or relationship with atmospheric properties that provide up-to-date concentrations and estimates or add to our understanding of spatiotemporal concentration trends.
Measurement and Modeling (M)	Studies describing methods of measurement of oxides of nitrogen by federal reference and equivalent methods, satellite remote sensing estimates, low-cost sensor estimates, research methods, or modeling techniques (e.g., chemical transport modeling) for characterizing oxides of nitrogen concentrations in ambient air, including the evaluation of measurement principles and modeling assumptions, examination of potential bias and uncertainties, and method comparisons that are relevant to the NAAQS or to studies in this ISA.

List of abbreviations in alphabetical order: ISA = integrated science assessment; NAAQS = National Ambient Air Quality Standards; STEM = sources, transport and transformation, exposure/extent, and measurement and modeling.
Note: A study must meet at least one requirement listed in the description field for at least one of the statements to be considered for inclusion in the chapter.

1.2 Sources

This section discusses available information on sources of oxides of nitrogen emissions. It describes the methods used to estimate oxides of nitrogen emissions, emissions trends over time, and the most recent relevant research on specific major anthropogenic and natural NO_X emissions sources.

1.2.1 Emissions Estimation

Emissions estimates are usually based on either measurements or model parameterizations of source data (often referred to as bottom-up estimates) or inferences from concentration data in areas where a particular source dominates (often referred to as top-down estimates). Much of the recently published bottom-up emissions data for the United States (U.S.) is based on the National Emissions Inventory (NEI) (U.S. EPA, 2023a). Canadian, European, and global emissions inventories (EC, 2024; Government of Canada, 2024; PNNL, 2021) are also vital not just for establishing global emissions trends and understanding international transport, but also for setting boundary and initial conditions for U.S. air

quality modeling. Most of the recent top-down emissions estimates are based on rapidly improving satellite remote sensing technology. As discussed below, both bottom-up and top-down approaches have strengths and limitations. Recent efforts have used them in combination to improve emissions estimation methods and representation of atmospheric processes in chemical transport modeling (CTM) (Toro et al., 2021).

The NEI is a comprehensive and detailed bottom-up estimate of air emissions of criteria pollutants like oxides of nitrogen, criteria pollutant precursors, and hazardous air pollutants from air emissions sources. The NEI is released every three years based primarily upon data provided by state, local, and tribal air agencies for sources in their jurisdictions and supplemented by data developed by the U.S. Environmental Protection Agency (EPA). The intent of the NEI is to create the most complete inventory possible for use in air quality modeling, national rule assessments, international reporting, and other reports. The process of estimating emissions, including measurement and estimation methods, is explained for each source in a detailed technical support document (U.S. EPA, 2023a). Certain provisions of the Clean Air Act require states to submit information on emissions to the EPA as part of their State Implementation Plans for the NAAQS program. For example, the Clean Air Act section 172(c)(3) requires certain states to provide "a comprehensive, accurate, current inventory of actual emissions from all sources of the relevant pollutant or pollutants in such [NAAQS nonattainment] area" to the EPA.

NEI sources include anthropogenic stationary and mobile sources, as well as natural sources, including wildfires and biogenic sources (U.S. EPA, 2023a) (see Section 1.2.2 for more detail). Data are reported for a total of 60 source sectors that are grouped into various source types to show their contributions to total U.S. emissions in Figure 1-1. Highway vehicles (26%) include all on-road vehicles (i.e., light-duty and heavy-duty vehicles, both gasoline- and diesel-powered). Non-road mobile sources (19%) include aircraft, commercial marine vessels, locomotives, and non-road equipment (such as construction or agriculture equipment). Stationary fuel combustion (25%) includes Electric Generating Units (EGUs), which generate electricity from fossil fuels (primarily coal), as well as commercial/institutional, industrial, and residential combustion of biomass, coal, natural gas, oil, and other fuels. Industrial processes (12%) include oil and gas production and cement manufacturing.

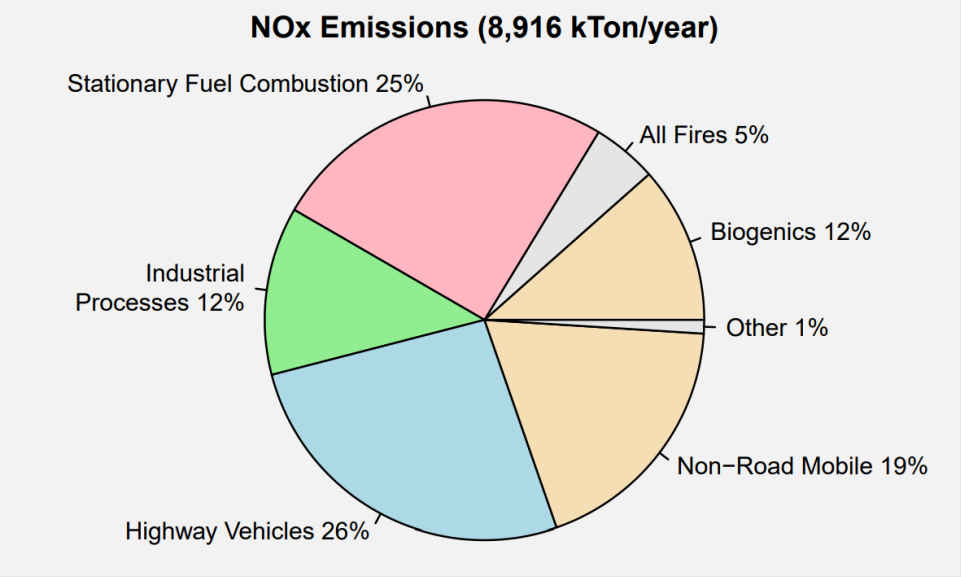

List of abbreviations in alphabetical order: NO_X = the sum of NO_2 + NO.
Note: Generated using data from the 2020 NEI.
Source: U.S. EPA (2023d).

Figure 1-1 Source distribution of United States NO_X emissions.

Natural sources of NO_X emissions include lightning (geogenic), plants and soils (biogenic), fires, and lightning (lightning NO_X is not currently a part of the NEI). Of the natural sources, the greatest contributor to NO_X emissions are biogenic sources. As shown in Figure 1-1, biogenic emissions account for 12% of total U.S. NO_X emissions in the year 2020—roughly double the 6% contribution reported in the EPA's 2016 Integrated Science Assessment for Oxides of Nitrogen – Health Criteria (hereafter 2016 Oxides of Nitrogen ISA) using 2011 data (U.S. EPA, 2016). This is because biogenic emissions remained relatively constant from 2011 to 2020 (1.03 million tons in 2020 [U.S. EPA, 2023a]), while total U.S. emissions decreased from about 17 million tons in 2011 (U.S. EPA, 2016) to about 9 million tons in 2020 (U.S. EPA, 2023a) per year. In the NEI and this document ton refers to a U.S. short ton (2000 lbs or 907 kg). Biogenic sources include both managed (e.g., fertilized) and unmanaged soils. Although the NEI does not distinguish between soil types, NEI guidance clarifies that fertilizer application is considered for some soils, indicating that some fraction of NEI biogenic emissions is agricultural (U.S. EPA, 2023b). There are differences in emissions uncertainties among the different source groups identified (e.g., higher uncertainties and greater seasonal differences for fires and biogenic emissions). These uncertainties are not quantified in the NEI, and thus the percentages shown in Figure 1-1 should be interpreted cautiously. A map showing county-level total NO_X emissions estimates using the 2020 NEI is shown in Figure 1-2.

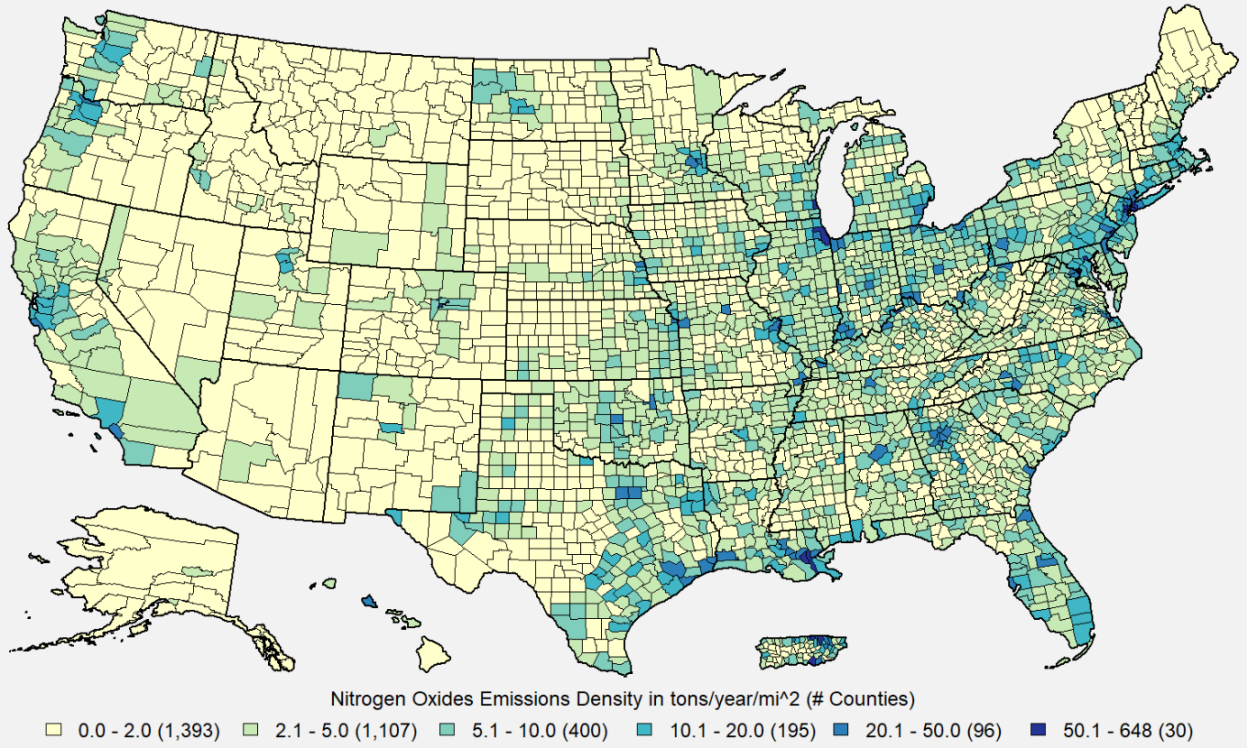

List of abbreviations in alphabetical order: NO_X = the sum of NO_2 + NO.
Note: Generated using data from the 2020 NEI.
Source: U.S. EPA (2023d).

Figure 1-2 United States county-level NO_X emissions density estimates in tons/year/mi^2.

Beginning in 1995, satellite-based remote sensing emerged as a new top-down tool for estimating emissions (see Section 1.4.3). While satellite data cannot directly estimate emissions, several techniques including inverse modeling, which infers underlying emissions based on remotely sensed variables, are used to estimate emissions. These methods are particularly useful for estimating NO_X emissions due to the short lifetime of NO_X, meaning tropospheric NO_2 concentrations are strongly correlated with local NO_X emissions, making high-resolution remote sensing measurements of NO_2 suitable for estimating spatially resolved NO_X emissions (Goldberg et al., 2024). Emission estimates can also be achieved by comparing inventory-based NO_X emissions directly to satellite NO_2 data using only measurements from days with stagnant wind conditions, or by using a CTM or a statistical framework involving an assumed NO_2 lifetime (Goldberg et al., 2024). Satellite capabilities have improved considerably with the recent launch of geostationary satellites with greater spatiotemporal resolution than their low Earth orbiting predecessors, with increased potential for characterizing major point sources, finer scale emissions patterns, urban-suburban differences, and emissions tracking from episodic sources such as wildfires and lightning (see Section 1.4.3). A summary of satellite platforms and space-based remote sensing NO_2 instruments relevant to North American studies is provided in Section 1.4.3.

Satellite-based methods that measure total NO_2 column abundance, the number of NO_2 molecules in the entire column of atmosphere above a defined area (see Section 1.4.3), have been especially useful for estimating emissions from non-point sources that are not easily sampled through direct measurements. These include oil and gas extraction operations, ships, biogenic and geogenic sources, international emissions that could influence United States air quality, and wildfires or other episodic events. Satellite-based methods have also been used to characterize seasonal, diurnal, and episodic variations in source emissions that can be challenging to observe by other means (Duncan et al., 2014; Streets et al., 2013). Recently, satellite-based data have been particularly useful in estimating EGU (see Section 1.2.5) and soil emissions (see Section 1.2.7.1). Under favorable circumstances, a single satellite overpass can identify urban plumes and estimate emissions (Goldberg et al., 2019). Improvements in satellite technology can also be used to estimate whole city NO_X emissions. For example, satellite-based total emissions estimates for major North American cities, including New York, NY, U.S.; Chicago, IL, U.S.; and Toronto, Canada have been derived and compared to conventional emissions inventories (Goldberg et al., 2019). More recent improvements in satellite capabilities relevant to emissions estimates, like sensitivity and spatial resolution for individual satellites, are described in Section 1.4.3.

Both bottom-up emissions inventory-based estimates and top-down satellite-derived estimates have strengths and limitations. The NEI database does not include sector emissions uncertainty estimates. The accuracy of individual emissions estimates may vary from facility to facility or county to county, and for some sources, data may be incomplete or lacking. For example, there are no lightning data in the NEI, a major natural source, especially over North America and in spring and summer (see Section 1.2.7.3). On the other hand, satellite-based emissions estimates are only inferred using remotely sensed variables leveraging statistical, inverse, or chemical transport models. Over time, the NEI has steadily become more detailed and incorporated recent research on more poorly characterized sources (Day et al., 2019). This steady responsiveness has also led to continually improving emissions data and allows for finer temporal and spatial scale comparison with top-down emission estimates.

1.2.2 Emissions Trends

Nationwide estimates based on emission trends indicate a 70% decrease in anthropogenic NO_X emissions from 2002 to 2023 (Figure 1-3). The overall decrease in NO_X emissions has been driven primarily by decreases from the three largest groups of anthropogenic emissions sectors. Specifically, compared to the 2002, estimates for 2023 indicate an 84% reduction in NO_X emissions from highway vehicles, a 54% reduction in NO_X emissions from non-road mobile sources, and a 68% reduction in NO_X emissions from stationary fuel combustion (a large fraction of which are EGUs). Trends in Figure 1-3 include past NEI emissions and projections (e.g., trends include 2023 as a projection) (U.S. EPA, 2024e).

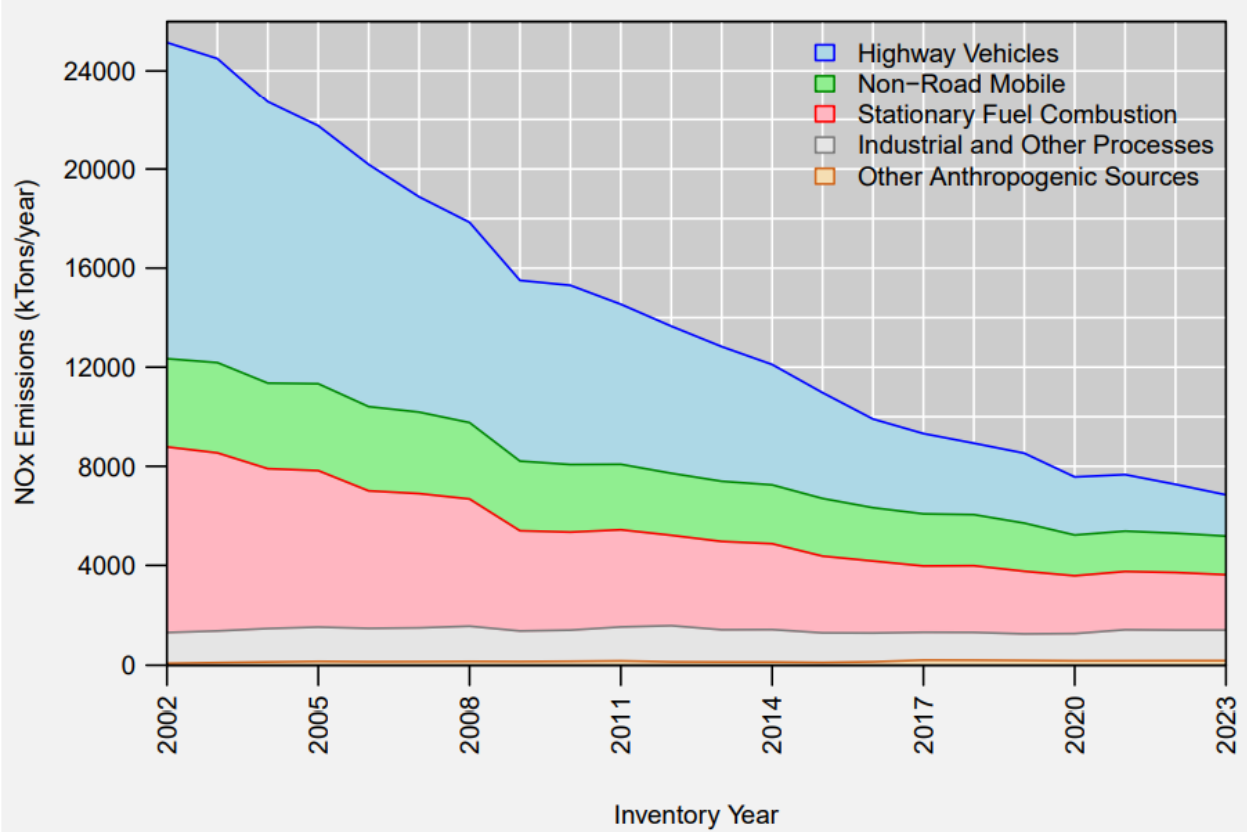

List of abbreviations in alphabetical order: NO_X = the sum of NO_2 + NO.
Source: U.S. EPA (2024e). Copyright permission pending.

Figure 1-3 United States anthropogenic NO_X emissions trends from 2002 to 2023.

As a result of the decreasing anthropogenic NO_X emissions shown in Figure 1-3, Figure 1-1 shows that biogenic emissions account for 12% of total U.S. NO_X emissions in the year 2020, roughly double the 6% contribution reported in the 2016 Oxides of Nitrogen ISA that used 2011 data (U.S. EPA, 2016) because biogenic emissions remained relatively constant from 2011 to 2020 (1.03 million tons in 2020 [U.S. EPA, 2023a]), while total U.S. emissions decreased from about 17 million tons in 2011 (U.S. EPA, 2016) to about 9 million tons in 2020 (U.S. EPA, 2023a) per year. In the NEI and this document ton refers to a U.S. short ton (2000 lbs or 907 kg). Biogenic sources include both managed (e.g., fertilized) and unmanaged soils. Although the NEI does not distinguish between soil types, NEI guidance clarifies that fertilizer application is considered for some soils, indicating that some fraction of NEI biogenic emissions is agricultural (U.S. EPA, 2023b). There are differences in emissions uncertainties among the different source groups identified (e.g., higher uncertainties and greater seasonal differences for fires and biogenic emissions). These uncertainties are not quantified in the NEI, and thus the percentages shown in Figure 1-2 should be interpreted cautiously.

Satellite-based remote sensing data also indicate decreasing NO_X emissions over the United States since 1996 (Geddes et al., 2015), similar to the NEI trend since 2002. Several studies have reported

that around 2009 or 2010, the rate of decline estimated from satellite-based observations became smaller than the rate of decline for satellite estimates before that time, but that the rate of decline estimated from the NEI exhibited little change, resulting in steeper declines for NEI than for satellite data after that time (Wang et al., 2021; Silvern et al., 2019; Jiang et al., 2018). For example, in one study NO_X emissions decreased 7% per year from 2005 to 2009, but only 2% per year from 2011 to 2015, matching surface measurements (Jiang et al., 2018). Possible explanations for this pattern are growing contributions from industrial and off-road sources, decreasing relative contributions from on-road gasoline emissions, and slower than expected decreases in on-road diesel emissions (Jiang et al., 2018). There also could be discrepancies between real-world and inventory-based vehicle emissions estimates (see Section 1.2.3). Because the flattening of total NO_X emissions after 2009 is observed in satellite-based data but not NEI data, a source not included or underestimated in the NEI could be driving this trend. Potential examples include lightning (see Section 1.2.7.3); fires, which are increasing but highly variable from year to year (see Section 1.2.7.2); soil emissions, which might be underestimated in the NEI (see Section 1.2.7.1), a possibility described in some detail by Wang et al. (2021); and/or NO_X formation from particulate nitrate photolysis (see Section 1.3.1) (Dang et al., 2023; Shah et al., 2023).

From summer satellite data available from 2005 to 2019 over the central United States, Wang et al. (2021) estimated that soil and lightning combined NO_X emissions decreased by about 4% per year until 2009. In contrast, after 2009 the trend reversed and combined soil and lightning emissions increased by 0.6% per year for the remainder of the period. For the central United States, Wang et al. (2021) estimated much smaller NO_X emissions from wildfires than from soil or lightning, with wildfires contributing less than 2% to total NO_X emissions compared to 11% for soil and 16% for lightning. However, in California there is some evidence that rising temperatures have contributed to the drying of forest fuels (Neighbour et al., 1990) and soil (Wang et al., 2023b), increasing both wildfire and biogenic soil NO_X emissions. In California, satellite-based NO_2 data trends sorted by land use showed a 3.7% per-year decrease in urban areas, no statistically significant trend in non-urban non-forested areas, and a 4.2% increase per year in remote forests (Wang et al., 2023b). Based on these observations, Wang et al. (2023b) concluded that, from 2009 to 2020, rising wildfire and soil emissions both contributed substantially to offset a decline in anthropogenic vehicle and fossil fuel emissions in non-urban parts of California, but that of the two sources, wildfires played a more important role than soil emissions.

Qu et al. (2021) observed no nationwide NO_2 trend in winter but a 19% increase in NO_2 for summer based on satellite data from 2010 to 2019. They reached a similar conclusion that, based on geographic and seasonal differences between monitoring network data, modeling results, and satellite-based NO_2 trends, it was that non-urban, warm season sources like wildfires or soil emissions were responsible for the flattening of the NO_2 emissions trend after 2009 observed in satellite data. These studies indicate that as fossil fuel sources decrease, non-fossil fuel sources with greater interannual variability like fires, soil, and lightning are making relatively larger contributions in rural areas that partially offset the decreasing trend in vehicle and other fossil fuel emissions. Further discussion of NO_X

emissions from wildfires, soils, and lightning, including evidence and explanation of their recent trends, are discussed in Section 1.2.7.

As NO_X emissions declined in the United States and Europe, global NO_X emissions trends showed little change between 2005 and 2014 (Miyazaki et al., 2017) due to NO_X emission increases in India, parts of China, and the Middle East (Jamali et al., 2020). This may mean higher contributions to ambient NO_X concentrations from international sources, especially for concentrations derived from satellite measurements because they are more strongly influenced by distant sources than ground level measurements (Jiang et al., 2022b). Indeed, increasing NO_X emissions from international sources have been suggested as an explanation for flattening trends in satellite-based NO_2 data despite continual decreases in U.S. anthropogenic NO_X emissions (Dang et al., 2023).

1.2.3 Highway Vehicles

Highway vehicles are the largest source of NO_X emissions nationally and the largest source in many of the areas in the United States with the highest ambient concentrations. Figure 1-1 shows the decline in NO_X emissions from highway vehicles since 2002. From 2014 to 2018, on-road NO_X emissions ranged from 9,575 to 10,300 tons/day (Li et al., 2021c). Highway vehicle emissions are frequently estimated with EPA's Motor Vehicle Emissions Simulator (MOVES) model (see Section 1.4.4). Comparison of this model to real-world driving emissions showed a reasonable agreement of results (Office of Transportation and Air Quality, 2021; Liu and Frey, 2015). While there have been improvements in data for real-world highway vehicle emissions, fewer data are available for contributions from high emitters, cold starts, and larger vehicles (Liu and Frey, 2015).

The greatest share of emissions is from heavy-duty diesel vehicles, which emit 1.3 million tons per year, accounting for 56% of U.S. on-road emissions and 15% of total U.S. NO_X emissions (U.S. EPA, 2023a). As a result of EPA rules tightening standards in successive tiers for criteria pollutant emissions from both light-duty and heavy-duty vehicles, vehicle NO_X emissions have decreased over time. For example, estimated NO_X emissions from light-duty passenger vehicles in 2013, after Tier 2 emissions standards were introduced, were 21% lower in Denver, CO and 43% lower in Tulsa, OK than in 2005 before Tier 2 emissions standards (Bishop and Stedman, 2015). This decrease has been gradual because a significant fraction of on-road vehicles remain in use for years after the latest standards are introduced (Li et al., 2020).

Since the 1990s, heavy-duty diesel vehicle emissions have decreased, but in 2013 NO_X emission factors (the amount of NO_X produced per amount of fuel burned) from heavy-duty diesel vehicles were still five to 10 times greater than from light-duty vehicles (Li et al., 2020). The national heavy-duty fleet emission factor was estimated by MOVES at 12.2 g NO_X/kg fuel, which agrees well with an independent on-road estimate of 12.2 g NO_X/kg fuel near Anaheim, CA (Haugen et al., 2018). Larson et al. (2017) reported NO_X emission factors for heavy-duty and light-duty vehicles of 14.8 g NO_X/kg fuel and 3.2 g

NO_X/kg fuel, respectively. In a recent tunnel study, the reported ratio of heavy-duty diesel to light-duty vehicle emission factors was 6 (Li et al., 2020).

Two areas of highway vehicle emissions uncertainty that have been discussed since publication of the 2016 Oxides of Nitrogen ISA are: 1) disagreement between the NEI and modeled emissions, and 2) differences between on-road emissions measurements and dynamometer testing results. The greatest of these discrepancies was between the NEI and modeled emissions. Several recent reports suggested that motor vehicle emissions estimates from the NEI and EPA emissions modeling platforms were overestimated by a factor of two in the summer (U.S. EPA, 2021; McDonald et al., 2018; Souri et al., 2016; Travis et al., 2016a; Canty et al., 2015; Anderson et al., 2014). These results led to an investigation of the discrepancy between ambient measurements and modeled estimates based on NEI data (U.S. EPA, 2021). It was found that model overpredictions were due to multiple confounding factors that each contributed to a portion of the bias, but that a major factor was too little vertical mixing at some times and locations in CTMs, a finding that led to model improvements (see Section 1.4.4).

Concerns about whether real-world emissions were adequately represented by test procedures arose when measured NO_X emissions exceeded the European standard by 260% during real-world, on-road driving (Weiss et al., 2012). These results suggested that dynamometer testing did not adequately capture on-road NO_X emissions by diesel cars. Real-world testing for Tier 2 diesel passenger vehicles in the United States also showed substantially higher-than-expected emissions for in-use diesel passenger vehicles (Thompson et al., 2014). One factor was the implementation of technology to activate emissions controls only during emissions testing by a leading manufacturer of U.S. diesel passenger vehicles, leading to an underestimation of NO_X emissions from diesel passenger vehicles by more than 36 million kg from 2008 to 2015. In 2015, the difference between emissions testing results and real-world observations was estimated to correspond to about 1% of total light-duty vehicle emissions (Barrett et al., 2015), corresponding to a considerably smaller impact compared to previously discussed errors in modeled emissions. However, these circumstances led to continued research on real-world, in-use vehicle emissions to complement emissions data obtained by standard test procedures, and this in-use vehicle testing has provided valuable information about passenger vehicle emissions.

Decreases in real-world emissions from individual light-duty gasoline vehicles were similar to decreases observed during dynamometer testing, as vehicles designed to meet Tier 2 NO_X emissions standards had 23 to 64% lower NO_X emissions than vehicles designed to meet Tier 1 NO_X emissions standards (Liu and Frey, 2015). Despite greater weight and higher fuel consumption, NO_X emissions from passenger trucks were similar to emissions from passenger cars, whereas hybrid electric vehicles had considerably lower NO_X emissions than conventional gasoline vehicles (Liu and Frey, 2015). Most recently, Yu et al. (2023) reported higher emissions for on-road vehicles (55 to 72% of total NO_X emissions) estimated in southern California from the Fuel-based Inventory of Vehicle Emissions (FIVE) than from the local emissions inventory of the South Coast Air Quality Management District (which estimated 43% of total NO_X emissions are attributed to on-road vehicles). These study results are

consistent with emission inventory data described earlier in this section, which show that although vehicle emissions have decreased, they still contribute substantially to, and in some locations may dominate, NO_X emissions.

Figure 1-4 shows field measurements of carbon monoxide (CO), hydrocarbon (HC), and NO emissions from light-duty highway vehicles at a typical urban interstate on-ramp in a Chicago, IL, U.S., suburb. Although CO and hydrocarbon emissions were measured earlier, measurements of NO emissions began in 1997 and decreased by 79% as progressively more restrictive emissions standards were introduced between 1997 and 2016 (Bishop and Haugen, 2018). In this study, there was also a much slower increase in NO emissions with vehicle age for Tier 2 than for Tier 1 vehicles. In addition, a greater fraction of emissions resulted from a smaller proportion of vehicles in more recent years: the emissions distribution across individual vehicles became increasingly skewed over time, with the highest emitting 1% of vehicles contributing a three times greater share to total emissions in 2016 than in 1997 (Bishop and Haugen, 2018). Passenger vehicles as a fraction of total vehicles decreased from 84% to 52% between 1992 and 2016. This shift in vehicle preferences to light-duty trucks did not appear to impact emissions trends because certifications were unified for cars and light-duty trucks (Bishop and Haugen, 2018).

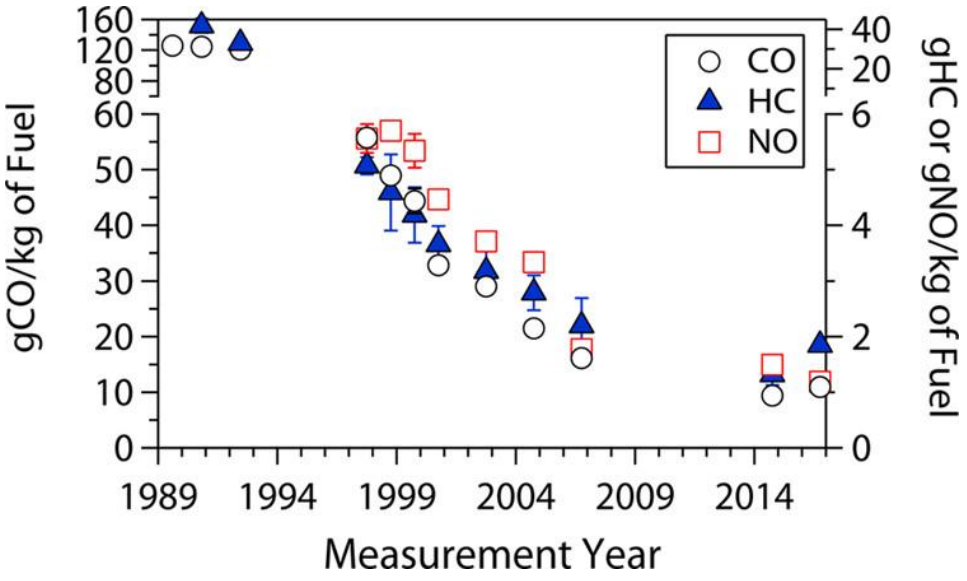

List of abbreviations in alphabetical order: CO = carbon monoxide; g = gram; HC = hydrocarbon; kg = kilogram; NO = nitric oxide.
Source: Bishop and Haugen (2018). Copyright permission pending.

Figure 1-4 Historical Chicago, IL, U.S., area real-world fleet emissions for carbon monoxide, hydrocarbons, and nitric oxide measured at an urban interstate on-ramp.

Decreasing NO_X emissions also have been documented through tunnel studies, which provide insight into real-world driving conditions but with the advantage of assessing a large vehicle fleet rather than just a single vehicle. Tunnel studies conducted 10 years apart in Pittsburgh, PA, U.S., indicated a

large reduction in NO_X emissions, with emission factors decreasing by 50 to 70% for both gasoline and diesel vehicles (Li et al., 2020). Results from historical studies similarly indicated a 70 to 80% decrease in light-duty vehicle emission factors between 2002 to 2015 and a rapid decrease in NO_X emissions from heavy-duty diesel vehicles (Li et al., 2020). However, tunnel measurements usually characterize emissions only from limited operating conditions. This is an important distinction, as vehicle starts (which are not reflected in tunnel studies) account for up to 8.3% of NO_X emitted from vehicles (Gately et al., 2017). This also sets tunnel studies apart from real-world driving conditions intended to capture a variety of driving conditions, in some cases resulting in even lower estimated NO_X emissions than dynamometer measurements. Modeled light-duty vehicle NO_X emissions are consistently higher than tunnel study results, reflecting a wider range of driving conditions that includes cold starts and transient operations. Decreasing NO_2 and NO_X concentrations have also been observed at many, but not all, near-road monitors in the United States (see Sections 1.4.2, 1.5.3).

Real-world emission estimates also indicate seasonal variations in highway vehicle NO_X emissions, with some studies reporting up to 70% higher emissions observed in winter than in spring (Bishop et al., 2022; Li et al., 2020) or summer (Saha et al., 2018; Wang et al., 2018). This is consistent with observations of NO_X emissions increasing with decreasing temperature (Grange et al., 2019). However, Toro et al. (2021) reported only small seasonal differences in on-road NO_X emissions based on NEI data. Several other factors influence real-world vehicle emissions, such as speed, acceleration, and road grade (Liu and Frey, 2015). The highest NO_X emissions generally occur at both low and high speeds, with the lowest emissions at moderate speeds of 40–50 mph (Liu and Frey, 2015). Vehicle NO_X emissions were also affected by global lockdown policies following the coronavirus disease (COVID-19) pandemic in 2020 (see Section 1.2.8).

1.2.4 Non-road Mobile Sources

Non-road mobile sources constitute 19% of total NO_X emissions in the United States (see Figure 1-2), though emissions from these sources have been decreasing since 2002 (see Figure 1-1). Examples of non-road mobile sources include locomotives, aircraft, commercial marine vessels, and non-road equipment, which make up 28%, 5%, 15%, and 52% of non-road mobile NO_X emissions, respectively, according to the 2020 NEI (see Figure 1-5). The relative contributions from different sources differ slightly from the recent analysis by Toro et al. (2021), because more recent NEI data are used and shipping emissions from federal waters are not included in Figure 1-5. EPA has set a series of standards to reduce NO_X emissions from non-road diesel sources similar to highway vehicles (see Section 1.2.3), referred to as Tier 1 to 4 standards. The most recent standard, Tier 4, was introduced in May 2004 and phased in from 2008 to 2015.

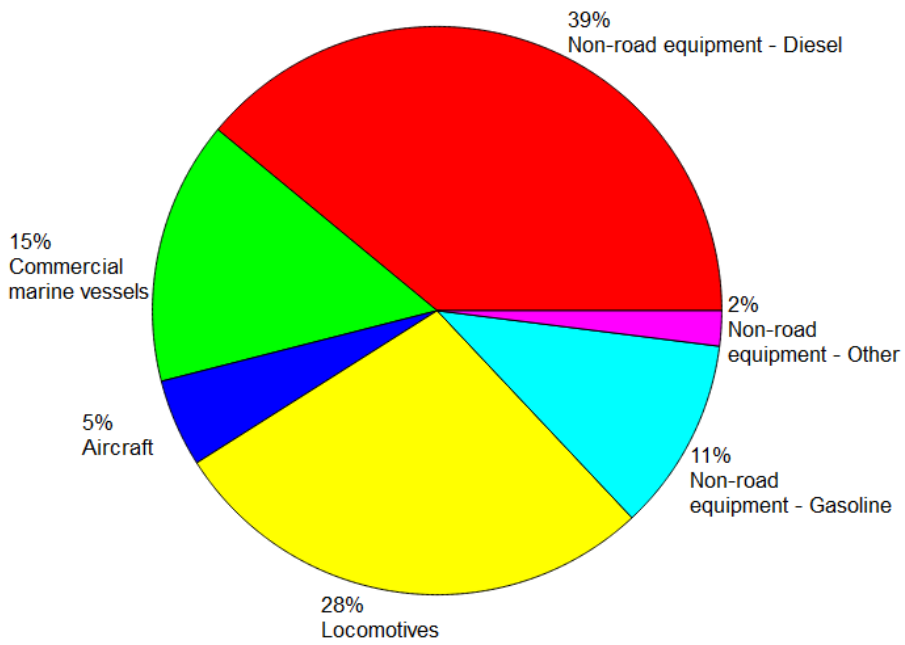

Source: U.S. EPA (2023a). Copyright permission pending.

Figure 1-5 Non-road mobile NO_X emissions quantified from the 2020 NEI.

Results from recent studies provide details on individual sources contributing to non-road mobile source emissions and are consistent with these NEI data. Emissions from locomotives can contribute significantly to the local areas in which they operate. Recent work measured NO_X emissions from 143 locomotives in Tacoma, WA, U.S., and found average emission factors of 51±2 g NO/kg fuel used and 4.2±0.2 g NO_2/kg fuel used (Breuer and Burgard, 2019).

Commercial marine vessels accounted for 14% of global nitrogen emissions at the time of the 2016 Oxides of Nitrogen ISA (U.S. EPA, 2016; Corbett et al., 1999). Similar to locomotives, ship emissions are spatially variable but can represent a substantial fraction of NO_X near port cities. In Houston, TX, U.S., roughly 50% of NO_X emissions were attributed to commercial shipping (U.S. EPA, 2016; Kim et al., 2011). A total of 1,170 tons of NO_X was emitted from ships in the Los Angeles, CA, U.S., and Long Beach, CA, U.S., ports during 2020 (Xiao et al., 2022). In that study, 40.2% of NO_X was attributed to cargo ships, 31.4% to container ships, 27.5% to oil tankers, and the remaining 0.9% to passenger ships and tugboats (Xiao et al., 2022). Reported fuel-based emission factors range from 24.1±1.4 g NO_X/kg fuel from passenger ships and ferries in San Francisco, CA, U.S., (Sugrue et al., 2022) to 72±24 g NO_X/kg fuel for large ocean-going ships in Vancouver, Canada (Burgard and Bria, 2016). Reported power-based emission factors range from 4.81 g NO_X/kilowatt-hour for diesel-engine recreational boats (Kiliç et al., 2022) to 11.91 g NO_X/kilowatt-hour for passenger ferries (Durmaz et al., 2017). A study conducted on cruise ships in the East China Sea measured average concentrations of 73.6 parts per billion by volume (ppbv) NO, 27.6 ppbv NO_2, and 0.39 ppbv nitrous acid (HONO) in ship

plumes (Sun et al., 2020). Global estimates of ship-produced HONO are 63.9±22.2 Gg/year (Sun et al., 2020).

It was stated in the 2016 Oxides of Nitrogen ISA that aircraft emissions contribute 2.6 to 15% of total ambient NO_X to areas within 3 km of airports (U.S. EPA, 2016; Carslaw et al., 2006; Unal et al., 2005). Global NO_X emissions from aircraft are estimated at 2 to 3 Tg/year (Turgut et al., 2013), with most NO_X emissions from aircraft occurring during the landing and takeoff cycles. NO_X emissions range from 8.59 to 82.47 kg NO_X per cycle depending on the type of aircraft (Ekici and Sevinc, 2022), with aircraft of higher mass emitting more NO_X (Turgut et al., 2013).

Construction machinery and mowing/agriculture equipment are non-road equipment that were not specifically discussed in the 2016 Oxides of Nitrogen ISA (U.S. EPA, 2016) but are included in the 2020 NEI and other studies. Recent studies have quantified NO_X emissions from construction machinery and agricultural equipment and determined they contribute 42% and 38%, respectively, to non-road diesel NO_X emissions (Toro et al., 2021). NO emission factors for diesel tractors mowing highway vegetation in New York ranged from 18 to 38 g/kg fuel, depending on mower type (Sonntag et al., 2015). Personal yard-tractor emissions ranged 2 to 8 g NO_X/wheel horsepower*hour (Li et al., 2021a). Average NO emissions factors for diesel-powered forklifts were 27.5±4.3 g/kg fuel (Pang et al., 2021). NO_X emission factors from construction machinery ranged 50–100 g NO_X/gal fuel, with significant NO_X emissions attributed to brake use (Cao et al., 2016). Oxides of nitrogen emissions as a function of fuel used for these types of non-road mobile sources are summarized in Table 1-2.

Table 1-22 Oxides of nitrogen emissions per amount of fuel used for various types of non-road mobile sources, as reported in the literature

Non-Road Mobile Source	Emissions Per Amount of Fuel Used	Source
Locomotive	51±2 g NO/kg fuel; 4.2±0.2 g NO_2/kg fuel	Breuer and Burgard (2019)
Commercial Marine Vessels	24.1±1.4 g NO_X/kg fuel from passenger ships and ferries	Sugrue et al. (2022)
	72±24 g NO_X/kg fuel for large ocean-going ships	Burgard and Bria (2016)
Aircraft	8.6–82.5 kg NO_X per landing and takeoff cycle	Ekici and Sevinc (2022)
Diesel Tractors	18–38 g NO/kg fuel	Sonntag et al. (2015)
Diesel-powered Forklifts	27.5±4.3 g NO/kg fuel	Pang et al. (2021)
Construction Machinery	50–100 g NO_X/gal fuel	Cao et al. (2016)

List of abbreviations in alphabetical order: g = gram; kg = kilogram; NO = nitric oxide; NO_X = the sum of NO_2 + NO.

1.2.5 Fuel Combustion and Utilities

As shown in Figure 1-2, stationary fuel combustion accounts for 25% of U.S. NO_X emissions, with the majority coming from EGUs (U.S. EPA, 2023a). A 33% decline in NEI estimates of total nationwide NO_X emissions from EGUs between 2008 and 2011 was described in the 2016 Oxides of Nitrogen ISA (U.S. EPA, 2016) (see Figure 1-1). This trend has continued: total U.S. NO_X emissions from EGUs were 2,089,000 tons/year in the 2011 NEI (U.S. EPA, 2013a) but decreased by 60% to 840,000 tons/year in the 2020 NEI (U.S. EPA, 2023a), mainly because of the shift away from coal for electric power generation. Recent evidence similarly shows an average decrease in NO_X emissions of 35% from 2005 to 2011 for 27 individual U.S. power plants at which emissions plumes could be isolated from other sources (de Foy et al., 2015). In addition, a 40% reduction in total U.S. NO_X emissions from EGUs from 1997 to 2012 has been attributed to an increasing fraction of electricity being generated by natural gas, in a shift away from coal as a fuel source, based on data from EPA's continuous emissions monitoring system (CEMS) (de Gouw et al., 2014).

As described in Section 1.2.1, satellite-based methods have been especially useful for estimating EGU emissions. The first use of satellite instrumentation for this purpose was reported by Kim et al. (2006) and was cited in the 2016 Oxides of Nitrogen ISA (U.S. EPA, 2016). It described a 35% decrease in NO_X emissions in the Ohio River Valley over the period 1997 to 2005 in response to 1998 regulatory requirements for EGU emissions. Other early satellite-based studies of U.S. EGU emissions also documented decreasing emissions, on average, and showed good agreement with modeling results (Russell et al., 2012; Kim et al., 2009).

Satellite instrumentation used to estimate NO_X emissions and surface concentrations is described in detail in Section 1.4.3, and most of the instruments described there have been applied to estimating emissions from EGUs (Liu et al., 2020; Goldberg et al., 2019; de Foy et al., 2015). Recent advances in satellite technology include greater NO_2 sensitivity and greater NO_2 spatial and temporal resolution, resulting in improved satellite capabilities for estimating EGU emissions (see Section 1.4.3). For example, the most recent satellite instrumentation has been used to derive NO_X emissions estimates for two large EGUs in the western United States, the Four Corners/San Juan Power Plant complex in NM and the Colstrip Power Plant in MT. These efforts were carried out to validate a satellite-based remote sensing methodology for estimating NO_X emissions using known, isolated sources with continuously monitored emissions and detectable daily plumes, which are among the largest point source NO_X emissions sources in the United States. Results for the Four Corners and Colstrip power plants agreed within 12% and 3% of emissions tracked hourly by CEMS, respectively (Goldberg et al., 2019).

1.2.6 Industrial Sources

Other anthropogenic sources include industrial activities, such as oil, gas, and cement production. Industrial nitrogen increased globally from 1960 to 2008, from 2.5 to 25.4 Tg N/year (Gu et al., 2013). Overall, industrial processes account for 12% of annual NO_X emissions in the United States (see Figure 1-2). More than half of U.S. industrial source NO_X emissions are from the oil and gas industry, with an additional 10% accounted for by cement industry emissions. The next largest industrial source is the pulp and paper industry, accounting for about 6% of industrial emissions, but NO_X emissions from paper production decreased by 40% from 1995 to 2010 (316,000 to 194,000 tons NO_X) (Pinkerton, 2014). Since 2002, industrial NO_X emissions have not decreased as much as NO_X emissions from mobile and stationary fuel sources (see Figure 1-1). Between 2017 and 2020, NEI emissions data show that industrial NO_X emissions decreased by 84,000 tons, or about 7%, compared to a 21% decrease for total U.S. NO_X emissions (U.S. EPA, 2023a).

Oil and gas production was discussed in the 2016 Oxides of Nitrogen ISA as an important source of NO_X in some regions: for example, in Dallas, TX, U.S., the industry around the Barnett Shale produces 30 to 46 tons of NO_X/day (U.S. EPA, 2016; Pacsi et al., 2013). Recent satellite measurements provide further detail into NO_X emissions from the largest oil and gas producing regions in the United States and suggest NO_X emissions of 4.8 to 81.1 tons/day across the largest producing regions (Dix et al., 2022). Inventory-based measurements suggest higher NO_X emissions of approximately 150 tons/day at the Permian Basin in Texas, approximately 75 tons/day at the Eagle Ford Shale in Texas, and approximately 45 tons/day at the Bakken Basin in North Dakota (Dix et al., 2020). Gas production at the Marcellus Shale in the northeastern United States emits 100 tons NO_X/day, accounting for 12% of NO_X emissions in that region (Roy et al., 2014). Ground-based monitors near the Marcellus Shale measured NO_2 values of 15 to 80 ppb (Long et al., 2019), similar to ground-based NO_2 measurements near oil and gas wells in California (21.4±14.6 ppb) (Gonzalez et al., 2022). Ethanol refineries also contribute NO_X to the atmosphere, such as one in Decatur, IL with emissions of 241 kg NO_X/hour or 0.53 g NO_X/kg ethanol (de Gouw et al., 2015). Canada is the world's fifth largest natural gas producer, with facilities such as one in British Columbia that emits approximately 1,700 tons NO_X/year near the United States border (Islam et al., 2020). In a recent study, satellite retrievals detected highly localized NO_2 hotspots over oil refineries near Baton Rouge, LA (Filonchyk and Peterson, 2023). The same study measured ground-based concentrations using a monitor located 2 km from the Baton Rouge, LA, oil refinery and detected average NO_2 concentrations of 18.6 ppb (34.9 μg/m^3) (Filonchyk and Peterson, 2023).

Cement production is another industrial process with nationally small (<1% of annual national NO_X) but regionally important and highly variable NO_X emissions (U.S. EPA, 2016; Walters et al., 1999). Cement and concrete production accounts for 7.8% of global NO_X emissions (Miller and Moore, 2020). In 2010, NO_X emissions from cement production in North America were 25,669 tons/year, equating to emission factors ranging from 1.88 to 2.71 kg NO_X/ton of cement produced (Brown et al., 2014).

1.2.7 Other Sources

A variety of other NO_X sources contribute to total U.S. NO_X emissions and are relevant to understanding trends and variability in atmospheric oxides of nitrogen concentrations. These sources are either natural or have both natural and anthropogenic components that are not always distinguished. The following section describes oxides of nitrogen emissions from soil, biomass burning, lightning, plants, animal waste, and marine microbes. As described in Section 1.2.2, NO_X emissions from wildfires and soil are increasing relative to fossil fuel sources and offsetting declines in anthropogenic emissions in non-urban areas (Wang et al., 2023b).

1.2.7.1 Soil Emissions

As U.S. NO_X emissions from other sources have decreased (see Figure 1-1), soil NO_X emissions are emerging as an increasingly important contributor to overall NO_X emissions (see Figure 1-6) (Geddes et al., 2022; Guo et al., 2020). Reports of the extent to which soil NO_X emissions already contribute to total NO_X emissions vary between studies and their locations, but there has been considerable effort to improve soil emissions parameterizations and reduce soil emissions uncertainties.

The NEI's biogenic sector includes emissions from soil and plants. Soil is a dominant source of NO_X emissions in areas of intensive agriculture with substantial fertilizer inputs, especially the Midwest and the Central Valley of California. Cropland soil emissions vary temporally, with largest emissions occurring when fertilizers are applied (Hudman et al., 2012). Hudman et al. (2010) estimated that 15–40% of total column NO_2 could be attributed to soil emissions during spring and summer months over the Great Plains of the United States (U.S. EPA, 2016). Soil NO_X is mainly emitted as NO through both microbial and abiotic processes (Huber et al., 2023; Rasool et al., 2016).

Soil NO_X emissions are variable and influenced by precipitation, irrigation, soil texture, soil drainage, nitrogen availability, and temperature (Almaraz et al., 2018). From dry soils, emissions sometimes occur in pulses after wetting of dry soil by precipitation or irrigation; NO_X emissions during these pulses can be many times greater than before or after pulsing and account for a large fraction of total soil NO_X emissions (Oikawa et al., 2015; Hudman et al., 2010). Accurate estimates of soil emissions are also challenging because a substantial fraction of soil emissions experience rapid uptake by vegetation canopies (Almaraz et al., 2018; Vinken et al., 2014). Improved modeling (and associated reductions of uncertainties) of soil NO_X emissions over the past 30 years have generally led to somewhat higher global soil NO_X emissions estimates with each improvement (Vinken et al., 2014).

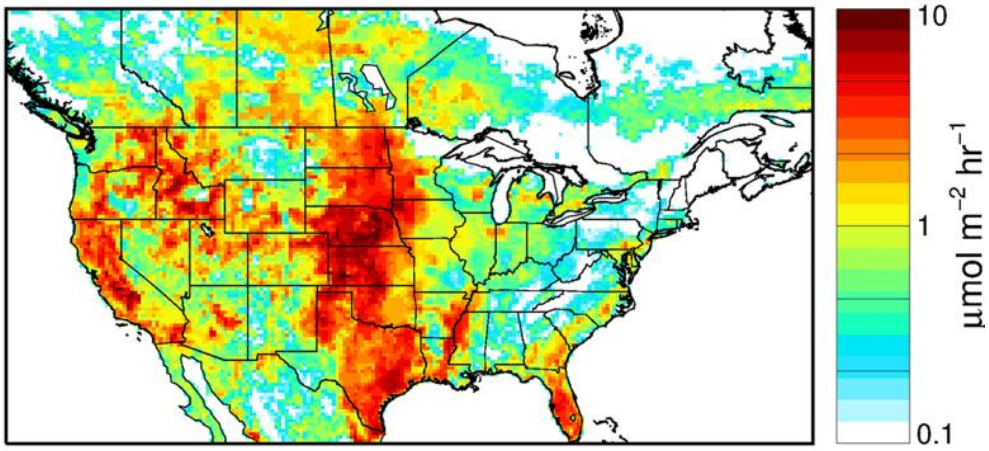

List of abbreviations in alphabetical order: h = hour; µmol = micromole; m = meter; NO_X = the sum of NO_2 + NO.
Source: Geddes et al. (2022). Copyright permission pending.

Figure 1-6 Estimated mean soil NO_X emissions from GEOS-Chem for July 2013.

In the agriculturally intensive San Joaquin Valley, CA, U.S., two different methods to estimate NO_X emissions have been compared: a spatial model of soil emissions and derivation of soil emissions from airborne-based observations of NO_X concentrations (Almaraz et al., 2018). Results indicated that fertilized cropland soil accounted for 20 to 32% of total statewide emissions, with the majority of NO_X emissions in the San Joaquin Valley. Emissions from natural soils contributed only 5 to 9% of total statewide emissions because of the impact of fertilizers in accelerating soil microbial processes (Almaraz et al., 2018). These results are consistent between methods and with previous research indicating agricultural soil emissions are responsible for more than 20% of global NO_X emissions and up to half of NO_X emissions in agricultural regions (Almaraz et al., 2018). Emissions have also increased in agricultural areas of California during the last 20 years. While some of this increase is probably due to increased NO_X emissions from mobile sources and other combustion sources linked to population growth in California's agricultural areas, increased fertilizer use is a major contributor (Almaraz et al., 2018).

Similarly, Sha et al. (2021) used an improved modeling scheme that accounted for NO_X emission pulses from previously dry soils wetted by precipitation or irrigation. The authors estimated that soil NO_X emissions increased monthly mean surface concentrations by 1.2 ppb statewide and by 3.0 ppb over croplands. Soil accounted for about 40% of California NO_X emissions in July 2018 and more than 50% in both rural regions with high fertilizer application and native drylands (Sha et al., 2021). In contrast, Guo et al. (2020) studied soil NO_X emissions from the San Joaquin Valley and from the entire state of California and reported much lower emissions. The authors estimated that soil NO_X emissions contributed 1.1% of total California NO_X emissions, 60% of which was from cropland and driven by fertilizer use. They emphasized that agricultural emissions were still a relatively minor source compared to traffic combustion in both urban and rural areas of the San Joaquin Valley (Guo et al., 2020). The differences between these studies suggest substantial uncertainty in soil NO_X emissions. To address this, several methodological improvements to soil NO_X emissions estimation have been carried out in recent years,

including allowing the classification of arid and non-arid land to vary with time (Sha et al., 2021), improving the temperature dependence function (Wang et al., 2023a), and improving the representation of soil moisture effects (Huber et al., 2023).

High soil emissions have also been estimated in the Midwest United States (Hudman et al., 2010). Travis et al. (2016b) reported that substantially greater contributions of combined soil and fertilizer emissions relative to NO_X emissions from combustion sources than those reported in the National Emissions Inventory reduced modeled ozone bias in the southeast United States. High soil NO_X emissions uncertainties are also evident in these regions. Vinken et al. (2014) estimated biogenic soil emissions using satellite observations from 11 world regions dominated by agricultural soil NO_X emissions, including two in parts of the midwestern and western United States. Although global and regional estimates were higher for satellite-based than for inventory-based estimates, the midwestern U.S. region was an exception, where soil NO_X emissions estimates were 40% lower for satellite-based estimates than for a priori emissions inventory estimates based on Hudman et al. (2012). Similarly, Travis et al. (2016b) also needed a strong reduction in soil NO_X emissions computed according to Hudman et al. (2012) in the southeast United States to achieve model agreement with atmospheric observations.

Soil NO_X emissions increase nonlinearly with increasing temperature, soil moisture, and fertilization, meaning that emissions from agricultural soils in hot climates are especially high. Some of the highest soil NO_X emissions ever observed are reported in the Imperial Valley, a high temperature agricultural region in California where soil NO_X emissions ranged up to 900 ng $N/m^2/s$, with highest emissions observed at temperatures between 27 to 40°C, moderate soil water contents, and within 23 days of fertilization (Oikawa et al., 2015). Number of days since fertilization was the strongest predictor of NO_X emissions, but pulsed NO_X emission responses to irrigation could be observed even more than 30 days after fertilization (Oikawa et al., 2015).

The temperature dependence of soil NO_X emissions contributes to seasonal emissions patterns, with warm season periods of higher emissions. For example, Yan et al. (2005) statistically modeled soil NO_X emissions and estimated that seasonally fertilized croplands made the greatest contribution to global NO_X emissions when several major types of soils were compared. They further estimated that northern hemisphere soil emissions fluctuated between about 100 Gg N/year in January to more than 500 Gg N/year in July (Yan et al., 2005), matching a similar seasonal pattern for NO_2 reactivity but exhibiting an opposite seasonal pattern to motor vehicle emissions, which are highest in winter (see Section 1.2.3). Considerable interannual variability of soil NO_X emissions based on CTM results have also been reported, with national monthly soil NO_X emissions for July ranging from 0.11 to 0.20 Tg from 1996 to 2014 (Geddes et al., 2022). There is also evidence that rising temperatures could be responsible for recent increasing trends in soil NO_X emissions. Romer et al. (2018) attributed increasing NO_X emissions at a forested site in the Southeast United States to the impact of increasing temperatures on soil microbes, and Wang et al. (2023b) showed that increasing soil NO_X emissions in California were associated with a 1.2°C per decade increase in temperature from 2009 to 2020.

Recent research on improving soil NO_X emissions estimates in the United States has also focused on the role of soil moisture. After updating soil moisture relationships to account for soil and ecosystem characteristics, Huber et al. (2020) estimated higher soil NO_X emissions in non-arid regions than had been estimated using a constant relationship between soil moisture and emissions, particularly in the eastern United States. Soil NO_X emissions are not only contributing a greater share of overall NO_X emissions as highway vehicle and EGU emissions decline but are also more sensitive to climate conditions than fossil fuel NO_X emissions because of their relationship to soil moisture (Huber et al., 2024; Huber et al., 2020). Soil moisture is challenging to represent because of high spatial variability and scarce observations (Huber et al., 2023). Recent modeling confirms that soil NO_X emissions have been underestimated in non-arid regions of the United States, including much of the eastern U.S., further highlighting the importance of climate-related soil NO_X emissions as non-agricultural anthropogenic NO_X emissions decline (Huber et al., 2023). Although the contributions of soil to NO_X emissions are increasingly recognized, temporal patterns are still poorly understood, with models underestimating emissions of soil NO_X in the spring and overestimating them in the summer (Huber et al., 2024).

As U.S. NO_X emissions from motor vehicles and power plants decline, significant NO_X contributions from soil emissions are not limited to highly fertilized intensive agricultural regions. For example, in a model grid containing Philadelphia, PA, more than 10% of estimated summer NO_X emissions were from soils (Geddes et al., 2022). Wang et al. (2023b) defined scrublands as shrublands, savanna, and grasslands, exclusive of croplands. They reported that scrublands accounted for 48.4% of California land cover compared to only 9.5% for croplands, that soil NO_X emissions have increased more from scrublands than other land use types, and that 63% of observed summer enhancements of NO_X emissions in scrublands could be attributed to soil NO_X emissions. Romer et al. (2018) also reported increasing NO_X emissions from non-agricultural soils in the southeastern United States. Increasing soil NO_X emissions in the southeastern United States could be affected by invasive kudzu (*Pueraria montana*), which can increase net nitrification by 500% and NO emissions from invaded soils by 100% (Hickman et al., 2010).

1.2.7.2 Biomass Burning

Fire emissions are estimated in the NEI which aggregates data using different methods (see Section 1.2.1), modeling (see Section 1.4.4), or through observational studies (some included below). Prescribed and agricultural fires were not separated from wildfires or other biomass burning emissions in the 2016 Oxides of Nitrogen ISA (U.S. EPA, 2016), though the NEI and recent work now consider these separate from wildfire. It was reported in the 2016 Oxides of Nitrogen ISA that biomass burning (i.e., wildfires, prescribed burns, and agricultural fires) represented approximately 15% of global NO_X emissions (U.S. EPA, 2016; Denman et al., 2007). The magnitude and type of NO_X emissions vary with the type of biomass burned, but in general NO emissions dominate during flaming combustion (Benedict et al., 2017; U.S. EPA, 2016; Urbanski, 2014; Burling et al., 2010). Emission factors of 2.3 to 5.1 g/kg

were previously reported for wildfires in the southeastern U.S. (U.S. EPA, 2016; Burling et al., 2010). Currently, all fires represent approximately 5% of NO_X emissions in the United States (see Figure 1-2).

Since the 2016 Oxides of Nitrogen ISA (U.S. EPA, 2016), biomass burning estimates have increased and now represent approximately 27% of global NO_X emissions (Bray et al., 2021). Average global biomass burning emissions from 2001 to 2015 were 4.53±0.51 Tg NH_3/year and 14.65±1.60 Tg NO_X/year, with NO_X emissions projected to increase to approximately 18.9 to 20.9 Tg/year by mid-century and 19.5 to 25.3 Tg/year by the end of the century (Bray et al., 2021). In 2013, wildfires emitted up to 44 Gg NO_X/year (Liu et al., 2017a). As wildfires become more frequent, particularly in the western United States, emissions are anticipated to increase. Wildfires in 2020 contributed up to 83% of total annual nitrogen emissions in the western United States, with modeled fire NO_X emissions estimates ranging from 1.7 to 11.8 Tg across the continental United States (Campbell et al., 2022). The first recorded gigafire was recorded in California in 2020, an extremely active fire year, so these modeled estimates represent the upper limit of fire emissions.

Fire emissions are sporadic, with high interannual and seasonal variability that create emissions hot spots. Wildfires occur most often in the summer and fall. For example, Wang et al. (2023b) identified a substantial rise in summertime NO_2 concentrations in forested environments, mostly driven by wildfire emissions. In the past decade, however, there have been more wildfires in winter and spring, seasons not historically associated with active wildfires (e.g., Palisades Fire in January 2025). Prescribed burning occurs most commonly in the springtime, and research has shown that biomass burning smoke from Mexico and Central America can be advected to the southern United States in springtime (Kaulfus et al., 2017; Rogers and Bowman, 2001).

Wildfires have been shown to affect ambient NO_X concentrations. For example, average background (naturally occurring) NO_X concentrations in Fort Collins, CO, U.S., were 5 ppb but increased to 16 ppb during a wildfire event (Benedict et al., 2017). Similarly, NO_2 concentrations doubled from 0.8 ppb to 1.6 ppb during California wildfires in 2013 (Burley et al., 2016). NO and NO_Y concentrations of approximately 12 ppbv and 100 ppbv, respectively, were reported during the Williams Flat fire in California in August 2019 (Bourgeois et al., 2022). Published NO_X emission factors upon burning are 1.9±1.1 g NO_X/kg peat (Watson et al., 2019), 1.0±0.1 g NO_X/kg boreal forest (Urbanski, 2014), and 2.0±1.0 g NO_X/kg conifer forest (Urbanski, 2014), which are largely consistent with NO_X emission factors derived more recently from satellite data (Jin et al., 2021). HONO concentrations up to 25 ppb were measured during the Australian wildfires in 2019-2020 and are similar to fires in the United States (Dufour et al., 2022).

Measurements of smoke plumes from crop burning in the southeast United States from 2016 to 2018 reached maximum values of 8 ppb NO and approximately 40 ppb NO_2, 12 ppb HONO, and 60 ppb NO_Y (Bourgeois et al., 2022). Across eight coniferous forest prescribed burn plots in North Carolina and California, average emissions were 0.84±0.34 g NO, 2.70±0.35 g NO_2, and 0.50±0.15 g HONO per kg of fuel (Burling et al., 2011). Across six chaparral and oak savannah prescribed burn plots in the

southwestern United States, average emissions were 0.75±0.24 g NO, 2.58±1.05 g NO_2, and 0.54±0.14 g HONO per kg of fuel (Burling et al., 2011). Agricultural burns had higher emission factors of 2.67 g NO_X/kg of fuel (Jin et al., 2021). While the amount of emissions from wildfires is typically greater than that from prescribed or agricultural fires (U.S. EPA, 2023a), these types of fire management strategies are increasing and contribute to concentrations of oxides of nitrogen in ambient air.

1.2.7.3 Lightning

Although NO_X emissions from lightning are not captured in the NEI, research indicates that up to 80% of upper tropospheric NO_X is produced by lightning (Zhu et al., 2019b), with the remaining percentage contributed by aircrafts (Zhang et al., 2020). Understanding the vertical distribution of NO_2 from these aboveground sources is critical for improving the accuracy of satellite data retrieval (see Section 1.4.3). While the vertical distribution of lightning-produced NO_X resides primarily in the troposphere, recent studies have identified the elevation of surface NO_X immediately following thunderstorm activity (Murray, 2016). For example, peak NO_2 concentrations reached 30 ppb over northern Alabama after thunderstorms, suggesting NO_X production from lightning in the boundary layer and subsequent convective transport to ground-level (Murray, 2016). In spring and summer, most lightning activity occurs over North America and the Atlantic Ocean (Gressent et al., 2014). Estimates of tropospheric NO_X production from lightning flashes have been reported as 101.17 mol NO_X/flash (Koshak et al., 2014) and 500 mol NO/flash (Zhu et al., 2019b), though lightning is a very spatially variable source. Annual global lightning NO_X emissions are estimated at 2 to 8 Tg N/year, which represents the widest range of uncertainty associated with any specific NO_X source category (Zhang et al., 2020; Koshak et al., 2014). Models have estimated a linear relationship between lightning NO_X production and changes in global surface temperature (0.44±0.05 Tg N/K) (Finney et al., 2016), suggesting that lightning may become an increasingly important source of NO_X as surface temperatures increase.

1.2.7.4 Other Biogenic Sources

Other biogenic NO_X sources include emissions from animal waste, plants, and microbes. Horse dung emits NO and HONO for up to a year, with emissions rates for most nitrogen species increasing over time (Maljanen et al., 2016). Horse manure releases more NO_X than dairy cow manure, representing a potentially important source of nitrogen-containing gases (Maljanen et al., 2016). Plant NO_X emissions were not quantified in the 2016 Oxides of Nitrogen ISA (U.S. EPA, 2016), though recent work shows leaf litter is a source of NO (Gritsch et al., 2016). Leaves represent a small portion of tree mass but a large fraction (33%) of nitrogen sequestered in trees (Coggon et al., 2016). Coniferous leaf litter releases the highest amounts of NO upon decomposition (207 µg NO/kg), with 2.4 to 7 times higher NO emissions than deciduous leaf litter (Gritsch et al., 2016). Warm temperatures and moist conditions enhance leaf

litter emissions (Gritsch et al., 2016). Microbial NO_X emissions are particularly important in the open ocean, where microbes contribute 58±3% of oceanic NO_X (Song et al., 2022). Overall, biogenic sources add relatively small contributions to overall concentrations of oxides of nitrogen in ambient air but may be temporally or spatially important.

1.2.8 COVID-19 Changes to NO_X Emissions

The COVID-19 pandemic and subsequent lockdowns altered global atmospheric NO_2 concentrations. In early 2020, NO_2 decreased 45.8% globally compared to the baseline period of 2015 to 2019 (He et al., 2021; Liu et al., 2021b). NO_2 concentrations dropped across all continents in 2020, with the largest reductions of 42.5% observed in Europe (He et al., 2021). NO_2 decreases attributed to COVID-19 lockdowns ranged from 9.2 to 43.4% among 20 cities in North America, with a median NO_2 decrease of 21.6% (Cooper et al., 2022; Goldberg et al., 2020). Across the United States, NO_2 declined by 25.5% during March and April of 2020 relative to 2017–2019 (Qu et al., 2021; Berman and Ebisu, 2020). The most notable declines were observed in urban areas, with NO_2 decreases of up to 31%, 49%, and 51% observed in Los Angeles, CA (Liu et al., 2021b), Las Vegas, NV (Chen et al., 2020), and Newark, NJ, respectively (Yao et al., 2022). Satellite-based measurements (see Section 1.3) comparing 21-day COVID-19 lockdown periods in 2020 to the same period in 2021 indicated 17%, 18%, and 22% lower NO_2 measurements in New York, NY; Washington, DC; and Chicago, IL, respectively (Huang et al., In Press). NO_2 concentrations from 240 U.S. ground monitoring stations were compared between April 2020 and April of the prior 5 years by Archer C et al. (2020). The authors reported large, statistically significant decreases in NO_2 concentrations at more than 65% of monitoring stations, with an average decrease of 2 ppb from the mean of the previous 5 years (Archer C et al., 2020).

In general, decreases in NO_X emissions during COVID-19 lockdowns were consistent with declining mobile emissions (Chen et al., 2020). Across the United States, on-road NO_X emissions decreased by up to 31% in April 2020 when lockdown measures were most stringent (Kondragunta et al., 2021). Traffic volume in Seattle, WA decreased by 37%, resulting in NO, NO_2, and NO_X decreases of 33%, 29%, and 30%, respectively (Xiang et al., 2020). Similarly, total traffic decreased by up to 26.4% in Cincinnati, OH during the stay-at-home order, corresponding to 30% NO_2 reductions compared to pre-pandemic concentrations (Tumbleson and Balachandran, 2022). In California, weekday traffic decreased 24 to 29% depending on the area, with corresponding significant declines of NO (32 to 35%) and NO_2 (15 to 29%) measured using ground-based monitors (Liu et al., 2021a). NO_2 decreased 10.8% at near-road monitoring stations in Atlanta, GA following COVID-19 lockdown measures (Huang et al., 2021).

Some studies have noted a rebound of NO_X concentrations with lifted COVID-19 lockdown restrictions (Yao et al., 2022; Liu et al., 2021b) or even an increase in heavy-duty vehicle traffic during the latter half of 2020 (Tumbleson and Balachandran, 2022). However, the San Joaquin Valley, Los Angeles, and San Francisco areas of California continued to have roughly 20% lower on-road NO_X

emissions through November 2020, months after lockdown restrictions were lifted, due to reduced mobile emissions associated with increased telework and remote work options (Kondragunta et al., 2021). Compared to the 2022 NEI (U.S. EPA, 2022), NO_X emissions are still lower than in 2020 (6,589 kt compared to 8,916 kt in 2020, a reduction of 26%).

1.2.9 Emissions Summary

Major categories of NO_X emissions in the United States are highway vehicles, non-road mobile sources, stationary fuel combustion, industrial processes, and biogenic/geogenic sources. Source contributions to total U.S. emissions based on the 2020 NEI are summarized in Figure 1-2. In urban areas, emissions are generally dominated by highway vehicles and non-road mobile sources, which make up more than three-quarters of emissions in areas with populations over 2.5 million. Episodic emissions from industrial and other anthropogenic sources can be locally or regionally significant. Advances in vehicle technologies and the shift away from coal for power generation have led to substantial reductions in NO_X emissions, with total national NO_X emissions declining by 70% nationally from 2002 to 2023 (Figure 1-1).

The decline in vehicle emissions coincides with recent increases in estimated fire and soil emissions in some locations. Therefore, although Figure 1-2 shows that highway vehicles and stationary fuel combustion remain the greatest sources of NO_X emissions in the United States, there are greater uncertainties and variability in fire and biogenic emissions, including those from soils. In addition, the seasonal pattern of motor vehicle emissions differs from fire and soil emissions (see Section 1.2.7), with fire and soil emissions highest in summer when NO_X is most reactive and motor vehicle emissions highest in winter when the longer NO_X lifetime (see Section 1.3.1) favors greater accumulation in the atmosphere and higher concentrations. The result is a decreasing trend but greater variability in NO_X emissions, especially in fire-prone or heavily agricultural regions with increasing annual emissions of more seasonally dependent emission sources like soil (see Section 1.2.7.1) and fires (see Section 1.2.7.2). It also highlights the need for more seasonal emissions data. Higher temporal resolution of geostationary observations from recently launched satellite instruments (Zoogman et al., 2017) could help meet this need if they can be used to better isolate and constrain emissions from specific sources (see Section 1.4.3).

1.3 Atmospheric Chemistry and Fate

This section presents the atmospheric chemistry for reactive oxides of nitrogen. Topics include atmospheric lifetimes, intermediate reactions, and sinks, and these topic discussions aid in the interpretation of NO_X concentrations that are most relevant for the review of the primary NAAQS. Particular attention is given to NO_2 as this is the indicator for oxides of nitrogen and most relevant to the

evaluation of health evidence. NO_Y includes NO_X (i.e., NO + NO_2) and other oxides of nitrogen including, but not limited to, nitric acid (HNO_3), HONO, dinitrogen pentoxide (N_2O_5), and nitryl chloride ($ClNO_2$). In addition, NO_Y includes organic nitrates ($RONO_2$) and peroxyacetic nitric anhydride (PAN; sometimes referred to as peroxyacetyl nitrate and its homologues. All reactive oxidized species except for NO_X are referred to as NO_Z, such that $NO_Z = NO_Y - NO_X$ (see Figure 1-7 and Figure 1-8). Detailed descriptions of NO_Y chemistry are included in this section because some NO_X species can temporally be transformed to NO_Y species (e.g., HONO, organic nitrates) before being transformed back into NO_X, thereby affecting NO_2 concentrations and trends even far from emission sources. Major developments in the atmospheric chemistry and fate of NO_X since the 2016 Oxides of Nitrogen ISA (U.S. EPA, 2016) center around improved understanding of wintertime NO_Y cycling and lifetimes, surfaces and particulate nitrate (pNO_3^-) as sources of HONO and recycled NO_X, and NO_Y chemistry in wildfire smoke. These topics, among others, are discussed below.

1.3.1 Formation, Reactions, and Sinks

Oxides of nitrogen in the atmosphere are primarily emitted as NO. For example, tail pipe emission studies show that 90% or more of highway vehicle NO_X emissions are emitted as NO, with the remaining 2 to 10% emitted as NO_2 in the United States (Zuraski et al., 2025; Wild et al., 2017). NO is rapidly (i.e., within seconds to hours) converted to NO_2. In the presence of sunlight, NO_2 can be quickly photolyzed back to NO. Because NO and NO_2 are quickly cycled back and forth, they are grouped together as NO_X. The conversion of NO to NO_2 is driven by oxidizing species such as O_3 or short-lived, unstable species identified as radicals, the most important of which is the hydroxyl radical (OH). Higher concentrations of oxidizing species and higher ambient temperatures accelerate the conversion of NO to NO_2. A by-product of NO_2 reduction to NO is the creation of O_3. As a result of NO_X cycling, the presence of NO_X is directly tied to O_3, which also affects human health and the oxidizing capacity of the atmosphere, as most recently discussed in the 2020 ISA for Ozone and Related Photochemical Oxidants (U.S. EPA, 2020a). HONO is also directly emitted from various sources. Figure 1-7 shows simplified reaction pathways for NO_X.

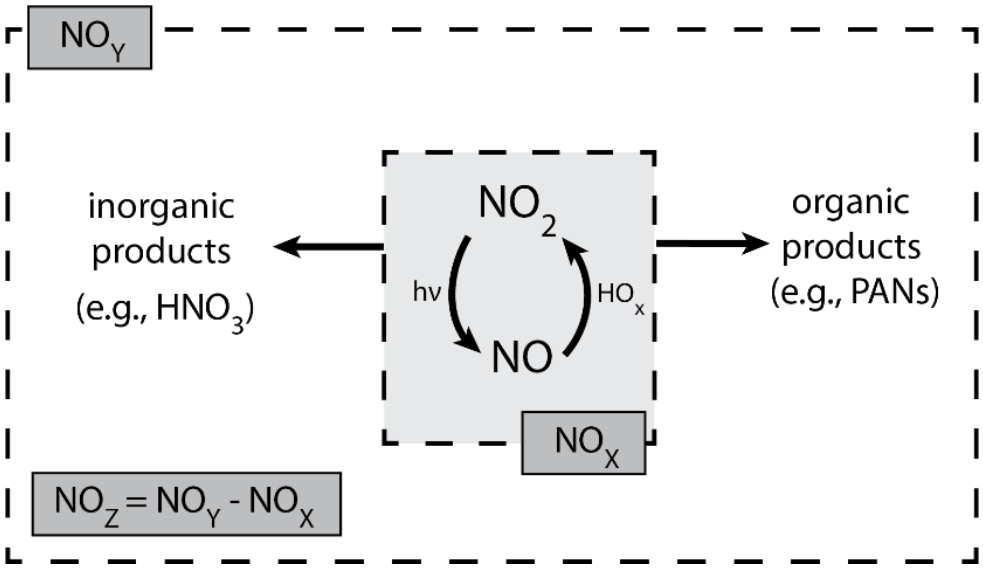

Note: The inner dashed box (shaded light gray) contains NO_X (NO + NO_2), interconverted by photolysis (hv) and HOx radicals (OH + HO_2). The outer dashed box contains other species formed from reactions of NO_X, which are referred to as NO_Z. Species shown in the outer and inner dashed boxes are collectively referred to as NO_Y.

Figure 1-7 Simplified schematic diagram of the cycle of reactive oxidized nitrogen species in the atmosphere.

The atmospheric lifetime for a chemical species is defined as the length of time a species persists against chemical transformation or depositional loss. NO_X lifetimes vary by time of day, season, meteorology, and presence of reactants and are non-linearly related to their own concentration. Averaged across midlatitude locations of the United States during summer, the lifetime of NO_X is approximately three hours (Martin et al., 2003). Urban areas often have shorter NO_X lifetimes than other areas in the United States due to more available reactants from anthropogenic emissions (Laughner and Cohen, 2019). A recent analysis of approximately 30 North American cities showed differences in urban weekday NO_X lifetimes depending on the chemical composition of each city (Laughner and Cohen, 2019). These authors additionally reported that NO_X lifetimes have significantly changed, some have increased while some have decreased, between 2005 to 2014 due to continued decreases in NO_X emissions (Laughner and Cohen, 2019). Other recent research efforts have also focused on determining wintertime NO_X lifetimes. Using observations from the Wintertime Investigation of Transport, Emissions, and Reactivity field campaign in the northeastern United States in 2015, daytime winter NO_X lifetimes were estimated to be 29-hours, while nighttime winter lifetimes were approximately 6-hours (Kenagy et al., 2018). Wintertime NO_X lifetimes are typically longer than summer ones due to reduced sunlight and available OH radicals, which slow chemical reactions, such as VOC reactivity.

Major NO_X sinks include other reactions forming more highly oxidized products and NO_X deposition, which typically occur on longer timescales than the conversion of NO to NO_2 (Jaeglé et al., 2018). The formation of HNO_3 is the dominant global NO_X sink and is often a terminal sink, meaning NO_X cannot be reformed. Organic nitrates (e.g., PAN) are produced in significant amounts in the presence

of volatile organic compounds (VOCs). Research has gone into understanding the partitioning between HNO_3 and organic nitrate production, as organic nitrates can rerelease NO_X through chemical reactions and thereby lengthen the lifetime of NO_X and increase NO_X concentrations far from emission sources. Production of organic nitrates can dominate HNO_3 production in rural locations during summer when VOC emissions from temperate flora are abundant (Alexander et al., 2020; Romer et al., 2016). For example, organic nitrates comprised between 30 to 45% of the total NO_Y budget during the Southern Oxidant and Aerosol Study field campaign in summer 2013 in the southeastern United States (Ayres et al., 2015). Chemical transport model simulations informed by observations have estimated organic nitrate lifetimes to be almost 3-hours during the summer (Zare et al., 2018b). During the winter, the oxidization of NO_X to organic products decreases significantly due to lower VOC emissions. Therefore, the relative importance of HNO_3 increases as a NO_X sink during the winter. For example, during a winter field campaign in the northeastern United States, 91% of NO_X was oxidized to produce HNO_3 (Jaeglé et al., 2018) due to low VOC reactivity (Kenagy et al., 2018). The small fraction of organic nitrates produced during winter have been estimated to have much longer lifetimes, up to 23 days (Jaeglé et al., 2018), lengthening NO_X lifetimes.

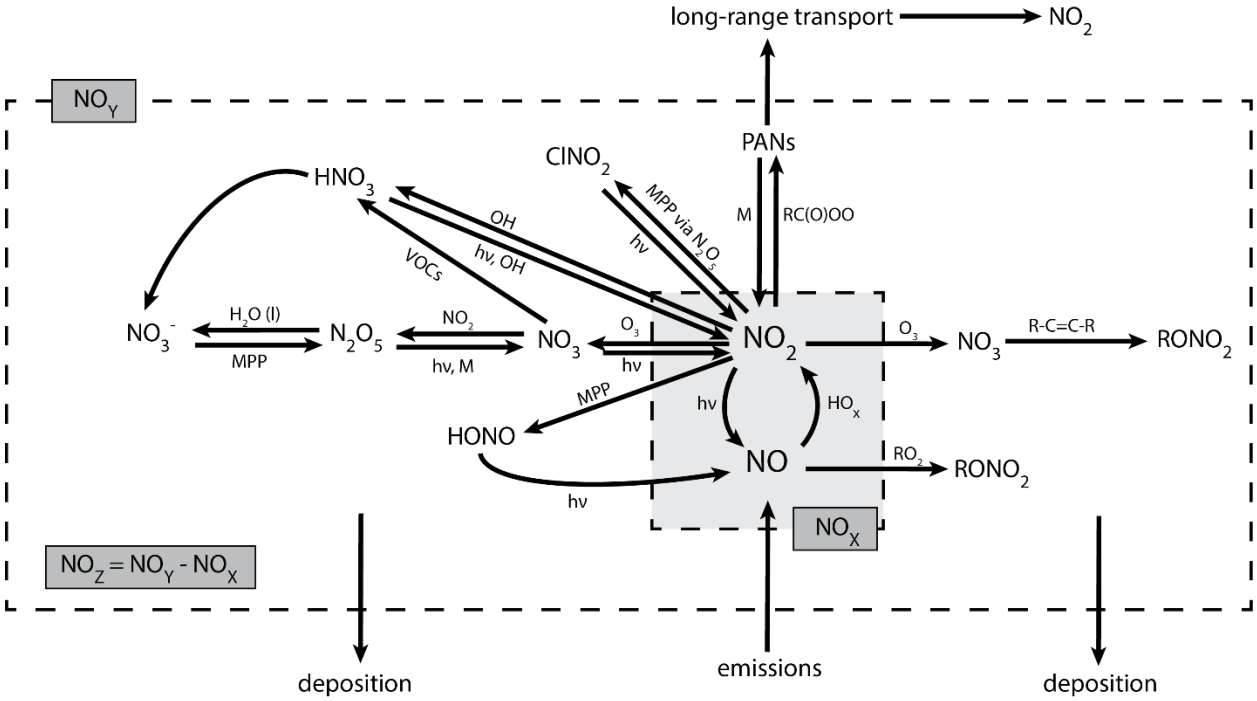

Note: The inner dashed box (shaded light gray) contains NO_X ($NO + NO_2$) interconverted by photolysis (hv) and HOx radicals ($OH + HO_2$). The outer dashed box contains other species formed from reactions of NO_X, which are referred to as NO_Z. Species shown in the outer and inner dashed boxes collectively referred to as NO_Y. M = species transferring/removing enough energy to cause a molecule to decompose/stabilize; hv = solar photon; MPP = multiphase process, R = organic radical.
Source: Figure modified from the 2016 Oxides of Nitrogen ISA (U.S. EPA, 2016).

Figure 1-8 Schematic diagram of the cycle of oxidized nitrogen species in the atmosphere, showing the complexity of relationships among inorganic and organic products that are simplified in Figure 1-7.

In general, there are multiple formation pathways for HNO_3 (see Figure 1-8). The oxidation of NO_2 with OH dominates during the day, whereas hydrolysis of N_2O_5 to HNO_3 dominates at night (Alexander et al., 2009). At night, HNO_3 formation occurs when nitrate radical (NO_3), produced by the oxidation of NO_2 with O_3, reacts with VOCs. Additionally, there are heterogeneous reactions that occur at night and can create HNO_3. N_2O_5 is formed from the reaction of the $NO_3$and NO_2, which can react with water-containing aerosols to produce condensed phase HNO_3 (Alexander et al., 2020). Condensed phase HNO_3 is preferentially produced at low temperatures, high relative humidities, and higher particle pH (Shah et al., 2018; DSDTT, 1988). Alternatively, N_2O_5 can also be photolyzed back into NO_2 in the morning, increasing daytime NO_X concentrations. Recent analysis from a field campaign along the U.S. East Coast found that nighttime heterogenous reactions with N_2O_5 are responsible for 62% of HNO_3 production, with 35% of HNO_3 production due to the daytime homogenous oxidation pathway (Jaeglé et al., 2018). Globally, however, both reaction pathways are equally important for HNO_3 production in the lower atmosphere (Alexander et al., 2020).

N_2O_5 can also collide with chloride-containing aerosols (e.g., sea spray or road salt) to produce $ClNO_2$ (McNamara et al., 2020; Thornton et al., 2010). The fraction of these collisions that result in a chemical reaction to form a new product is referred to as that product's reactive uptake coefficient. There is much active research to determine the reactive uptake coefficient for $ClNO_2$. The reaction rate depends on chloride concentration, relative humidity, particle size and viscosity, and interfacial processes (Galib and Limmer, 2021; Gaston and Thornton, 2016; Gržinić et al., 2015; Gaston et al., 2014). Because of these factors, reported uptake coefficients over the United States vary widely (McDuffie et al., 2018a; McDuffie et al., 2018b). Determining $ClNO_2$ uptake coefficients is important because $ClNO_2$ thermally dissociates during the day, releasing two gas-phase Cl and NO_2. Therefore, conditions that favor $ClNO_2$ production at night can increase NO_2 concentrations at sunrise.

Organic nitrates are formed from the oxidation of NO_X with biogenic VOCs, and they can serve as a major daytime temporary NO_X reservoir (Kenagy et al., 2018). Classes of organic nitrates include peroxy nitrates (RO_2NO_2, sometimes referred to as SPNs) and alkyl nitrates ($RONO_2$, sometimes referred to as SANs). Approximately 10% of NO_X over the northeastern United States during winter is converted to organic species (Jaeglé et al., 2018). Recent research using 15-years of in-situ observations has shown that NO_X losses via $RONO_2$have been increasing in relative importance (Present et al., 2020; Zare et al., 2018a). The photodecomposition of organic nitrates releases NO_X and is therefore a significant driver of the homogenization of NO_X concentrations worldwide, particularly in the remote troposphere (Romer et al., 2016).

PAN, an organic nitrate, is an important secondary photochemical air pollutant and a major temporary reservoir for NO_X (Juncosa Calahorrano et al., 2021). Production occurs when VOCs, including biogenic VOCs such as isoprene and acetaldehyde, react with NO_2 during the day in the presence of N_2 or O_2 (Fischer et al., 2014). In addition, acetaldehyde and nitrate can form PAN at night. In polluted urban environments, PAN concentrations are expected to be high because of higher

concentrations of precursor compounds from anthropogenic emissions. The main sink for PAN is thermal decomposition, which can re-release NO_X at sunrise, but PAN is relatively stable at low temperatures.

HONO can be emitted directly from combustion or soil microbial processes (discussed in Section 1.2) or created through secondary formation pathways. A recent meta-analysis integrated 46 observational data sets and concluded that there are two dominant HONO formation pathways: (1) homogeneous and heterogeneous reactions on surfaces (i.e., aerosols or ground) in conjunction with NO_X, and (2) photodecomposition of N-containing compounds and pNO_3^- (Jiang et al., 2022a).

Formation pathway 1 is sometimes referred to as the "NO_X dominated" pathway, whereby OH combines with NO on a surface to produce HONO (Reaction 1 [R1]) or NO_2 is converted to HONO on humid surfaces (Reaction 2 [R2]). R1 is thought to dominate during the day, when OH is available from the photolysis of O_3 and HONO, while R2 dominates at night when relative humidities are higher. Recent research has shown that HONO formation scales linearly with relative humidity (Diao et al., 2016) and that the surfaces on which HONO can form include soot, humic acid or films (Ricker et al., 2022; Han et al., 2016), sulfur dioxide (SO_2)and dust (Ma et al., 2017), wetted aerosols (Lu et al., 2018), and urban grime (Yu et al., 2022).

Formation pathway 2 occurs when pNO_3^- photolyzes in the presence of Cl-containing aerosols to produce NO_2 (Ye et al., 2017). This "renoxification" process typically dominates in marine, coastal, and mountain environments, while formation pathway 1 dominates in polluted inland areas (Sarwar et al., 2024; Jiang et al., 2022a). The identification of pNO_3^- as a source of HONO and NO_2 is a major development since the 2016 Oxides of Nitrogen ISA (U.S. EPA, 2016), because it was previously thought that pNO_3^- was a terminal sink for NO_X (Andersen et al., 2023; Reed et al., 2017; Ye et al., 2016). The creation of NO_X from this pathway lengthens NO_Y lifetimes, particularly in remote locations such as over the ocean (Sarwar et al., 2024).

HONO reservoirs change diurnally. HONO accumulates during nighttime in continental sites, particularly in urban-influenced airsheds, via direct emissions and R2. At sunrise, HONO can decompose into NO (thereby recycling NO_X) and OH (Karamchandani et al., 2015; Levy et al., 2014). Since the last NO_X ISA, day-time field measurements have shown higher-than-expected HONO mixing ratios. A field campaign in California showed substantial HONO deposition onto ground surfaces at night. Once deposited, HONO reacts with carbonates or soil (VandenBoer et al., 2014). During the daytime, this deposited HONO is displaced from soils by gaseous reactions with hydrogen chloride (HCl) or HNO_3, elevating daytime ambient HONO concentrations (Tsai et al., 2018; VandenBoer et al., 2015). HONO is also thought to be released from other types of ground-based surfaces including snowpack (Chen et al., 2019). However, field observations from the southeastern United States did not find that ground sources significantly contributed to the HONO budget (Ye et al., 2018). Overall, the relationship between NO_X and HONO remains unresolved and requires additional research (Pusede et al., 2015).

In addition to chemical transformations that result in terminal sinks for NO_X, deposition occurs when NO_X (or any NO_Y product) is physically deposited out of the atmosphere. As some NO_Y species can partition into the particulate phase (e.g., organic nitrates and HNO_3), it is important to consider depositional processes in models, and models that fail to accurately capture physical losses misrepresent ambient NO_X concentrations. There are two types of deposition. Dry deposition occurs when gases or particles fall out of the atmosphere. Wet deposition occurs when NO_Y species act as cloud condensation/ice nuclei or when NO_Y species are scavenged below the cloud and rained out. Wet deposition trends typically follow precipitation patterns, with wet deposition comprising a higher fraction of total N deposition in wetter areas. Due to decreases in NO_X emissions, NO_X deposition decreased by 31% in 2011 than in 2000 in the United States (Lloret and Valiela, 2016). N deposition rates further decreased during the 2010s, suggesting a slowdown in the rate of N deposition decline due to slower decreases in emissions reductions (Benish et al., 2022). However, deposition of reduced forms of N has increased since 2000 due to increases in fertilizer production and use and now accounts for roughly 50% of total reactive N deposition across the United States (Lassiter et al., 2023; U.S. EPA, 2020b; Walker et al., 2019; Lloret and Valiela, 2016).

1.3.2 Chemistry in Wildfire Smoke

Since the 2016 Oxides of Nitrogen ISA (U.S. EPA, 2016), there has been increased attention to NO_X chemistry in wildfire smoke. Understanding the impact of wildfire emissions on ambient NO_X concentrations is important, as fire activity has increased over the past decade, increasing NO_X emissions. Wildfires directly emit NO and NO_2 and growing evidence shows that wildfire smoke is an excellent environment for producing secondary NO_Y compounds such as HONO (Chai et al., 2021; Peng et al., 2021) and PAN (Lin et al., 2024). NO_X lifetimes in wildfires are highly varied and are, in part, a function of emissions and wind speeds (Jin et al., 2021). Satellite measurements found NO_X lifetimes ranged from approximately seven hours in fires with low wind speeds and less than 1-hour in large fires with high wind speeds (Jin et al., 2021). The abundance of VOCs in wildfire plumes increases the conversion of NO to NO_2 and to secondary NO_X reactions (Pouyaei et al., 2023). In addition, HONO is consistently elevated in fresh wildfire plumes, and HONO emissions have been previously underestimated by a factor of 2 to 4 (Theys et al., 2020). In smoke plumes sampled in the western United States during 2018, NO_X and HONO were elevated near the actively burning area and rapidly converted to more oxidized forms within 90 minutes or 40 km of the burn site (Jin et al., 2023; Juncosa Calahorrano et al., 2021). At sites farther than 40 km downwind, average NO_X measurements were an order of magnitude lower than at the burn site (Pouyaei et al., 2023). In smoke plumes more than four hours old, the dominant NO_Y species were peroxy acyl nitrates (including PAN) and other organic nitrates, comprising approximately 37% and 23% of NO_Y, respectively (Juncosa Calahorrano et al., 2021); these percentages are similar to those reported from box model results (Peng et al., 2021). This is significant because the photolysis of PANs could contribute to downwind NO_X concentrations far from the burn location. In addition, heterogeneous

reactions produce HONO in aged smoke (Peng et al., 2022). These observations are consistent with those over the southeastern United States showing that HONO concentrations exceeded 4 ppbv in air masses from agricultural burns (Neuman et al., 2016). NO_3 formation also can occur during smoke plumes (Selimovic et al., 2020) and may be favored over N_2O_5 formation at night (Decker et al., 2019).

1.4 Measurement and Modeling Methods

Measurement of oxides of nitrogen has been an active area of research for many years. The 2016 Oxides of Nitrogen ISA (U.S. EPA, 2016) provided a broad overview of progress in several areas, including atmospherically relevant interferences with the Federal Reference Method (FRM) for NO_2; advances in optical methods (e.g., differential optical absorption spectroscopy (DOAS), laser-induced fluorescence (LIF), cavity attenuated phase shift (CAPS), and quantum cascade-tunable infrared laser differential absorption spectrometer (QC-TILDAS)); evolution of satellite-based methods; and current ambient air monitoring networks that included NO_2 measurements.

This section expands on methods and measurement progress described in the 2016 Oxides of Nitrogen ISA (U.S. EPA, 2016) by synthesizing recent information on the measurement and modeling of oxides of nitrogen. It starts with an overview of the FRM and Federal Equivalent Methods (FEMs) for NO_2 monitoring, with particular emphasis on newer advances like photolytic conversion, DOAS, and CAPS. Measurement methods that are not used as FRMs or FEMs but that are widely used in the exposure and health studies described in this ISA (e.g., LIF, photoacoustic spectroscopy, and cavity ringdown methods).

Measurements, in turn, are used to inform CTMs through providing boundary and initialization conditions or model nudging. In addition, measurements can also be used to compare to model simulations to evaluate model performance. Moreover, satellite-derived observations are used in conjunction with measurement-informed CTMs to infer surface concentrations. Recent advances in atmospheric modeling relevant to predicting concentrations and understanding processes for oxides of nitrogen are described. Separate sections discuss advances in satellite remote sensing technology and applications, along with low-cost community sensor methods. Finally, national monitoring networks and up-to-date monitoring locations are summarized.

1.4.1 Federal Reference and Equivalent Methods

This section describes methods that are federally approved to measure ambient NO_2, the oxides of nitrogen indicator, and other oxides of nitrogen. FRMs and FEMs are used by states and other organizations to ensure that their collection of air quality data is accurate and consistent (U.S. EPA, 2024b). FRM and FEM are defined at 40 CFR Part 53, 53.1. Generally speaking, the U.S. EPA designates

FRMs to provide the most fundamentally and scientifically defensible concentration measurements and to serve as a basis for judging other measurement methods. If a method for measuring the concentration of an air pollutant is found to be equivalent to an FRM, the U.S. EPA designates it as an FEM. FEMs are generally newer, innovative technologies that can reduce operating costs or meet multiple monitoring objectives while providing an equivalent level of quality to be used in decision-making.

Comparatively, few FEMs have been developed since the designation of the oxides of nitrogen criteria air pollutant, and these were limited to methods based on long-path DOAS as an alternative to chemiluminescence. Just before the publication of the 2016 Oxides of Nitrogen ISA (U.S. EPA, 2016), additional FEMs were developed based on both an adapted chemiluminescence measurement and CAPS methods. Further development of FEMs has continued with the recent approval of additional chemiluminescence methods based on photolytic conversion of NO_2 to NO, an alternative method based on selective direct absorption at 405 nanometers (nm), and improved CAPS methods (U.S. EPA, 2023c).

The current FRM based on chemiluminescence reaction of NO with O_3 is described in Section 1.4.1.1, with recent advances in photolytic conversion to reduce interference described in Section 1.4.1.2. FEMs developed and improved since the 2016 Oxides of Nitrogen ISA include Cavity Attenuated Phase Shift (CAPS) spectroscopy and Differential Optical Absorption Spectroscopy, described in Sections 1.4.1.3 and 1.4.1.4, respectively. Details on detection limits, ranges, interferences, and response times differ with particular variations of these methods and are documented in references found in (U.S. EPA, 2024a).

1.4.1.1 Chemiluminescence

The gas phase chemiluminescence measurement principle and calibration procedure for the measurement of NO_2 in the atmosphere is established at 40 CFR Part 50, Appendix F. This method, used by the FRM for monitoring NO_2 in ambient air, involves the conversion of NO_2 to NO using a molybdenum oxide (MoOx) surface substrate at 300 to 400°C and quantification of a chemiluminescence signal after reaction of O_3 with NO at low pressure. The chemiluminescence signal results from the sum of NO sampled in the air before conversion, plus the NO converted from NO_2, or NO_X ($NO+NO_2$). Because the chemiluminescence-based FRM cannot detect NO_2 specifically, NO must also be measured in parallel by the same method but without the initial NO_2 to NO conversion step, and then subtracted from the NO_X measurement to determine NO_2 as the difference between the converted NO that has passed over the heated MoOx substrate and the unconverted NO originally present in the airstream. This same chemiluminescence method is also the basis for a widely used NO_X stationary source emissions monitoring method (U.S. EPA, 2020c).

The FRM is subject to positive interference by NO_X oxidation products that can also be converted to NO over the MoOx substrate. These interferences, first reported in the mid-1970s (Winer et al., 1974), were reviewed extensively in the 2016 Oxides of Nitrogen ISA (U.S. EPA, 2016). Interferences apply

mainly to NO_Z products (see Figure 1-7), including HNO_3, PAN, and alkyl nitrates. Numerous studies on NO_X interferences between the work of Winer et al. (1974) and others summarized in the 2016 Oxides of Nitrogen ISA (U.S. EPA, 2016) consistently indicate that measurement of NO_X by the FRM is an overestimate because other oxides of nitrogen (i.e., NO_Z, see Section 1.3) also contribute to the measurement. The sensitivity of the FRM to potential interference by individual NO_Z compounds is variable and depends on the characteristics of individual monitors (e.g., inlet design, substrate composition and temperature, and interactions of atmospheric species with the reducing substrate [U.S. EPA, 2016]). Greater interference was reported for PAN and other organic nitrates than for HNO_3 (U.S. EPA, 2016; Dunlea et al., 2007).

Research on interferences associated with NO_2 analysis by chemiluminescence has continued since the 2016 Oxides of Nitrogen ISA (U.S. EPA, 2016). In environments where the sum of more highly oxidized nitrogen species (NO_Z) concentrations is greater than 4% of NO_2 concentrations, correction after analysis has been recommended to meet the recently developed European data quality objectives of 15% accuracy for ambient air NO_2 analysis (Doval Miñarro et al., 2013). In cases where NO_Z concentrations exceed NO_2 concentrations, use of this method should be avoided (Doval Miñarro et al., 2013). At high enough ratios of HONO to NO_X, which are possible during biomass burning, HONO interference can occur and cause overestimation of NO_2 concentrations (Gingerysty et al., 2021). In addition to other species that form NO in the conversion step, there are also potential interferences from atmospheric species that undergo competing chemiluminescent reactions with O_3. Interferences by terpenes and short-chain alkenes like ethylene have been quantified and found to be important in high VOC environments such as forests (Alam et al., 2020).

As pointed out in the 2016 Oxides of Nitrogen ISA (U.S. EPA, 2016), interference from highly oxidized N-containing species like HNO_3 and PAN is likely to be more important at low concentrations or downwind of fresh emissions sources, and less important in urban areas influenced by fresh NO_X combustion emissions. Although large NO_2 overestimates have been reported (e.g., 27 to 132% overestimation across recent co-located comparisons of thermal- and photolytic conversion-based chemiluminescence methods [Zhang et al., 2018]), it is also important to consider the concentrations and geographic context of monitors evaluated in this kind of analysis. State and Local Air Monitoring Stations (SLAMS) network monitors are frequently situated in densely populated urban areas, near roads or other locations strongly influenced by fresh emissions from local sources, where NO_2 concentrations are highest. In these locations, the relative contributions of species like HNO_3 or PAN compared to NO and NO_2 are likely to be considerably less than would be typical in a national scale analysis. To illustrate, Lassiter et al. (2023) reported that NO_X accounted for 98% of NO_Y in a comparison of co-located NO_X and NO_Y monitors across EPA's largely urban National Core (NCore) network designed for multipollutant monitoring (Weinstock, 2012).

1.4.1.2 Photolytic Converters

Since 2012, an automated method based on the NO-O_3 chemiluminescence reaction replacing thermal MoOx oxidation with photolytic conversion of NO_2 to NO has been approved as an FEM (U.S. EPA, 2016). Direct comparisons of measurements between chemiluminescence analyzers using thermal and photolytic conversions were summarized in the 2016 Oxides of Nitrogen ISA (U.S. EPA, 2016; Steinbacher et al., 2007). These comparisons showed that methods based on thermal conversion overestimated NO_X due to positive interferences from other species besides NO_2, especially in summer (see Section 1.4.1 and the 2016 Oxides of Nitrogen ISA (U.S. EPA, 2016)). Like earlier studies, Jung et al. (2017) also found slightly lower efficiencies for photolytic (95%) than thermal (100%) conversion and that thermal conversion overestimated NO_2 concentrations by 20% relative to photolytic conversion across all concentrations in a suburban sampling site in South Korea. They also found that the extent of overestimation was dependent on measurements of mass concentration of $PM_{2.5}$ and proposed a simple correction. However, other studies have suggested that differences between the methods are caused by negative interference for photolytic conversion-based methods due to photochemical production of radicals during the conversion (U.S. EPA, 2016; Kleffmann et al., 2013; Villena et al., 2012). Negative interferences using the photolytic conversion, occurring from the production of radicals by the photolysis of VOCs that could also react with NO, were also reviewed. However, negative artifacts were most apparent for high VOC concentrations and could be reduced by using a smaller spectral range.

More recent work has provided greater detail on the conversion efficiency and interferences related to photolytic conversion. It was reported that photolytic conversion is sufficiently efficient, with 96% conversion achievable independent of relative humidity if residence time is optimized (Jordan et al., 2020). However, as FEMs based on chemiluminescence with photolytic conversion are more widely used, interferences associated with the photolytic conversion process have also been identified. About 5% of PAN present in the sampled air decomposes to NO_2 in the instrument before conversion, leading to interference with NO_2 measurement (Reed et al., 2016). Direct photolysis of HONO has been observed to occur at a rate of about 6% of the rate of NO_2 conversion. Interference from other thermally labile compounds (e.g., other PAN, alkyl nitrates, nitric acid, $IONO_2$, $BrONO_2$, $ClNO_2$, N_2O_5, $CH_3O_2NO_2$, and HO_2NO_2) has been observed or predicted (Jordan et al., 2020; Reed et al., 2016), and a thorough investigation of interferences associated with the photolytic conversion process was recently published (Jordan et al., 2020).

The possibility of interference by more oxidized species might explain the observation of high NO_2 concentrations measured in remote areas, where concentrations of highly oxidized species are higher than in areas near fresh emissions sources (Reed et al., 2016). Surface-promoted photochemistry and secondary chemistry on internal tubing can also contribute to measurement interferences (Jordan et al., 2020). However, these interferences can be made negligibly small if photolytic cell pressures are sufficiently low, sampling flow rates are sufficiently high, tubing length is minimized, and instrumental temperatures are properly managed (Jordan et al., 2020).

1.4.1.3 Cavity Attenuated Phase Shift Spectroscopy

At the time of the 2016 Oxides of Nitrogen ISA, one new CAPS methods had just been approved as FEMs with another approved in 2020 (U.S. EPA, 2024b). CAPS spectroscopy was praised for requiring less user intervention and having lower operating costs compared to DOAS or LIF methods (U.S. EPA, 2016). CAPS can measure NO_2 at concentrations between 0 and 320 ppb with a detection limit of 60 ppt (U.S. EPA, 2016; Kebabian et al., 2008) by measuring NO_2 light absorption at 450 nm in a resonant optical cavity using a blue light emitting diode as a light source (Sobanski et al., 2021; Sadanaga et al., 2016). CAPS methods experience interference from water due to Rayleigh scattering effects and are often used with driers at the inlet to mitigate this issue (Sobanski et al., 2021). Thermal dissociation CAPS was developed for the measurement of total peroxy nitrates and organic nitrates, reaching detection limits of 21 pptv with an integration time of 2 minutes (Sadanaga et al., 2016).

1.4.1.4 Differential Optical Absorption Spectroscopy

Optical absorption spectroscopy takes advantage of light absorbing properties of a substance and their relationship to concentration to obtain a path-integrated measurement of trace gas concentrations in the ultraviolet (UV) and visible spectral regions. DOAS is a type of optical absorption spectroscopy that uses a continuous light source over a broad frequency range, such as sunlight or a lamp with a continuous emission spectrum, and measures absorption of a substance at characteristic absorption frequencies from the difference between an observation and a reference spectrum of the continuous emission source. DOAS has been widely used in satellite retrievals, aircraft measurements, and ground-level monitoring platforms. Ground-level mobile DOAS methods have been developed with 0.63 nm spectral resolution in the 309–351 nm wavelength region (Johansson et al., 2014). DOAS methods that are not FEMs used in aircraft observations are discussed in Section 1.4.2 and DOAS methods used in satellite observations are discussed in Section 1.4.3.

1.4.2 Ambient Monitoring Networks

NO_2 is the indicator for the NAAQS for oxides of nitrogen. Ambient air NO_2 concentrations are measured by FRMs and FEMs at monitoring stations within networks operated by state, local, and tribal air agencies and typically funded in part by EPA. EPA provides monitoring requirements for NO_2 and other pollutants in 40 CFR Part 58, with station and network design requirements contained in Appendix D, quality assurance requirements contained in Appendix A, and probe and monitoring path siting requirements contained in Appendix E (https://www.ecfr.gov/current/title-40/chapter-I/subchapter-C/part-58/appendix-Appendix%20E%20to%20Part%2058). There were 482 monitoring stations reporting hourly NO_2 concentration data to EPA during the 2021 to 2023 period; locations of these monitoring stations are shown in Figure 1-9. The large majority of monitors providing ambient data for use in NAAQS

implementation activities are part of the SLAMS network, comprising over 80% of all NO_2 monitoring stations, a majority of which are in urban and suburban areas. This network relies on a chemiluminescent FRM and on FEMs that use either chemiluminescence or direct NO_2 measurement methods. Data produced by chemiluminescent FRM analyzers include NO, NO_2, and NO_X measurements, while some direct methods provide NO_2, NO, and NO_X, or just NO_2. All FRM and FEM data outputs are routinely reported by state and local air monitoring agencies to EPA's Air Quality System (AQS) and often through other means to the public.

Two important subsets of SLAMS stations are the near-road network and the NCore multipollutant monitoring network leveraged by the Photochemical Assessment Monitoring Stations (PAMS) network. The near-road network was required as part of the 2010 review of the NAAQS for oxides of nitrogen and began operation in 2014 and is the primary component of the network used to understand mobile source exposure. Near-road stations are required in each metropolitan area with a population of 1 million or more, and an additional near-road station is required in each metropolitan area with either (1) a population of 2.5 million or more, or (2) one or more roadway segments with an average daily traffic volume of 250,000 or more vehicles per day (see 40 CFR, App. D, 4.3.2). Near-road monitors must be as near as practicable to the road, and not greater than 50 meters from the nearest edge of the traffic lanes (see 40 CFR Part 58, App. E, 2.5.4), with inlets placed between 2.0 to 7.0 meters above ground level See 40 CFR Part 58, App. E, 2.1(f) (https://www.ecfr.gov/current/title-40/chapter-I/subchapter-C/part-58/appendix-Appendix%20E%20to%20Part%2058). There were 73 near-road monitors in operation during the 2021 to 2023 period.

The 2010 rulemaking also required NO_2 monitoring at area-wide sites in urban areas having 1 million or more persons (40 CFR Part 58, App. D, 4.3.3). Many of those required area-wide monitors leveraged the existing NCore network consists of approximately 60 urban (and 20 rural monitoring stations), with each state required to have at least one NCore station. The PAMS network is required to operate within any NCore site in urban areas with a population of 1 million or more persons (based on the most recent census; 40 CFR Part 58, App. D, 5(a)). PAMS sites are required to measure NO, NO_2, NO_Y, and other O_3 precursors during the months of June, July, and August, although some precursor monitoring may be required for longer periods of time (40 CFR Part 58, App. D, 5(g)). Those NCore/PAMS sites that are also used to satisfy area-wide NO_2 requirements, as well as NO_Y monitoring and associated NO measurements, make those measurements year-round (40 CFR Part 58, App. D, 4.3.3). Finally, it is notable that the Pandora network used for comparing ground-level to satellite NO_2 measurements (see Section 1.4.3) is integrated into the PAMS network. Finally, there are also a number of Special Purpose Monitors (SPMs), which are often operated by air agencies for short periods of time (i.e., less than 3-years) to collect data for targeted human health and welfare studies. The SPMs are typically not used to assess compliance with the NAAQS (see 40 CFR Part 58, Subpart C, 58.20).

To provide an assessment of data quality, monitoring agencies must perform quality assurance (QA) checks at least once every two weeks to derive estimates of precision and bias for NO_2 and other

gaseous criteria pollutant measurements using calibration gas. For NO_2 monitors, the data quality goal for precision and bias is 15%. Ambient air quality data and associated QA data must be submitted to EPA within 90 days after the end of each calendar quarter. Additionally, each monitoring agency is required to certify all FRM/FEM data submitted to AQS annually, taking into consideration any QA findings. A data certification letter must be sent to the relevant EPA Regional Administrator by May 1st of the following year (see 40 CFR Part 58, App. A).

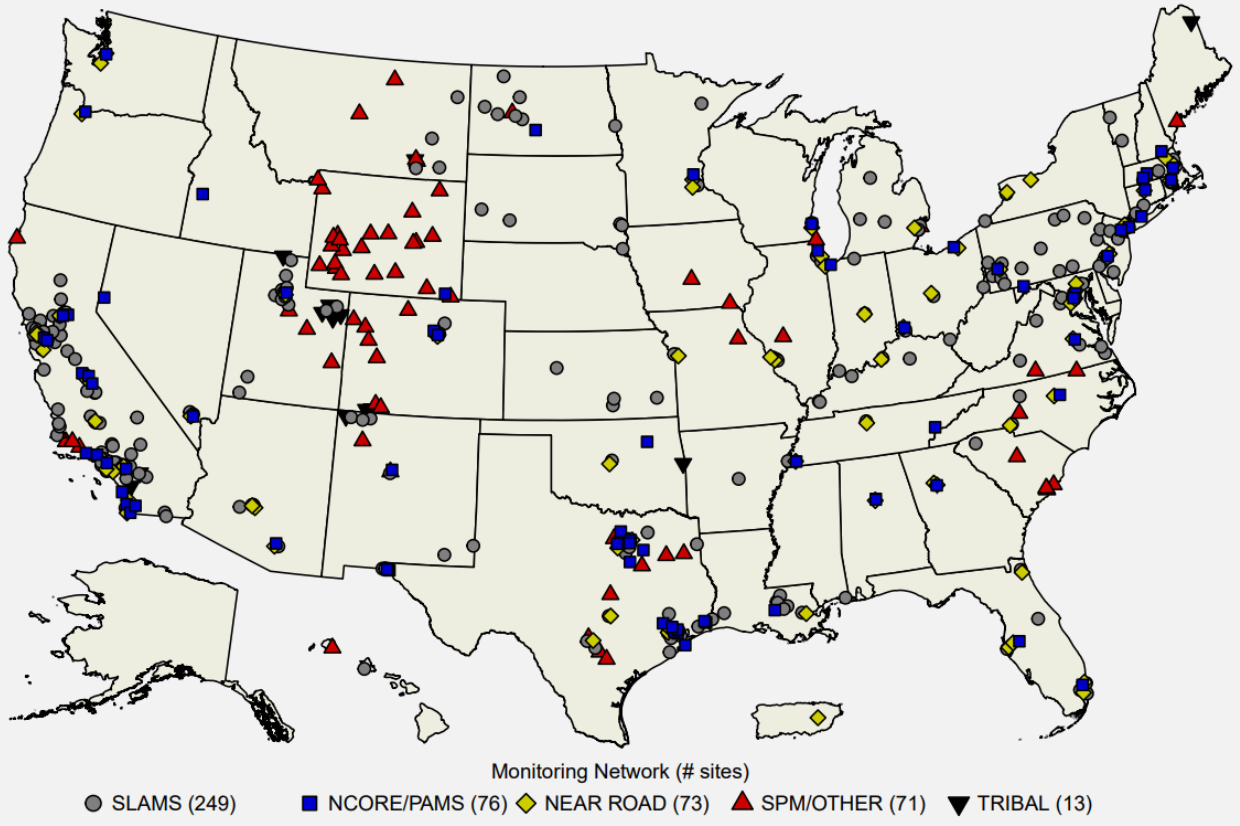

List of abbreviations in alphabetical order: NCORE = National Core; PAMS = Photochemical Assessment Monitoring Station; SLAMS = State and Local Air Monitoring Stations; SPM = Special Purpose Monitor.
Source: U.S. EPA (2023d). Copyright permission pending.

Figure 1-9 Map of United States NO_X monitoring stations reporting data to EPA, 2021 to 2023.

1.4.3 Other Methods for Measuring NO_X

The 2016 Oxides of Nitrogen ISA noted several fluorescence and spectroscopy methods used for NO_2 measurements in field campaigns and sometimes in aircraft: LIF, QC-TILDAS, long path absorption photometry (LOPAP), cavity ring down spectroscopy, and photoacoustic spectroscopy (U.S. EPA, 2016). Since then, new spectroscopy techniques have been developed for HONO detection. UV-light emitting

diode-based incoherent broadband cavity-enhanced absorption spectroscopy is a technique that allows for non-invasive optical monitoring with detection limits of 56 pptv and 112 pptv for HONO and NO_2, respectively (Yi et al., 2021). Long path DOAS, LOPAP, QC-TILDAS, and stripping coil visible absorption photometry were all used to measure HONO during the Spring 2009 SHARP campaign in Houston, TX (Pinto et al., 2014). A high precision photoacoustic spectroscopy-based NO_2 analyzer with sub-ppb detection and 1-second response time capability was also developed (Qi et al., 2024). Aircraft-based DOAS instrumentation, such as the Geostationary Trace Gas and Aerosol Sensor Optimization (GeoTASO) and GEOstationary Coastal and Air Pollution Events (GEO-CAPE) Airborne Simulator (GCAS) instruments (Judd et al., 2019), as well as that used by Schoenhardt et al. (2015), are useful to convert column information to ground-level concentrations and have been used to validate model-generated NO_2 vertical profiles (Cooper et al., 2020). Emissions monitoring methods include methods based on chemiluminescence (see Section 1.4.1.1), ion chromatography, ultraviolet spectrophotometry, and colorimetry (U.S. EPA, 2024a).

1.4.4 Low-Cost Sensors

Advances in air pollution sensor technology have enabled the development of small, low-cost systems to measure outdoor air pollution, often using metal-oxides or electrochemical means to determine NO_2 concentrations (Russell et al., 2022; SCAQMD, 2021). In general, electrochemical sensors perform marginally better than metal-oxide methods and have been used to measure NO_2 concentrations up to 120 ppb (Russell et al., 2022). To understand the capability of emerging air sensor technologies, the Community Air Sensor Network (CAIRSENSE) project deployed low-cost, continuous air pollution sensors at a regulatory air monitoring station near Decatur, GA (Jiao et al., 2016). Relationships between the electrochemical NO_2 measurements from these sensors and a reference monitor varied, with Pearson correlation coefficients ranging from −0.25 to 0.76 across a variety of sensors tested (Jiao et al., 2016), demonstrating high uncertainty in their accuracy. A separate study performed in the United Kingdom (U.K.) deployed low-cost electrochemical NO_2 sensors that closely represented monitor concentrations after adjusting for ambient temperature (Frederickson et al., 2022). Unfortunately, the calibration process for low-cost sensors is lengthy and often necessitates weeks to months of co-location (Zamora et al., 2023) or comparison to reference instruments to establish calibration equations (Weissert et al., 2020). While still in development, low-cost air pollution sensors show promise for accurately capturing concentration variation, particularly in areas close to pollution sources.

1.4.5 Satellite Remote Sensing

Since the 2016 Oxides of Nitrogen ISA, there has been an increase in the number of papers developing and leveraging remote sensing products. In addition, the geostationary satellite Tropospheric Emissions: Monitoring Pollution (TEMPO), a National Aeronautics and Space Administration (NASA)

product that provides high-resolution air quality measurements, including NO_2 vertical columns, on an hourly resolution over the United States, is expected to produce data that will inform numerous papers in the near future as near-real time data is available in 2025 (Zoogman et al., 2017). Given the increasing importance of satellite data in studying the atmospheric chemistry of NO_X, we provide an extended overview of remote sensing methodology in this ISA. Because of the high spatial variability in NO_2 concentrations (see Section 1.5) and the relatively sparse coverage of ground-level NO_2 monitoring network (see Section 1.4.2), satellite retrieval data are effective for supplementing gaps in NO_2 ground-level concentration monitoring data (see Section 1.4.2) and providing insight into NO_2 concentrations in regions without prior or regular observations (Geddes et al., 2015). However, as described in the 2016 Oxides of Nitrogen ISA (U.S. EPA, 2016), pollutant concentrations are not directly measured by satellite remote sensing instrumentation, and information on NO_2 surface concentrations must be inferred from satellite-based measurements. In contrast to ground-based monitoring methods (see Section 1.4.2), satellite-based remote sensing determines the vertically integrated number of NO_2 molecules per unit area between Earth's surface and the tropopause, a quantity that is referred to as the tropospheric vertical column density of NO_2. This value is a fundamentally different quantity than a point-based ground level air concentration, and differences between these types of measurements present a serious challenge for comparing satellite and ground observations for both assessing data quality and estimating concentrations away from monitors. The strengths and weaknesses of satellite remote sensing technology stem mainly from this principal feature of satellite-based atmospheric measurement methods.

Apart from differences in measurement methods, satellite-based remote sensing data and monitoring network data also provide different perspectives on national levels, distributions, and trends of NO_2. While ground-level monitors are located mainly in urban and suburban locations, satellite coverage reflects actual land use patterns, with observations mainly from rural and remote areas and occasional urban hot spots. For example, in one comparison a national annual trend of -1.5%/year for satellite NO_2 data was less than half the magnitude of the annual trend of -3.9%/year for EPA's Air Quality System (AQS) ground-level monitoring network data (Zhang et al., 2018). National scale long-term trends for ambient NO_2 concentrations are explored in more detail in Section 1.5.

1.4.5.1 Satellite Platforms and Instruments

Unique spectral features in the visible blue 400 to 500 nm wavelength range make NO_2 suitable for detection by satellite-based remote sensing. As described in the 2016 Oxides of Nitrogen ISA, NO_2 tropospheric vertical column density has been monitored globally by satellites using optical absorbance spectroscopy, including DOAS (see Section 1.4.1.4), to measure spectra of backscattered sunlight (i.e., sunlight reflected back in the direction it came from with a phase angle of less than 90 degrees) in this wavelength range since the 1990s (U.S. EPA, 2016; Boersma et al., 2004; Martin et al., 2002). This started with the Global Ozone Monitoring Experiment (GOME) in 1995, which measured NO_2 at a 40 km x 320 km spatial resolution (Burrows et al., 1999). In 2011, the U.S. NASA established the Air Quality

Applied Sciences Team (AQAST), which in 2016 became the Health and Air Quality Applied Systems Team (HAQAST), to assist U.S. air quality managers with the provision and use of satellite-based data. Table 1-3 provides summary information on the satellite-based platforms that are most relevant for atmospheric measurement of NO_2 over North America.

Table 1-33 Selected satellite platforms for atmospheric NO_2 measurement

	GOME	SCHIAMACHY	OMI	GOME-2	OMPS	TROPOMI	TEMPO
Satellite Platform	ERS-2	ENVISAT	Aura	METOP-A	NOAA-20	Sentinal-5	IS40e
Sponsoring Agency	ESA	ESA	NASA	ESA/EUMETSAT	NASA/ NOAA	NASA/ESA	NASA
Operational Period	1995–2003	2002–2012	Since 2004	Since 2006	Since 2017	Since 2018	Since 2023
Global Coverage	3 d	6 d	Daily	1.5 d	Daily	Daily	Geostationary
Spatial Resolution (km)	40 × 320	30 × 60	13 × 24	40 × 80	17 × 13	3.5 × 7	2 × 4.75
Spectral Range (nm)	240–790	240–2400	270–500	250–790	345–390	270–500	290–740

List of abbreviations in alphabetical order: ENVISAT = Environmental Satellite; ERS-2 = European Remote Sensing Satellite-2; ESA = European Space Agency; EUMETSAT = European Organization for the Exploitation of Meteorological Satellites; GOME = Global Ozone Monitoring Experiment; METOP-A = Meteorological Operational Satellite-A; NASA = National Aeronautics and Space Administration; NOAA = National Oceanic and Atmospheric Administration; IS40e = Intelsat 40e; OMI = Ozone Monitoring Instrument; OMPS = Ozone Mapping and Profiler Suite; SCIAMACHY = Scanning Imaging Absorption Spectrometer for Atmospheric Chartography; TEMPO = Tropospheric Emissions: Monitoring of Pollution; TROPOMI = Tropospheric Monitoring Instrument.
Source: Modified from Streets et al. (2013). OMPS data from Huang et al. (In Press). TROPOMI data from Pinardi et al. (2020). TEMPO data from Zoogman et al. (2017). All other satellite data are based on the original table by Streets et al. (2013). Copyright permission pending.

Subsequent satellite-based DOAS methods in current or recent use include the Scanning Imaging Absorption Spectrometer for Atmospheric Chartography (SCIAMACHY), a larger scale version of GOME designed to investigate the impact of tropospheric pollution from industrial activity and biomass burning by determining NO_2 and other trace gases and aerosol abundances in the troposphere (Fox, 1995); the Ozone Monitoring Instrument (OMI), designed for improved spatial resolution to investigate urban scale spatial variability of NO_2 and other pollutants (Levelt et al., 2006b; Levelt et al., 2006a); the GOME-2 (Callies et al., 2000), a UV-visible spectrometer that measures backscattered solar radiation in the 240 to 790 nm wavelength region with spectral resolution ranging from 0.2 to 0.5 mm and ground pixel (smallest unit of a digital image) sizes of 40 km × 40 km (Pinardi et al., 2020); and the Ozone Mapping and Profiler Suite (OMPS) instrument launched by NASA/NOAA in 2017 as a part of the Joint Polar Satellite Systems (JPSS) mission that provides independent measurements useful to intercalibrate and cross-validate with other satellite instruments (Huang et al., 2022).

The most recently developed instruments in Table 1-3 are the TROPOspheric Monitoring Instrument (TROPOMI), launched in 2017 onboard the Sentinel-5P spacecraft, and TEMPO, launched in April 2023. Like most artificial objects in space, OMI and TROPOMI have low-Earth orbits, meaning

they orbit the Earth in 128 minutes or less at an altitude of 1200 km or less, passing over different parts of the Earth in each of their approximately 11 orbits per day. In contrast, TEMPO is in a geostationary orbit, meaning an orbit that is fixed relative to the Earth's surface, which allows hourly resolution not possible with earlier satellite-based DOAS instrumentation. TEMPO provides the greatest temporal and spatial resolution among the satellites in current use, with enhanced capabilities for observation of diurnal variation of NO_X concentrations and emissions (Zoogman et al., 2017).

The recently deployed TROPOMI is a DOAS method (see Section 1.4.1.4), based on the 405 to 465 nm spectral window that has been used to collect NO_2 data since 2018 (Goldberg et al., 2021a). TROPOMI has at least six times higher spatial resolution and one to five times higher signal-to-noise ratio compared to OMI (Cooper et al., 2020; Pinardi et al., 2020), providing the ability to differentiate fine-scale spatial variability within urban areas and to precisely locate traffic, airports, ports, power plants, and major industrial operations for emissions estimates (Goldberg et al., 2021a). Uncertainty, stability, bias, spatial resolution, and scale of emissions estimates have been directly compared between TROPOMI and OMI, highlighting the enhanced capabilities of TROPOMI for NO_2 measurements (Sekiya et al., 2022; Goldberg et al., 2021a; van Geffen et al., 2020; Zhao et al., 2020). As a result of these improvements, NO_2 retrievals that required a year or more for previous satellite-based instruments like OMI could be achieved in less than 5 months with TROPOMI (Goldberg et al., 2019).

TEMPO is intended to achieve hourly resolution not possible with earlier satellite-based DOAS instrumentation and provide the greatest temporal and spatial resolution among the satellites in current use (Zoogman et al., 2017). Publicly available NO_2 data from TEMPO were released in May 2024, but no studies within the scope of this ISA have yet been published. Because it is geostationary, TEMPO improves upon TROPOMI by providing even higher spatial (~2 km^2 × ~4.75 km^2) and hourly temporal resolution of NO_2 and O_3 estimates. This is expected to allow for more detailed observations to fill some of the major knowledge gaps related to neighborhood-scale emissions (see Section 1.2), atmospheric chemistry (see Section 1.3), and spatial variability (see Section 1.5), as well as air quality forecasting. For example, high spatial resolution and hourly data will allow for a greater understanding of processes such as the release of NO_X from photosensitive compounds at dawn or from compounds along the coast that may be affected by Cl-containing sea spray particles.

1.4.5.2 Satellite Data Retrieval

The 2016 Oxides of Nitrogen ISA described a three-step process for retrieval of NO_2 tropospheric vertical column density for satellites that were then in operation: (1) determining the total NO_2 slant-path column abundance by spectral fitting of solar backscatter measurements; (2) removing the stratospheric contribution using data from remote regions where the tropospheric column abundance is small; and (3) applying an air mass factor (AMF) to convert tropospheric slant columns into vertical columns. Satellite-based DOAS instrumentation like that used with OMI and TROPOMI retrieves the atmospheric optical

depth, or natural logarithm of the ratio of incident to transmitted radiant energy flux through the atmosphere, along an average path between the instrument and the Earth's surface (i.e., the slant path). The slant-path column abundance of an absorbing species like NO_2 is its abundance in a column of the atmosphere rising from a defined area of the Earth's surface along the slant path and is determined by the best fit to reference spectra. The conversion of slant-path column abundance to vertical column abundance is accomplished using a scaling factor called the AMF. The AMF is not just a simple ratio of the slant-path and vertical path lengths, because the intensity of backscattered sunlight from Earth's surface is influenced by atmospheric and ground surface properties that are inferred in retrieval algorithms.

Inaccuracies in these properties can result in 50 to 100% uncertainty in measured NO_2 vertical column abundance (Herman et al., 2009). For polluted air, AMF is often the largest component of retrieval error (Boersma et al., 2004; Heland et al., 2002) and understanding what determines AMF is an active area of research. For example, it was recently estimated that accounting for nitrate photolysis increased AMF by 7% and for airplane emissions increased AMF by 2% because they produce NO_2 at a higher altitude than surface sources, resulting in a greater deviation from typical assumptions about the vertical distribution of NO_2 than NO_2 emitted from surface sources. This impacts satellite-derived surface concentration estimates because they are particularly sensitive to what AMF values are used (Dang et al., 2023). Retrieval error over regions abundant in NO_2 is usually dominated by error in AMF (U.S. EPA, 2016), an observation also supported by more recent studies (Laughner et al., 2019; Goldberg et al., 2017; Lorente et al., 2017; Laughner et al., 2016).

The magnitude of the AMF error depends on assumptions about NO_2 vertical profile shape, surface reflectivity, clouds, and aerosols. The vertical distribution of NO_2 is usually unknown and must be represented by an estimated or predicted profile (Zhang et al., 2018; Boersma et al., 2011). In the earliest satellite retrievals, high AMF error was partly due to AMF being estimated from *a priori* vertical NO_2 profiles. Replacing these with profiles from fine-resolution models improves retrieved vertical column densities (Cooper et al., 2020). There has been considerable recent progress in reducing both AMF errors and overall retrieval uncertainty. For example, agreement with ground-level measurements was improved by estimating vertical profile shape factors using a high-resolution Community Multiscale Air Quality (CMAQ) simulation constrained by aircraft measurements to recalculate tropospheric AMFs and NO_2 tropospheric vertical column densities in summertime in the eastern United States (Goldberg et al., 2017). This resulted in up to 160% increases in city centers and 20–50% decreases in rural areas for tropospheric vertical column densities, and better agreement with both Pandora measurements (see Section 1.4.3) and urban ground-level monitoring data (Goldberg et al., 2017).

Further reductions of AMF error have been achieved by simulating *a priori* vertical NO_2 profiles with higher spatial and temporal resolution. In Atlanta, GA, U.S., NO_X emissions estimated from daily, high spatial resolution *a priori* profiles were approximately 100% greater than those based on spatially coarse a priori profiles, and 26 to 40% lower than those based on retrievals using monthly averaged

profiles (Laughner et al., 2016). Other improvements in AMF error have also been reported (Laughner et al., 2019; Lorente et al., 2017). However, oversampling (see Section 1.4.3) can complicate the contribution of AMF error to overall uncertainty because AMF is often determined at even coarser spatial resolutions than satellite column measurements. In addition to AMF, other important contributors to uncertainties in tropospheric vertical column NO_2 satellite retrievals include surface reflectance, tropospheric/stratospheric separation, uncertainties in CTMs typically used for modeling the vertical NO_2 distribution, surface pressure and reflectance anisotropy in rugged terrain, cloud and aerosol radiance, and boundary layer dynamics (Zhang et al., 2018).

A prominent feature of the evolution of satellite NO_2 measurement technology is the steady improvement in spatial resolution (see Table 1-3, Section 1.4.5.1). According to the 2016 Oxides of Nitrogen ISA (U.S. EPA, 2016), a high degree of spatial variability within urban areas is common, as well as substantial smaller scale NO_2 concentration gradients, especially near roads and other major sources. This pattern has been confirmed in more recent studies (see Sections 1.5.3 and 1.5.4). For example, the greater sensitivity and spatial resolution provided by TROPOMI (see Section 1.4.5.1) allow for shorter averaging times than required by previous instruments to observe spatial variability with similar resolution. Long-term spatial patterns can be discerned with single-day measurements, although a full month of sampling (or potentially longer in winter, when conditions are less ideal for satellite retrieval) has been recommended to achieve better characterization of spatial patterns (Goldberg et al., 2021a). High spatial resolution NO_2 concentration estimates are useful not only for broadening spatial coverage beyond the limitations of ground-level monitoring networks, but also for more accurately quantifying urban NO_2 exposures (described in detail in subsequent chapters of this ISA). There is a distinction between the native resolution of the satellite instrument based on its pixel size and the even finer scale resolution that can be produced through statistical methods made possible by day-to-day changes in satellite track position, which result in different locations for pixel centers each day (Russell et al., 2010). These statistical methods are commonly referred to as oversampling and their influence on data uncertainty is an active area of research.

1.4.5.3 Inferring Surface Concentration from Satellite Data

The 2016 Oxides of Nitrogen ISA and references therein (U.S. EPA, 2016; Boersma et al., 2004; Martin et al., 2002) explained the need for additional steps to infer ground-level concentrations from satellite-based column measurements and reviewed combining satellite data with CTMs as one possible method to accomplish this. Estimating ground-level concentration from tropospheric vertical column density requires at a minimum CTM or an alternative method to simulate the relationship between ground-level concentration and the tropospheric vertical column density (Cooper et al., 2020; Geddes et al., 2015; Lamsal et al., 2008). In practice, this can lead to complex approaches often involving satellite oversampling, data fusion, hybrid modeling, and machine learning approaches. Uncertainty in satellite-derived NO_2 concentrations has been approached by cross-validating modeled concentrations with

ground-level concentrations from national network monitoring stations (see Section 1.4.2). For example, the integration of machine learning algorithms with satellite-based NO_2 measurements, land-cover variables, meteorological variables, and simulation results from CTMs into an ensemble model to predict national NO_2 concentrations at high spatiotemporal resolution resulted in an overall cross-validated r^2 of 0.788 (Di et al., 2020). Because ensemble models like this are typically used to derive surface concentrations from satellite data, further results of Di et al. (2020) and other satellite-based derivations of surface concentrations are discussed in Section 1.4.4.

A continuing issue with satellite-based NO_2 surface concentrations has been a low bias in comparison to ground-based monitoring data, with satellite-based estimates tending to underestimate surface concentrations relative to ground-based monitoring data (Cooper et al., 2020; Gu et al., 2017; Geddes et al., 2015). This is due in part to substantial surface NO_2 concentration variability within the coarse spatial resolution of satellite products, resulting in an underestimation of NO_2 surface concentration peaks (Cooper et al., 2020). Cooper et al. (2020) developed and demonstrated the successful application of a new algorithm for TROPOMI-inferred surface NO_2 concentrations that reduced this bias, but found that in addition to improved satellite resolution, it also required updating assumptions about vertical mixing.

To facilitate a direct comparison of OMI, TROPOMI, and OMPS satellite observations with a consistent set of ground-based observations, a ground-based network of 13 monitoring stations using Pandora DOAS instrumentation, the Pandonia Global Network (PGN), was established (Herman et al., 2019a; Rawat et al., 2025). Multi-axis DOAS combines measurements from different viewing directions at altitudes up to 3 km from surface (Lauster et al., 2021). Ground-based multi-axis DOAS has been employed as part of the global Pandora network since it was first established in 2019 (Park et al., 2022; Herman et al., 2019a; Rawat et al., 2025). The Pandora network is integrated into the existing Photochemical Assessment Monitoring Station (PAMS) network (see Section 1.4.2) and has proved useful for directly comparing satellite and ground-based DOAS measurements (Herman et al., 2019b).

Comparisons of OMI and PGN observations consistently show satellite data underestimate NO_2 tropospheric vertical column densities by 50 to 100% in polluted areas (Herman et al., 2019b). Remote sensing observations from TROPOMI were generally well correlated with ground-based Pandora observations ($r^2 = 0.73$), though they showed a bias of -22.8% (Nawaz et al., 2024). The smaller bias for TROPOMI than for OMI suggests improved performance for newer TROPOMI satellite technology. OMPS NO_2 tropospheric vertical column density observations were less well correlated ($r^2 = 0.40$) with data from 13 U.S. Pandora stations over a period of more than two months and averaged a positive bias of 14.8%. However, the bias was negative (mean relative difference = -34.6%, $r^2 = 0.43$) for observations greater than 12×10^{-15} molecules/cm^2, and more consistent with the TROPOMI observations. Airborne observations from GCAS (see Section 1.4.2) were strongly correlated ($r^2 = 0.79$) with a small positive normalized mean bias of 3.4% compared to Pandora observations (Nawaz et al., 2024).

In other studies, TROPOMI data correlated well (slope = 1.03, r^2 = 0.92) with ground-based spectrometric data in the New York City, NY, U.S., area (Judd et al., 2020); met design bias requirements of <10% compared with ground-based spectrometric data in Toronto, Canada (Zhao et al., 2020); and showed generally good consistency with ground-level concentrations (Goldberg et al., 2021a). Zhang et al. (2018) were able to greatly improve agreement in long-term trends between OMI and AQS network data by updating established data processing procedures to better accommodate albedo and lightning-affected data, and by removing unexplained artifacts over remote ocean areas with minimal marine traffic.

1.4.6 Modeling

Many recent health studies use modeling approaches to estimate exposures to NO_2 and other oxides of nitrogen. These can be geophysical models that resolve chemical and physical processes using equations, empirical models that rely on statistical relationships, or data assimilation models that integrate observational data with model predictions. This section provides high-level summaries of modeling techniques commonly used in and/or relevant to health studies. The summaries are not intended to be comprehensive reviews of modeling techniques used to estimate oxides of nitrogen in ambient air, but rather to provide background information for models discussed in later chapters of this ISA.

The 2016 Oxides of Nitrogen ISAs contain detailed descriptions of CTMs (U.S. EPA, 2020b, 2016). EPA develops and maintains the CTM CMAQ, which has a spatial resolution of 12 km x 12 km and a temporal resolution of 1-hour (U.S. EPA, 2016; Byun and Schere, 2006) but can also be run at a finer spatial and temporal resolutions. CMAQ can simulate NO_Y species such as NO, NO_2, HNO_3, PAN, alkyl nitrates, and particulate nitrate at various pressure levels (Cai et al., 2016). CMAQ version 5.4, released by EPA in 2022 (U.S. EPA RD, 2022), includes several improvements important for NO_Y chemistry, such as updated Cl and other halogen chemistry, and pNO_3^- chemistry (Sarwar et al., 2024) as well as a bi-directional ammonia deposition model, and development of the Detailed Emissions Scaling, Isolation, and Diagnostic module (Appel et al., 2021). CMAQ updates prior to release of version 5.4 also addressed and reduced overestimated summertime values in modeled results compared to ambient measurements reported in a series of recent publications (see Chapter 2, Section 2.3.1.2), with the greatest improvement occurring with the introduction of CMAQv5.1 due to improved treatment of vertical mixing that reduced model overpredictions (Toro et al., 2021). Recent studies have demonstrated larger and more variable biases in modeled surface NO_2 concentrations compared to modeled NO_2 tropospheric column density, suggesting modeled vertical mixing as a large source of uncertainty when trying to estimate NO_2 (Kuhn et al., 2024; Nawaz et al., 2024).

CMAQ relies on emission inventories such as the EPA's MOVES (see Section 1.2.3), a bottom-up emissions model used to estimate emissions from on-road vehicles (Office of Transportation and Air Quality, 2021). Recently a new chemical mechanism called the Community Regional Atmospheric Chemistry Multiphase Mechanism (CRACMM) has been incorporated into CMAQ (Place et al., 2023).

CRACMM predicts multiple endpoints (e.g., NO_X, PM, O_3, and reactive organic species), which better match observations than previous chemical mechanisms in CMAQ (Pye et al., 2023). Multiple studies have compared CMAQ simulations to remote sensing and ground measurements and found that CMAQ generally overestimates NO_X in populated areas and underestimates NO_X in rural environments (East et al., 2022; Toro et al., 2021; Choi, 2014). Recent work by Toro et al. (2021) compared NO_X estimates from photochemical simulations in CMAQ for the years 2002 to 2016 and compared NO_X concentrations to surface network measurements to discern CMAQ performance by U.S. region, season, and time of day. Nationally, summertime morning (4 to 9 AM) NO_X bias was between 28 to 57% from 2002 to 2012, but then dropped to 7% in 2013 and then to -2 to 2% from 2014 to 2016 (Toro et al., 2021). Wintertime evening NO_X bias shifted from 92 to 142% in 2002 to 2012 simulations to 12 to 27% in 2013 to 2016 simulations (Toro et al., 2021), suggesting CMAQ revisions have resulted in improved estimates over time.

Since the 2016 Oxides of Nitrogen ISA, the Air QUAlity TimE Series Project (EQUATES) has been developed, using CMAQv5.2.3, the standardization of emission inventory calculations, and chemical mechanisms to allow for long-term analysis of air quality trends from 2002 to 2019 (Foley et al., 2023). EQUATES can also be used in epidemiologic studies and critical load analyses. Since publication, EQUATES has been used to study surface-level mobile emissions (Kerr et al., 2023), long-term trends in sulfate and nitrate concentrations in Barbados (Gaston et al., 2024), and nocturnal NO_X chemistry (Hoffman et al., 2024).

Other CTMs used to estimate NO_2 and NO_X concentrations include GEOS-Chem, Comprehensive Air Quality Model with Extensions (CAMx), Weather Research and Forecasting model coupled with Chemistry (WRF-Chem), and Monitoring Atmospheric Composition and Climate MACC. GEOS-Chem is a global scale CTM with spatial resolution as low as 2 km (Bindle et al., 2021). Recently, GEOS-Chem has been used to predict atmospheric composition forecasting information (Knowland et al., 2022). GEOS-Chem simulates atmospheric concentrations of NO_X and NO_Y and has also been used to simulate NO_2 tropospheric column densities (see Section 1.4.1.2) (Bindle et al., 2021). CAMx is a photochemical grid model that has been used to estimate hourly to annual NO_Y in the United States (Goldberg et al., 2016). CAMx overestimated NO_Y by 86.2% in the Baltimore/Washington DC area in July 2011 when compared to the 2011 NEI, spurring Goldberg et al. (2016) to develop a revised CAMx framework to better match NO_Y observations, through differences in source attribution and updates to gas-phase chemistry.

The WRF-Chem is a CTM that integrates meteorology and chemistry to simulate atmospheric processes. A study conducted over Europe compared modeled NO_2 tropospheric column densities from WRF-Chem, satellite observations from TROPOMI, and NO_2 profiles obtained from Maximum-differential optical absorption spectroscopy (MAX-DOAS) (Kuhn et al., 2024). The authors identified average daytime and nighttime model biases of 3% and 13.8%, respectively, when compared to TROPOMI retrievals, suggesting a slight overprediction of NO_2 from WRF-Chem (Kuhn et al., 2024).

WRF-Chem model comparisons to MAX-DOAS retrievals were much more variable, with biases ranging from -5.9–50.7% depending on model parameters (Kuhn et al., 2024). Similarly, Liu et al. (2017b) combined NO_2 column retrievals from TEMPO with meteorology and chemical variables from WRF-Chem to predict urban NO_X concentrations in Denver, CO. The TRACER-AQ campaign in Houston, TX during September 2021 combined NO_2 columns from ground-, airborne-, and satellite-based spectrometers. Together, these studies suggest an underestimation of NO_X emissions from urban sources in WRF-Chem simulations.

The MACC project is a global model for aerosol and reactive gases (Wagner et al., 2015). MACC can simulate surface and tropospheric NO_2 at different altitudes at a spatial resolution of 100 km × 100 km (Wagner et al., 2015). MACC specializes in unique events such as volcanos and fires, but still tends to underestimate the spatial distribution and magnitude of tropospheric NO_2 in the United States when compared with satellite observations. The Copernicus Atmospheric Monitoring Service (CAMS) builds upon MACC with the addition of other chemical species, such as PAN (Wang et al., 2020). In Wang et al. (2020), CAMS underestimated NO_X in the middle and upper troposphere (above 8 km), but overestimated NO_X in the lowest layer (under 2 km).

The American Meteorological Society and EPA Regulatory Model (AERMOD) and the Atmospheric Dispersion Modeling System are plume-dispersion models that can predict NO_2 at 1 hour time scales and spatial scales ranging from approximately 10 meters to 50 km (U.S. EPA, 2024d; Carruthers et al., 2017). Recent additions to AERMOD enable hourly NO_2 concentration estimates based on reduced form ozone chemistry and plume entrainment, NO2 photolysis, and combined plume treatments (U.S. EPA, 2024d).

Land use regression (LUR) models often combine monitor data and satellite-based concentration estimates with population density, land use characteristics (e.g., road density or emissions sources), and meteorology information to predict NO_2 concentrations at fine (30 to 500 m^2) or global spatial scales (Larkin et al., 2023; Larkin et al., 2017; Lee and Koutrakis, 2014). Further details and applications of LUR models to predict surface NO_2 concentrations can be found in Chapter 2.

Ensemble models, such as that used by Di et al. (2020), combine multiple machine learning algorithms (e.g., neural networks, random forest, and gradient boosting), predictor variables provided from CTMs, and ground-based monitoring data. The model used by Di et al. (2020) used 1 km^2 resolution across the contiguous United States and showed a linear relationship between modeled and observed NO_2 ($r^2 = 0.788$). Model performance was analyzed seasonally and geographically, giving r^2 values of 0.729 and 0.844, respectively. In general, predictions best matched monitoring station results in the urban areas of the United States. Performance was worse in mountainous regions, such as the Rocky and Appalachian Mountains, where station monitors are sparse. Seasonal differences were minor, with slight overpredictions of NO_2 in winter and spring compared to summer and autumn.

The high spatial variability of NO_2 concentrations across the urban gradient presents challenges, given sparse monitoring coverage in many populated areas. Concentrations from a single monitor and concentrations averaged over several monitors can miss substantial spatial deviations, limiting their representativeness to small spatial areas and secondary pollutants (which are less spatially variable than primary pollutants) (Yu et al., 2018). Several approaches have been developed to characterize NO_2 concentrations between monitors in the absence of spatially sufficient monitoring, including spatial interpolation approaches with or without additional data (e.g., inverse distance weighting, kriging, and tessellation); satellite-derived measurements; hybrid approaches combining modeling and measurements; generalized additive and LUR models, and outputs from models such as the CMAQ or Research Line Source (RLINE) models (Kerr et al., 2023; Larkin et al., 2023; Anenberg et al., 2022; Di et al., 2020; Yu et al., 2018). Yu et al. (2018) summarized and compared results from 14 of these methods for developing spatiotemporal concentration fields to characterize spatial variability of concentrations for all criteria pollutant indicators, including NO_2, in Atlanta, GA. Poor performance was observed for inverse distance weighting, kriging, and tessellation of NO_2 data without dense network monitoring coverage. Satellite retrieval-based methods captured urban gradient spatial concentration variations (Lee et al., 2023; Judd et al., 2019); however, there can be errors associated with estimating ground-level concentrations from total air column satellite measurements, missing data from cloudy days, and other uncertainties (see Section 1.4.3). Hsu et al. (2024) used assimilated data to demonstrate that the newest generation of geostationary satellites substantially reduced uncertainties in emissions estimates as determined by root mean square errors and coefficient of determinations in comparisons between idealized true values and assimilated satellite data in 23 of 29 major urban U.S. regions compared to the previous generation of low Earth orbiting satellites. Newer methods have been deployed using models combined with street-level imaging (Suel et al., 2022), aircraft-based measurements of tropospheric vertical column densities (Li et al., 2021b), and low-cost sensors (see Section 1.4.4) (Guaman et al., 2022). Substantial errors and biases were observed for CMAQ and RLINE model outputs without adjustment, but these could be improved using hybrid data fusion methods that combine air quality model outputs with observational data (see Section 1.4.4) (Yu et al., 2018).

Since the last ISA, improvements have been made to models that predict NO_X concentrations. These include updated chemical transport modules, increased use and development of ensemble models, and model validation and correction using observational data. Seasonally, models tend to perform better in summer and autumn compared to winter and spring, where model biases are more common but are an area of active research. Generally, NO_X is best modeled in urban areas and near large industrial sources where there are more monitoring stations compared to rural locations with fewer monitors to constrain model performance.

1.5 Ambient Concentrations of NO_X and Copollutants

In this section, spatial and temporal trends in surface level NO_2 concentrations in ambient air are discussed as well as NO_X and copollutant associations. The 2016 Oxides of Nitrogen ISA (U.S. EPA, 2016) summarized key findings in trends in NO_2 concentrations in ambient air in the United States. One major focus was on near-road NO_2 concentration gradients. NO_2 lifetimes are as short as 1-hour (see Section 1.3.1) (U.S. EPA, 2016), and are affected by microscale plume dynamics such as building downwash, low wind speeds, and plume rise (U.S. EPA, 2024d), leading to substantial concentration decreases as one moves away from busy roads and major industrial sources (see Section 1.2) and making accurate concentration measurements challenging, particularly when monitoring coverage is sparse. Approaches to address the challenges this spatial variation creates include supplementation of monitoring data with higher resolution satellite-based remote sensing data (see Section 1.4.3), various modeling or hybrid measurement/modeling approaches (see Section 1.4.4), and spatial saturation sampling at the neighborhood level with low-cost sensor technology (see Section 1.4.4) (U.S. EPA, 2016).

It should be noted that pollutant measurements can be reported as concentrations, as is the case in most peer-reviewed publications, or as design values, which are used for regulatory purposes. A design value is a statistic that summarizes pollutant concentrations in ambient air for an area in terms of the indicator, averaging time, and form for a given standard such that its comparison to the level of the standard indicates whether the area meets or exceeds the standard (U.S. EPA, 2023d). The annual NO_2 NAAQS is set at a level of 53 ppb, based on an annual average of NO_2 concentrations (U.S. EPA, 2016). The 1-hour NO_2 standard is set at a level of 100 ppb based on the 3-year average of the annual 98^{th} percentile of the 1-hour daily maximum NO_2 concentrations as stated in 50 CFR, Appendix S (U.S. EPA, 2017).

1.5.1 Current National Scale Trends

Figure 1-10 shows annual NO_2 design values from 2023 for air quality monitors across the United States. No monitors recorded annual NO_2 design values above 53 ppb. Of the 410 stations, 74% had annual design values less than 10 ppb. In the northeastern United States, southern California, and other urban locations (e.g., Los Angeles, CA; Houston, TX; and Chicago, IL), annual design values were typically higher, between 11 and 20 ppb. Six stations (1%), located in the Los Angeles Basin and the Central Valley of California, Denver, CO and Phoenix, AZ, had annual design values between 21 and 27 ppb. The highest design value reported was 27 ppb, which was measured at a near-road site in Los Angeles, CA.

Figure 1-11 shows 1-hour NO_2 design values from the 2021 to 2023 period. All design values during this period were below 100 ppb. Most stations (71%) had 1-hour design values between 31 to 60 ppb. These stations were located throughout the United States, with only coastal stations on the west

coast and rural stations in parts of the western United States showing design values below 31 ppb. Urban areas near New York, NY; Denver, CO; and parts of Los Angeles and the Central Valley of California had design values over 61 ppb. The highest 1-hour NO_2 design value was 71 ppb and was measured at the same location as the highest annual NO_2 design value at a near-road site in Los Angeles, CA.

Table 1-4 shows NO_2 concentration summary statistics across the United States based on daily maximum 1-hour (MDA1) and daily 24-hour average (DA24) metrics from 2021 to 2023 for sites that had at least 75% data capture during this period. Over the past three years, mean MDA1 and DA24 concentrations have generally been similar across much of the United States, except in the West North Central region, which has lower concentrations due to more rural sampling stations compared to other geographic regions.

Overall, measurements of higher NO_2 concentrations match known NO_X emissions patterns and correlate well with U.S. urban areas, interstates, manufacturing facilities, airports, and ports (Goldberg et al., 2024). In urban Houston, TX, high NO_2 design values were due to petrochemical refining, whereas in urban Baltimore, MD, high NO_2 values were due to the confluence of highways, the Baltimore Port, and a Baltimore incinerator (Goldberg et al., 2021b). In addition to urban areas, some rural areas have recently experienced increased NO_2 concentrations (e.g., in the Permian Basin in West Texas, Eagle Ford shale areas of South Texas, the Williston Basin of western North Dakota, and other locations in Utah and Colorado) (Dix et al., 2020). These areas correlate with known areas of oil and gas production (Goldberg et al., 2021b).

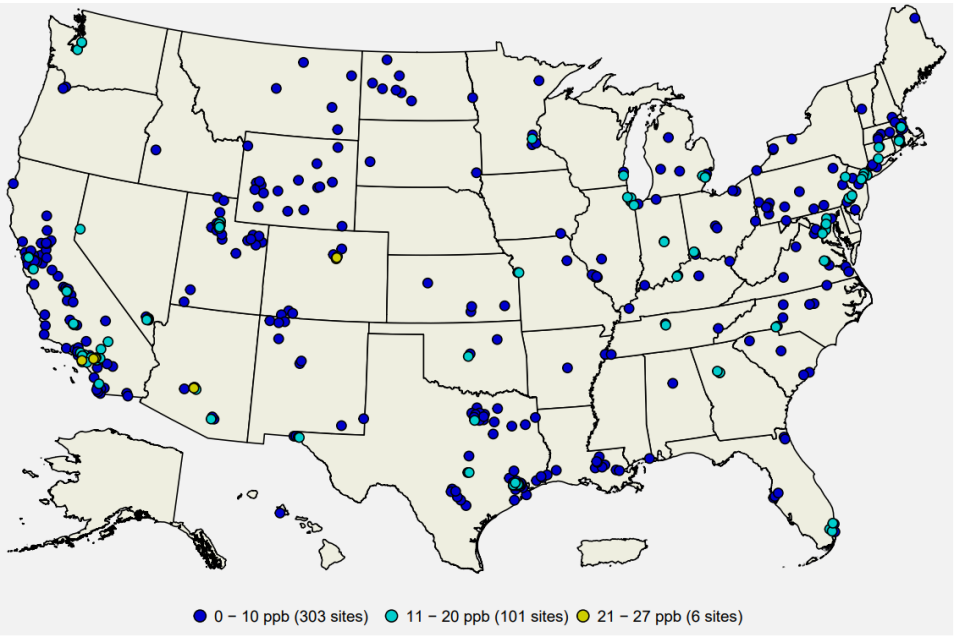

List of abbreviations in alphabetical order: ppb = parts per billion.
Note: values in ppb.
Source: U.S. EPA (2023d). Copyright permission pending.

Figure 1-10 Annual average NO_2 design values, based on data from 2023.

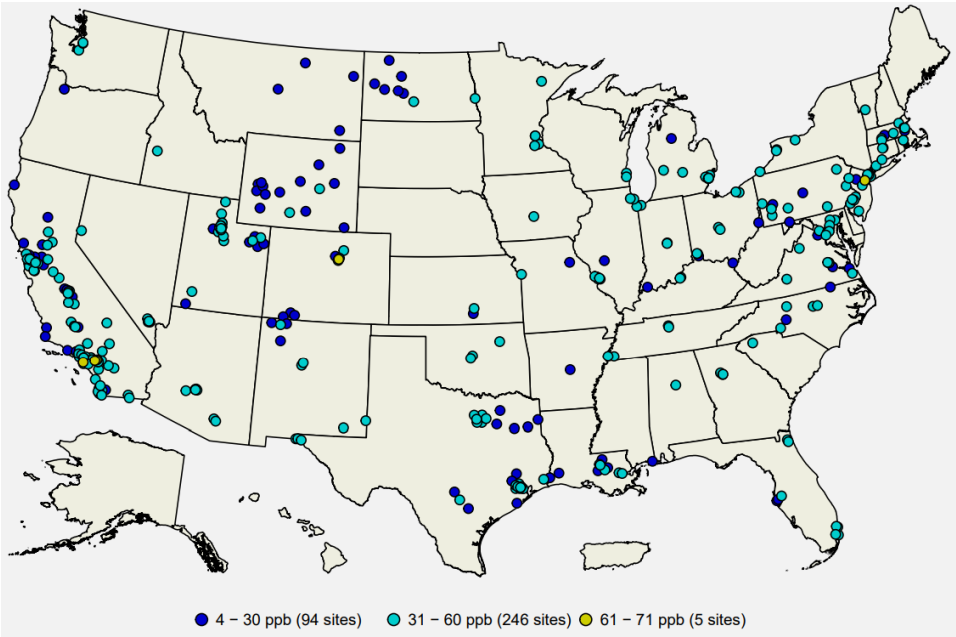

List of abbreviations in alphabetical order: ppb = parts per billion.
Note: values in ppb.
Source: U.S. EPA (2023d). Copyright permission pending.

Figure 1-11 Three-year averages of the annual 98th percentile daily maximum 1-hour average NO_2 design values for the 2021 to 2023 period.

Table 1-44 Summary statistics based on two daily NO_2 NAAQS metrics: the daily maximum 1-hour metric and the daily 24-hour average metric for 2021 to 2023

Metric	Region	N.stations	N.obs	Mean	SD	Min	P1	P5	P10	P25	P50	P75	P90	P95	P98	P99	Max	Max.station
MDA1	All	404	418,695	16.7	12.2	-3.0	0.7	1.8	3.0	6.8	14.1	24.6	34.3	39.8	45.6	49.7	315.3	201950001
MDA1	Central	31	32, 249	19.2	11.6	-0.7	1.5	3.3	5.1	9.9	17.6	27.0	35.1	40.0	45.8	49.2	109.2	295100094
MDA1	East North Central	20	20,511	17.0	10.9	-0.2	1.0	1.9	3.4	8.5	15.7	24.1	32.2	37.0	42.4	46.0	107.4	191770006
MDA1	Northeast	58	60,379	19.0	11.6	-2.0	1.3	3.0	5.0	9.8	17.7	26.9	35.0	39.8	45.4	49.3	97.0	340170006
MDA1	Northwest	6	6,279	21.2	9.6	1.6	4.0	6.7	9.2	14.0	20.6	27.4	33.5	37.7	43.0	47.4	78.5	530330030
MDA1	South	66	66,104	14.3	11.0	-1.8	0.8	2.2	3.2	5.9	11.3	20.4	30.5	36.0	41.8	45.9	315.3	201950001
MDA1	Southeast	39	40,243	16.6	10.5	-1.0	1.0	2.5	4.1	8.1	15.0	23.5	31.2	36.0	41.1	44.8	94.8	120110035
MDA1	Southwest	56	58,601	17.8	13.6	-0.7	0.6	1.3	2.7	6.7	14.3	27.0	38.2	43.4	49.2	53.3	113.0	490210005
MDA1	West	94	99,104	19.0	12.9	-0.9	0.9	2.2	4.0	8.4	16.6	27.7	37.4	42.5	48.4	52.8	119.1	010010015
MDA1	West North Central	34	35,228	5.8	6.2	-3.0	0.0	0.7	1.0	1.9	3.7	7.4	13.9	18.8	24.8	29.4	111.9	560210100
DA24	All	404	418,695	7.9	6.9	-3.3	0.1	0.7	1.3	2.8	5.9	11.0	17.4	21.8	27.1	30.8	64.1	060374008
DA24	Central	31	32,249	9.1	6.4	-1.3	0.6	1.4	2.2	4.3	7.6	12.6	18.1	21.6	25.8	28.3	44.0	170310076
DA24	East North Central	20	20,511	8.1	5.6	-0.9	0.4	1.1	1.8	3.8	7.0	11.4	15.8	18.8	22.3	24.6	36.5	261630093
DA24	Northeast	58	60,379	9.3	6.7	-2.7	0.6	1.5	2.2	4.2	7.7	12.9	18.5	22.2	26.9	30.4	53.0	340390004
DA24	Northwest	6	6,276	10.7	5.5	1.0	2.1	3.2	4.1	6.5	10.0	14.2	17.9	20.4	23.6	26.0	53.6	530330030
DA24	South	66	66,104	6.2	5.3	-2.3	-0.2	0.8	1.3	2.5	4.6	8.2	13.5	17.0	21.3	24.0	47.5	482011052
DA24	Southeast	39	40,243	7.7	5.7	-1.6	0.5	1.1	1.8	3.4	6.2	10.7	15.7	19.1	22.9	25.5	37.1	517600025
DA24	Southwest	56	58,601	8.3	8.0	-1.9	0.1	0.6	1.1	2.6	5.5	11.3	19.9	25.5	31.5	35.6	60.5	080310028
DA24	West	94	99,104	9.4	7.8	-1.4	0.1	1.0	1.9	3.7	7.1	13.2	20.7	25.4	30.6	34.2	64.1	060374008
DA24	West North Central	34	35,228	2.1	2.2	-3.3	-0.0	0.2	0.4	0.8	1.5	2.8	4.6	6.2	8.6	10.6	27.6	460990009

List of abbreviations in alphabetical order: DA24 = daily 24-hour average; max = maximum; max.station = AQS ID number for the monitoring station corresponding to the observation in the max column; MDA1 = daily maximum 1-hour; min = minimum; NAAQS = National Ambient Air Quality Standard; NO_2 = nitrogen dioxide; N.obs = number of observations; N.stations = number of stations; P1, P5, P10, P25, P50, P90, P95, P98, P99 = 1st, 5th, 10th, 25th, 50th, 90th, 95th, 98th, 99th percentiles; SD = standard deviation.
Region Notes: Central = Illinois, Indiana, Kentucky, Missouri, Ohio, Tennessee, West Virginia; East North Central = Iowa, Minnesota, Michigan, Wisconsin; Northeast = Connecticut, Delaware, Maine, Maryland, Massachusetts, New Hampshire, New Jersey, New York, Pennsylvania, Rhode Island, Vermont; Northwest = Alaska, Idaho, Oregon, Washington; South = Arkansas, Kansas, Louisiana, Mississippi, Oklahoma, Texas; Southeast = Alabama, Florida, Georgia, North Carolina, South Carolina, Virginia; Southwest = Arizona, Colorado, New Mexico, Utah; West = California, Hawaii, Nevada; West North Central = Montana, Nebraska, North Dakota, South Dakota, Wyoming.

Source: U.S. EPA (2023d). Copyright permission pending.

As described in Section 1.4.3, satellite remote sensing data are useful for filling gaps in sparse ground-level monitoring network coverage to get a more complete picture of national scale spatial variability. Figure 1-12 shows the average of TROPOMI NO_2 data over the first 20-month record (May 1, 2018 to December 31, 2019). The largest U.S. cities can be clearly identified as major sources of NO_X emissions. In addition, major road networks, power plants, oil and gas production operations, and mining operations in rural areas, which are indistinguishable from background with earlier satellite products, are resolvable with TROPOMI. For example, increased vertical column densities can be seen between Dallas, TX and Austin, TX, which correspond to the location of Interstate 35 (Goldberg et al., 2021a). As described in Section 1.4.5.3, additional steps are needed to calculate ground-level NO_2 concentrations from satellite-based column measurements, so increases in vertical column densities do not necessarily mean increases in surface concentrations. Vertical column density data, however, is still useful for determining emission hotspots or locations for further study that ground-based monitor networks may not capture because of their more limited spatial coverage.

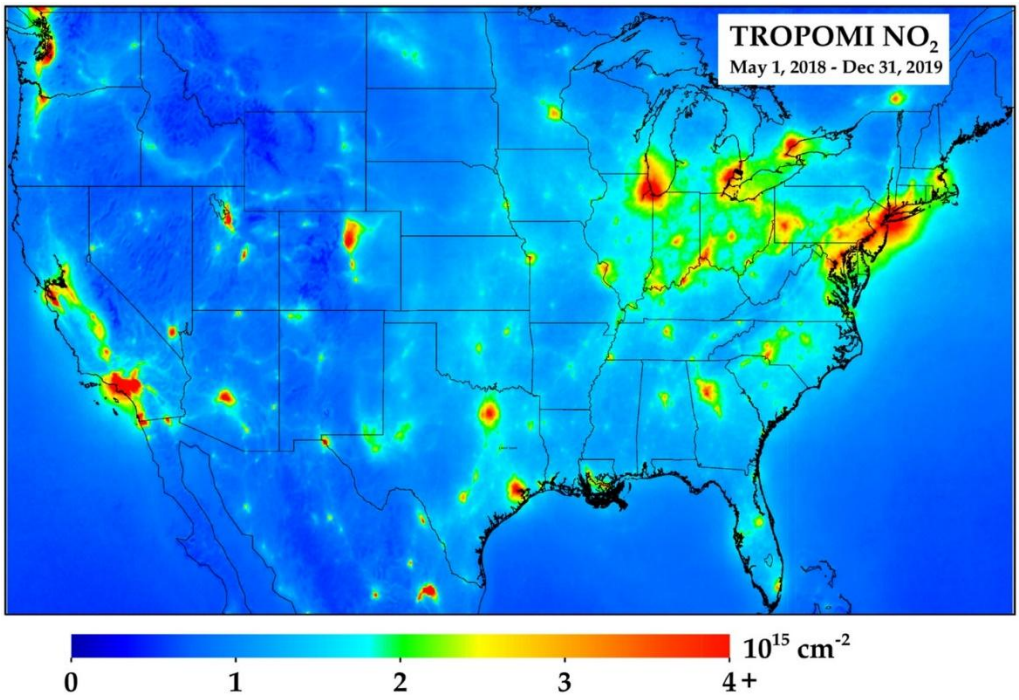

Source: Goldberg et al. (2021a). Copyright permission pending.

Figure 1-12 TROPOMI NO_2 tropospheric vertical column density (molecules/cm^2) sampled to 0.01° × 0.01° spatial resolution from May 1, 2018 to December 31, 2019.

1.5.2 Urban Scale Spatial Trends

The 2016 Oxides of Nitrogen ISA (U.S. EPA, 2016) described how a major benefit of the emergence of satellite measurement technologies is their capability for fine spatial resolution of NO_2 measurements (see Section 1.4.3). This is important because NO_2 concentrations generally exhibit a strong urban to rural concentration gradient, with concentrations decreasing substantially as one moves from an urban center to rural fringes due to the short lifetime of NO_2 (Bowling et al., 2018; Messier et al., 2018; Novotny et al., 2011). An example of this NO_2 concentration pattern from Minneapolis, MN is shown in Figure 1-13. Using a LUR model that combined ground-based and satellite-based data (as described in Section 1.4.6), Novotny et al. (2011) observed high spatial variability for NO_2 concentrations within urban areas. Urban spatial variation was most strongly influenced by proximity to roads, the extent of nearby impervious surfaces, and the extent of tree canopy in the vicinity. Indeed, NO_2 concentrations increased with proximity to major roads and extent of impervious surfaces and decreased with increasing extent of tree canopy coverage. Minor roads, elevation, and distance from the coast were less influential for NO_2 concentrations.

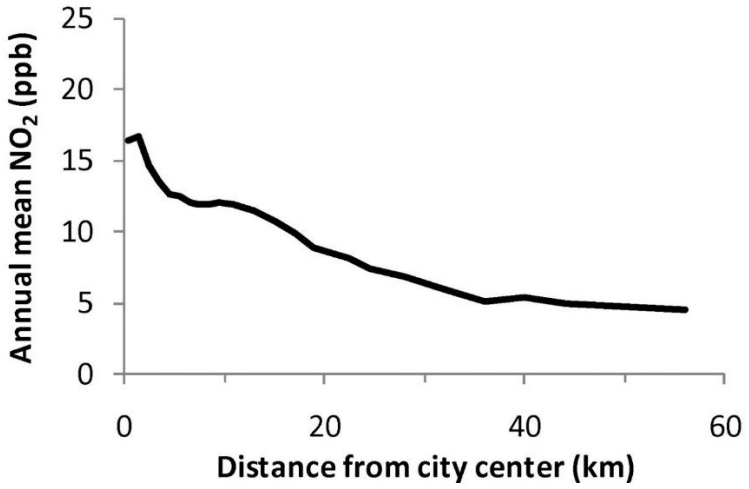

List of abbreviations in alphabetical order: km = kilometer; NO_2 = nitrogen dioxide; ppb = parts per billion.
Source: Novotny et al. (2011). Copyright permission pending.

Figure 1-13 2006 mean annual NO_2 concentration versus distance from Minneapolis, MN, U.S., city center.

Apte et al. (2017) used professionally driven fleet vehicles equipped with air quality instruments as mobile monitors for repeated sampling of every street in a 30 km^2 area of Oakland, CA, U.S., for one year. They mapped annual daytime NO and NO_2 concentrations at 30-meter intervals to develop the largest urban air quality data set of its type. They observed small-scale variations in concentration of up to five to eight times within individual city blocks, due to either traffic congestion or identifiable neighborhood sources (e.g., recycling businesses, warehouses, auto and tire shops). A characteristic

feature of the data was the presence of persistent hot spots on road segments <100 meters in road length, where on-road pollutant concentrations exceeded nearby on-road concentrations measured along the mobile monitor's route outside the hotspot by 50% or more. The hotspots were frequently associated with intersections, vehicle repair shops, or industrial sites associated with truck traffic. Sample collection was instantaneous, but reported concentration data for each 30-meter road segment were integrated over an average of 31 days and 1000 samples collected at different times of day. In general, spatial variability was consistently observed over much finer scales than can be observed using monitoring network measurements or predicted by air quality models. NO and NO_2 concentrations on residential streets were consistent with observations of the nearby regulatory monitor, but median NO and NO_2 concentrations on major highways serving the area were higher than the regulatory monitors by factors of 4.8 and 1.8, respectively. NO concentrations on designated truck routes connecting major highways to industrial areas were 1.9 to 3.6 times higher than on other streets (Apte et al., 2017). Apte et al. (2017) were also able to make some general observations about spatial concentration patterns for NO and NO_2. Distance-decay relationships for NO and NO_2 concentrations show elevated concentrations following a concentration gradient within 200 to 500 meters from busy roads to less busy areas. (U.S. EPA, 2016). Spatial variation of peak concentrations was consistent with general urban background concentrations dominating NO levels for low-traffic residential streets, while transient peaks reflected concentrations on major roads and near industrial operations.

More recently, Bowling et al. (2018) leveraged the electrified light rail network in Salt Lake City, UT, U.S., to take continuous measurements of NO_2 and other air pollutants. The authors observed strong spatial and temporal changes in NO_2 concentrations within the city. The highest NO_2 concentrations were observed in the urban core of Salt Lake City near a railyard station (with non-electrified trains), where concentrations exceeded 25 ppb. Other localized hot spots near roadways reached nearly 20 ppb, but NO_2 concentrations decreased to <10 ppb outside the urban core of the city.

1.5.3 Near-road Trends

The 2016 Oxides of Nitrogen ISA (U.S. EPA, 2016) summarized results from numerous studies that characterized near-road gradients around single road segments, including many studies that were analyzed in a meta-analysis by Karner et al. (2010). This meta-analysis consistently showed that NO concentrations in ambient air decreased sharply and NO_2 concentrations decreased more gradually moving from the edge of the road to a distance of several hundred meters away. The NO and NO_2 concentration gradients in these studies were influenced by traffic volume, wind direction and speed, time of day, season, day of the week, and meteorological conditions (U.S. EPA, 2016; Karner et al., 2010). The 2016 Oxides of Nitrogen ISA (U.S. EPA, 2016) also presented preliminary data from EPA's near-road network, which showed higher NO_2 concentrations near roads with heavy traffic than at other monitors in the same city.

Three recent studies have expanded on the near-road studies and the preliminary near-road network results described in the 2016 Oxides of Nitrogen ISA (U.S. EPA, 2016) by assessing trends based on the national near-road monitoring network (Gantt et al., 2021; Lal et al., 2020; DeWinter et al., 2018). DeWinter et al. (2018) assessed national scale air monitoring results during the first two years of near-road network operation, 2014 and 2015; compared them to the levels of the primary NO_2 NAAQS and other monitoring stations within the same urban areas; and explored impacts of traffic volume and fleet mix on near-road NO_2 concentrations. The overall maximum hourly concentration of near-road NO_2 over this 2-year period was 258 ppb, but there were only two occurrences (in 2014) and five occurrences (in 2015)—a total of 0.0015% of the total hourly observations—when a daily 1-hour maximum concentration exceeded 100 ppb. The 98th percentile of 1-hour maximum NO_2 concentrations remained below 100 ppb at all near-road monitoring stations. The highest annual average NO_2 concentration was 27.1 ppb in Anaheim, CA, U.S., (in 2014) and 29.9 ppb along Interstate 10 in Ontario, Canada (in 2015), both well below 53 ppb (DeWinter et al., 2018). Elevated near-road NO_2 concentrations were attributed to multiple factors, including higher traffic volumes, higher fractions of heavy-duty vehicles, lower traffic speeds, greater traffic congestion, depressed or below grade roadways, lower wind speeds, and wind direction (DeWinter et al., 2018). The two 1-hour maximum measurements greater than 100 ppb were observed at the Fort Lee sampling station located near the eastbound entrance of the 14-lane George Washington Bridge connecting New Jersey and New York (DeWinter et al., 2018).

Table 1-5 compares near-road and non-near-road monitors within 10 km of each other from January 2017 to December 2018. The average near-road monitor NO_2 concentration for 55 monitors is 15.9±5.8 ppb, or 6.2 ppb (64%) higher than the average of 9.7±4.1 ppb for 66 non-near-road monitors within 10 km of a near-road monitor (Lal et al., 2020). All NO_2 concentrations were below 53 ppb, the annual NAAQS, for all near-road and non-near-road monitors throughout the study (Lal et al., 2020).

Table 1-55 Comparison of two-year average NO_2 concentrations at near-road and non-near-road monitoring stations

	Near-road stations	Non-near-road stations within 10 km
2 yr Average NO_2 Concentration	15.9 ppb	9.7 ppb
Standard Deviation	±5.8 ppb	±4.1 ppb
Number of Monitors	n = 55	n = 66

List of abbreviations in alphabetical order: km = kilometer; n = number; NO_2 = nitrogen dioxide; ppb = parts per billion; yr = year.
Source: Lal et al. (2020). Copyright permission pending.

When hourly NO_2 measurements from 44 near-road network stations were compared in a pairwise manner to non-near-road urban monitors within 10 km of the near-road monitor, near-road NO_2 concentrations were an average of 5.0 ppb higher than non-near-road NO_2 concentrations, with a 95% confidence interval of 3.4 to 6.5 ppb (Lal et al., 2020). On average, higher concentrations were consistently observed at near-road monitors for each hour of the day and all seasons, and strong

agreement was observed between near-road NO_2 concentrations and annual average daily traffic (Lal et al., 2020).

Gantt et al. (2021) evaluated hourly near-road network data from 2013 to 2018 and estimated that near-road NO_2 concentrations were, on average, 6.9 ppb greater than hourly concentrations at non-near-road monitors. The most significant NO_2 concentration difference between near-road and non-near-road was 9 ppb and occurred between 2:00 to 4:00 PM. NO concentration differences were higher between near-road and non-near-road monitors, reaching concentration differences of 25 ppb during morning rush hour (5:00 to 8:00 AM).

The near-road network has now been in place long enough to make observations of changes in NO_2 and NO_X concentrations over 10-years of monitoring data possible. Near-road monitoring sites are shown in Figure 1-9, and they also make up a subset of the monitors for which current design values are shown in Figure 1-10 and Figure 1-11. Figure 1-14 shows changing near-road concentration patterns from 2014 to 2023 in two locations during ozone season. In Figure 1-14A, a decreasing trend was observed at the Anaheim, CA near-road monitor, especially before 2019. Other near-road monitors (see Figure 1-9) also show a similar decreasing trend over this period, but there are a number of near-road monitoring sites where decreasing trends are not observed. For example, in Figure 1-14B, little change in concentration was observed over the same period for a near-road I-610 monitoring site in Houston, TX.

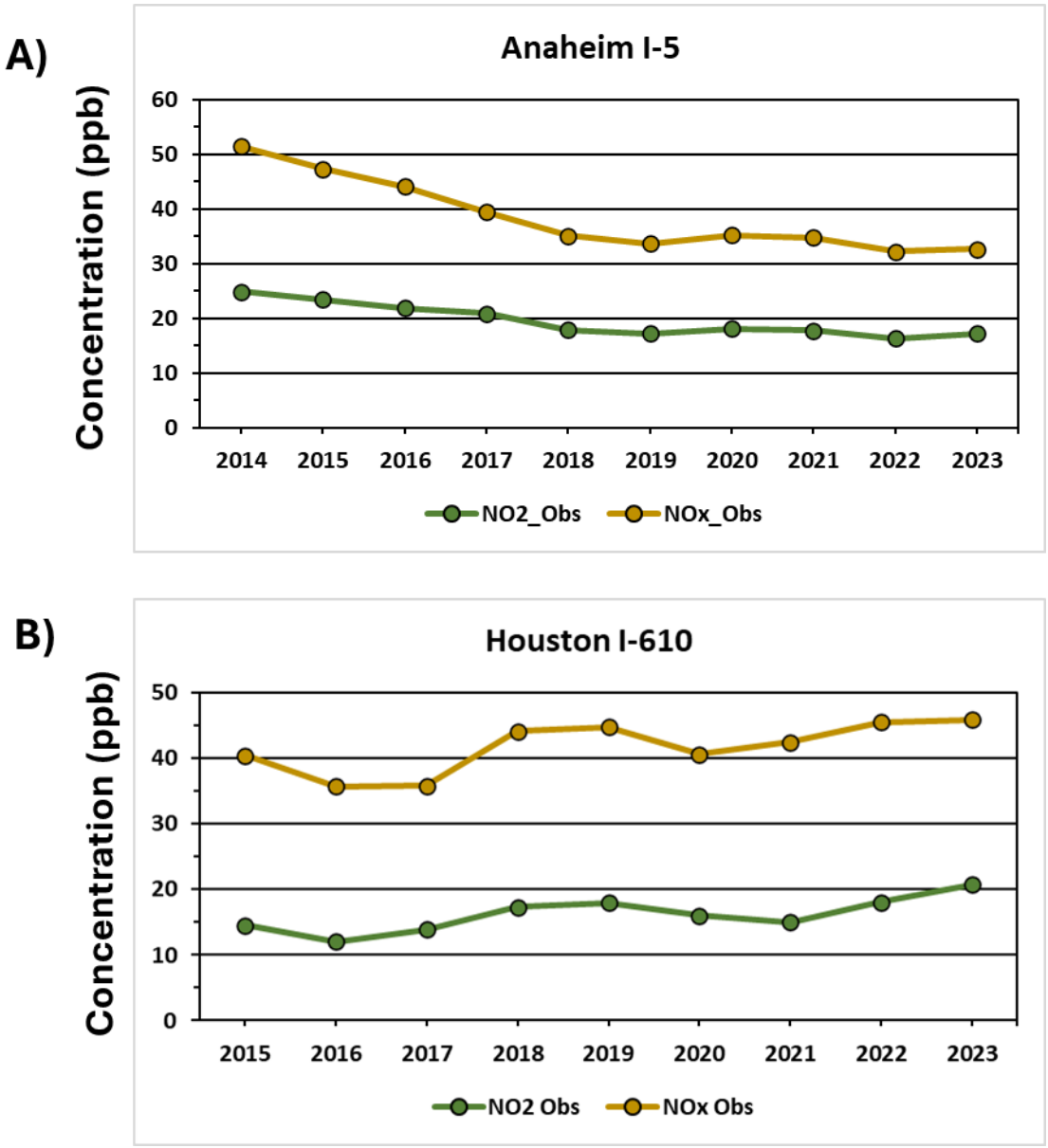

Notes: Obs = observed concentration (ppb). A) Anaheim, CA, U.S., and B) Houston, TX, U.S.
Source: U.S. EPA 2025 analysis of Air Quality System network data 2014 to 2023 (https://www.epa.gov/air-trends/nitrogen-dioxide-trends).
Copyright permission pending.

Figure 1-14 NO_2 and NO_X concentration trends at near-road monitors in Anaheim, CA, U.S., and Houston, TX, U.S.

Richmond-Bryant et al. (2017) modeled hourly on-road and near-road NO_X and NO_2 concentrations in Las Vegas, NV, U.S. Generally, concentrations decreased with increasing distance from the road, with median decreases of 16% observed 10 m from the road and 21% observed 20 m from the road. On-road concentrations were highest in the morning and late afternoon, correlating with traffic patterns. Average on-road concentrations were estimated to be 33 and 73 ppb for NO_2 and NO_X,

respectively, with maximum concentrations reaching 105 and 264 ppb for NO_2 and NO_X, respectively (Richmond-Bryant et al., 2017).

A meta-analysis reported average concentration decay rates over downwind distance from major roads of 0.0004 ppb/m for NO_2 and 0.0027 ppb/m for NO_X (Liu et al., 2019). Using a mobile laboratory for repeated rush hour measurements, locations 500 meters and 50 meters from a major road in Detroit, MI, U.S., were found to have a 17.0 ppb difference in NO and a 17.7 ppb difference in NO_X (Baldwin et al., 2015). Near Durham, NC, U.S., the combined effect of higher emissions and slower downwind dispersion led to 20% higher near-road hourly NO_X concentrations in winter than in summer (Saha et al., 2018). Elevated concentrations of NO_X near roads, versus at urban background stations, were also observed in New York, NY, U.S., and Rochester, NY, U.S, especially during daytime hours (Rattigan et al., 2020). Liu et al. (2021a) demonstrated that near-road NO and NO_2 concentrations could be directly and quantitatively related to changes in vehicle activity due to COVID-19 restrictions in northern and southern California (see Section 1.2.8). Although these recent studies, combined with previous studies reported in the 2016 Oxides of Nitrogen ISA (U.S. EPA, 2016), show consistent near-road gradient patterns for oxides of nitrogen, the complexity of traffic patterns can lead to spatial and temporal variations in NO_X and other pollutant concentrations, making spatially and temporally resolved traffic activity data an important factor for more accurately estimating near-road concentrations (Filigrana et al., 2020).

1.5.4 National and Regional Temporal Trends

EPA monitoring data and numerous external studies show that average U.S. NO_2 concentrations have decreased considerably since monitoring began several decades ago as policies for NO_X emissions reductions have been implemented (Sicard et al., 2023; Anenberg et al., 2022; Jaffe et al., 2022). Studies using the AQS monitoring network found that ground-based NO_2 concentrations have decreased 38 to 42% from 2005 to 2018 (Lamsal et al., 2015; Tong et al., 2015). Since then, NO_2 concentrations on average have continued to decline. Figure 1-15 shows station-level trends of annual NO_2 design values at U.S. monitoring stations from 2000 to 2023. All monitors (except for four in North Dakota and one each in Texas, New Mexico, Wyoming, and South Dakota) show decreasing NO_2 concentrations. Station-level trends in 1-hour NO_2 concentrations show similar decreases over the same time period (see Figure 1-16).

Since OMI satellite measurements began in 2005 to the mid-2010s, vertical tropospheric NO_2 column density over the eastern United States decreased by 35 to 40% (Krotkov et al., 2016; Tong et al., 2015). Decreased NO_2 concentrations are due to lower NO_X emissions, which decreased over U.S. urban areas by 49% as estimated by OMI (Lu et al., 2015), and catalytic reduction on point sources and vehicles (Krotkov et al., 2016). Beginning in about 2010, OMI vertical tropospheric NO_2 column density trends flattened despite NO_2 surface concentration and NO_X emissions continuing to decrease. Studies have suggested multiple hypotheses for this trend divergence. Silvern et al. (2019) attributed flattening OMI

NO_2 trends to increased geogenic sources such as lightning and soils. Indeed, soil NO_X emissions could be much higher than currently estimated, though uncertainty is high (see Section 1.2.7). Jiang et al. (2018), however, attribute the OMI NO_2 flattening to growing relative contributions of industrial, area, and off-road sources, decreasing relative contributions of on-road gasoline sources, and slower than expected decreases in on-road diesel emissions. The COVID-19 pandemic demonstrated how significant decreases in on-road sources could affect concentrations in ambient air. During the COVID-19 pandemic and subsequent lockdowns, NO_X emissions decreased drastically, resulting in NO_2 decreases of 9.2–43.4% among 20 cities in North America, with a median NO_2 decrease of 21.6% (Goldberg et al., 2020) (see Section 1.2.8).

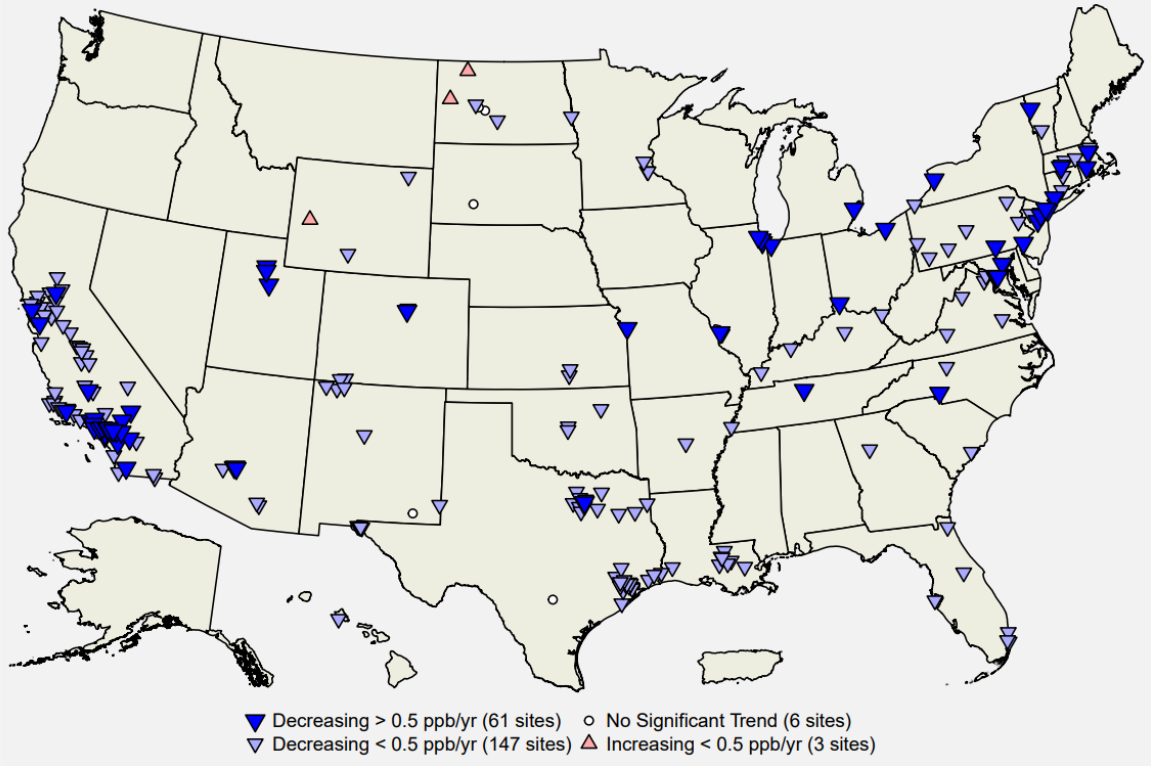

List of abbreviations in alphabetical order: ppb = parts per billion; yr = year.
Source: U.S. EPA (2023d). Copyright permission pending.

Figure 1-15 Station-level trends in annual average NO_2 concentrations based on data from 2000 to 2023.

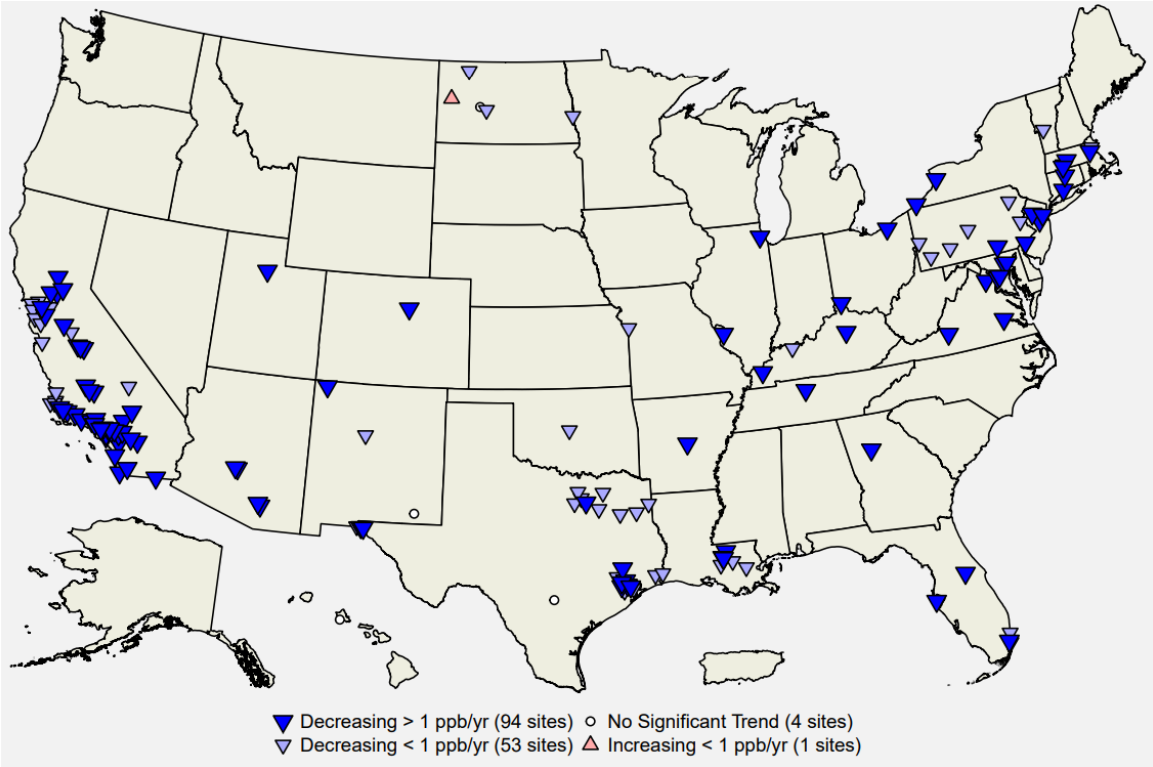

List of abbreviations in alphabetical order: ppb = parts per billion; yr = year.
Source: U.S. EPA (2023d). Copyright permission pending.

Figure 1-16 Station-level trends in three-year averages of the annual 98th percentile daily maximum 1-hour average NO_2 concentrations from 2000 to 2023.

While long-term NO_2 concentrations have decreased nationally, NO_2 has not decreased at the same rate everywhere across the United States. Both ground-based monitors and remote sensing studies show that urban areas across the United States experienced the most dramatic decreases in NO_X (Goldberg et al., 2021b). In recent satellite-based studies focused on rural and urban U.S. land area all together, NO_2 amounts decreased faster over the eastern United States, a region that tends to have higher NO_X emissions due to vehicle traffic and industrial sources (Jamali et al., 2020; Miyazaki et al., 2017). However, a major east-west geographic difference in NO_2 concentration trend is not evident in Figures 1-15 and 1-16, which are based on mainly urban national network monitors. NO_2 concentrations decreased by an average of 38% in New England and 41% in the Mid-Atlantic region from 2005 to 2013 (Lamsal et al., 2015). In New York, NY, NO_X concentrations in the early 1990s ranged from 70 to 120 ppb but have since decreased by 5%/yr (Civerolo et al., 2017). Despite these decreases, cities remain areas of higher NO_2. Decreases in NO_X were even smaller than 2%/yr in rural New York stations, due to lower initial NO_X concentrations (Civerolo et al., 2017). Interestingly, NO_2 monitoring at Whiteface Mountain in New York, which is not shown in Figures 1-15 or 1-16 because it is not a part of the SLAMS monitoring network (see Section 1.4.2) has shown increasing $NO_2 + NO_Y$ concentrations since 2011, which currently

remains unexplained but may be associated with the slowing of NO_X emissions decreases or increased background NO_X (Brandt et al., 2016).

California has also experienced dramatic decreases in average annual NO_X concentrations over the past decades. Surface NO_2 concentrations decreased by 29% from 2005 to 2010 in Los Angeles, CA (Huang et al., 2014) and 43% in southern California from 2003 to 2013 (Lamsal et al., 2015), despite increased population size and vehicle use. Similar to New York, the largest decreases were in urban areas such as the Los Angeles Basin (Lurmann et al., 2015; Huang et al., 2014) and in the East Bay region of Northern California (Civerolo et al., 2017; Su et al., 2015). The Central Valley of California also experienced a 37% decrease in NO_2 concentrations from 2005 to 2013 (Lamsal et al., 2015). Because NO_X can be a precursor for both pNO_3^- (a component of $PM_{2.5}$) and O_3, these NO_X reductions also have resulted in decreases in these in these and other pollutants (Pusede et al., 2016). Table 1-6 summarizes regional long-term trends based on network monitoring data from 2010 and 2023.

Table 1-66 Regional trends in annual 98th percentile of daily max 1-hour average NO_2 concentrations at United States monitoring network stations

	Number of Stations	2010 (ppb)	2023 (ppb)	% Decrease
Ohio Valley	9	48	37	-22%
Upper Midwest	5	32	25	-22%
Northeast	22	50	40	-19%
Southeast	14	44	33	-26%
South	34	39	30	-23%
Southwest	17	45	37	-17%
West	43	47	36	-24%
Northern Rockies/Plains	17	22	15	-34%

List of abbreviations in alphabetical order: NO_2 = nitrogen dioxide; ppb = parts per billion.
Source: U.S. EPA (2024c). Copyright permission pending.

At a handful of rural stations, long-term NO_2 levels increased 10 to 30% from 2005 to 2014 (Duncan et al., 2016). NO_2 levels increased in the Permian Basin in West Texas, in Eagle Ford shale areas of South Texas, in the Williston Basin of western North Dakota, and in other locations in Utah and Colorado (see Section 1.5.1) (Dix et al., 2020). Increases in NO_X emissions in these locations are associated with oil and natural gas operations, including flaring and the consumption of fossil fuels by heavy machinery and vehicles (Duncan et al., 2016). NO_2 concentrations at these stations can be more than 5-times higher than NO_2 concentrations upwind of these stations (Goldberg et al., 2021a). Interestingly, the Marcellus Shale region of Pennsylvania has, on average, not shown an increase in NO_2

concentrations, even though large emissions can be seen using satellites (Dix et al., 2022). This may be due to masking of NO_2 increases in western Pennsylvania by dramatic NO_2 reductions in the northeastern United States (Duncan et al., 2016).

1.5.5 Seasonal, Diurnal, Weekday, and Weekend Temporal Trends

The 2016 Oxides of Nitrogen ISA synthesized data on seasonal and diurnal NO_2 concentration patterns, reporting considerably higher NO_2 concentrations in winter and at night (U.S. EPA, 2016; Vette et al., 2013; Polidori and Fine, 2012; Monn et al., 1997). Seasonal variability in 24-hour average NO_2 concentrations were described in the 2016 Oxides of Nitrogen ISA (U.S. EPA, 2016; Monn et al., 1997), which reported strong NO_2 seasonal variability with higher concentrations in winter and lower concentrations in summer. Recent data from 2021 to 2023 show similar trends for both the MDA1 and the DA24 metrics (see Table 1-7). Mean winter and summer concentrations for the MDA1 metric were 20.2 ppb and 13.2 ppb, respectively. For the DA24 metric, mean winter and summer concentrations were 10.3 ppb and 6.0 ppb, respectively. Similar trends were reported by Novotny et al. (2011) for hourly concentrations in 2006, ranging from a 14.0 ppb national winter median to an 8.3 ppb national summer median. These seasonal differences showing higher concentrations in winter than summer are consistent with emissions data from satellite emissions data (see Section 1.2.2) as well as from highway vehicle emissions and near road observations (see Section 1.2.3), as expected considering that highway vehicles are the greatest NO_X source, especially in highly populated areas (see Section 1.2.3). They are also consistent with seasonal variations in atmospheric lifetimes (see Section 1.3). TROPOMI satellite data show that NO_2 concentrations are also higher when temperatures exceeded 32°C than on days when temperatures are between 26 to 32°C (Goldberg et al., 2021b).

Table 1-77 National distribution of NO_2 concentrations by season for data reported to Air Quality Systems from 2021 to 2023

Metric	Season	N.stations	N.obs	Mean	SD	Min	P1	P5	P10	P25	P50	P75	P90	P95	P98	P99	Max	Max.station
MDA1	All	406	418,695	16.7	12.2	-3.0	0.7	1.8	3.0	6.4	14.1	24.6	34.3	39.8	45.6	49.7	315.3	201950001
MDA1	Winter	394	100,944	20.2	13.1	-1.0	0.7	2.0	3.9	9.0	19.0	29.6	38.1	42.9	48.7	53.0	109.2	295100094
MDA1	Spring	392	103,636	15.9	12.2	-2.0	0.6	1.5	2.5	5.5	13.0	23.7	34.0	39.4	45.1	48.9	113.0	490210005
MDA1	Summer	395	103,747	13.2	9.9	-1.2	0.8	1.8	2.8	5.3	10.8	18.6	27.2	32.9	39.2	43.2	119.1	060010015
MDA1	Autumn	394	102,645	17.7	12.3	-3.0	0.7	1.8	3.0	7.4	15.7	25.7	35.0	40.4	46.3	50.5	315.3	201950001
DA24	All	404	418,695	7.9	6.9	-3.3	0.1	0.7	1.3	2.8	5.9	11.0	17.4	21.8	27.1	30.8	64.1	060374008
DA24	Winter	394	100,944	10.3	8.1	-1.8	0.1	0.9	1.7	4.0	8.4	14.7	21.6	26.2	31.6	35.3	64.1	060374008
DA24	Spring	392	103,636	6.9	6.0	-2.3	0.1	0.6	1.1	2.5	5.0	9.6	15.3	19.2	23.9	27.0	57.7	060374008
DA24	Summer	395	103,747	6.0	5.1	-1.9	0.1	0.7	1.2	2.4	4.5	8.0	12.8	16.2	20.7	24.1	53.6	530330030
DA24	Autumn	394	102,645	8.5	7.1	-3.3	0.1	0.7	1.3	3.2	6.6	12.0	18.4	22.7	27.8	31.3	62.0	060374008

List of abbreviations in alphabetical order: N.stations = number of stations; N.obs = number of observations; SD = standard deviation; min = minimum; P1, P5, P10, P25, P50, P90, P95, P98, P99 = 1st, 5th, 10th, 25th, 50th, 90th, 95th, 98th, 99th percentiles; max = maximum; max.station = AQS ID number for the monitoring station corresponding to the observation in the max column.

Note: Summary statistics are based on the two daily NO_2 NAAQS metrics: the daily maximum 1 hour (MDA1) metric and the daily 24-hour average (DA24) metric. These statistics are presented for year-round (all) and each season (winter = Dec–Feb, spring = Mar–May, summer = Jun–Aug, autumn = Sep–Nov). Concentrations listed in ppb.

Source: U.S. EPA (2023d). Copyright permission pending.

Improved satellite technology provides opportunities for further research on weekly concentration patterns in urban settings. Using TROPOMI, Goldberg et al. (2019) estimated total NO_X urban emissions in Chicago, IL, to be 45% higher on weekdays than weekends, a pattern reported in the 2016 Oxides of Nitrogen ISA (U.S. EPA, 2016; Choi et al., 2012; Pollack et al., 2012). More recent research has shown larger differences in NO_X concentrations between weekends and weekdays in commercial versus residential areas of Chicago, IL (de Foy, 2018). Other studies have reported 16 to 60% lower NO_2 concentrations on Saturdays and Sundays compared to weekdays in urban areas (e.g., Los Angeles, CA) (Wang et al., 2022; Goldberg et al., 2021b; de Foy et al., 2016; Valin et al., 2014) and up to 30% lower NO_2 concentrations in the San Joaquin Valley in California (de Foy and Schauer, 2019). Weekend NO_X concentrations were lower than on weekdays in Pittsburgh, PA (Li et al., 2020) and in Fresno, CA (de Foy et al., 2020), consistent with lower heavy-duty diesel traffic on weekends. More recent research suggests that the weekday-weekend NO_X cycle is weakening over U.S. and European cities, which the authors attribute to declining anthropogenic emissions, the growing importance of background NO_2, and longer NO_2 lifetimes due to lower OH and other oxidant levels (see Section 1.3) (Laughner et al., 2019; Stavrakou et al., 2020). In the United States, 16 out of 51 nonattainment areas for O_3 showed that the day-of-week trend was disappearing during summer months (May – September), which may indicate the increasing importance of sources without day-of-week activity patterns, such as soil NO emissions (see Section 1.2.7.1) (Simon et al., 2024).

Hourly and daily data often exhibit distinct patterns, with highest NO_X concentrations during both morning and evening rush hours, or sometimes midday if heavy-duty diesel vehicles are a particularly important source (Toro et al., 2021; Mukerjee et al., 2019; U.S. EPA, 2016). In Chicago, IL, U.S., AQS data from 2005 to 2016 showed that NO_X emissions peaked mid-morning and stayed high until after the evening rush hour, with only a slight decrease in the early afternoon (de Foy, 2018). In some urban and suburban locations, NO_X concentrations have two daily peaks, with a midday minimum that may be associated with lower traffic emissions, higher O_3 concentrations, and a deeper mixed layer that supports enhanced atmospheric mixing (Squizzato et al., 2018). In a Pittsburgh, PA, U.S., tunnel study, NO_X concentrations had one peak near midday, which was consistent with the peak volume of heavy-duty diesel vehicles (Li et al., 2020).

1.5.6 Copollutant Associations

The relationship between NO_2 and copollutants provides useful context for understanding the degree to which effects reported in health studies are specifically associated with NO_2 versus other pollutants that co-occur over space and time. For example, since O_3 is a secondary pollutant formed in the atmosphere from precursor emissions, its correlation with primary pollutants such as NO_X can vary substantially by location (U.S. EPA, 2013b). Copollutant relationships are influenced by season, time of day, meteorology, source environment, and other factors. Since early air pollution research in the United

States in the 1950s, it has been well established that pollutant mixtures can be broadly classified into cold and warm weather types. Cold season mixtures are generally characterized by primary combustion emissions and low oxidant levels (Finlayson-Pitts and Pitts, 2000), while warm season pollutant mixtures are more characterized by higher concentrations of oxidants, leading to parallel production of both $PM_{2.5}$ and O_3 (U.S. EPA, 2004). Such differences also have been recently documented in an extensive database of air pollutant measurements in China, which shows negative associations between particulate matter and O_3 in colder regions and in winter, and positive associations in warmer regions and in summer (Zhu et al., 2019a).

These two distinct types of air pollution mixtures reflect complex relationships between NO_X and its copollutants, $PM_{2.5}$ and O_3. NO_X and $PM_{2.5}$ are both components of fresh combustion emissions, but NO_X is also a precursor for O_3 (see Section 1.3.1). As a result, there is some degree of association between NO_X and both $PM_{2.5}$ and O_3. The chemistry of O_3 formation typically results in successive concentration peaks throughout the day, occurring first for NO in the morning, followed by NO_2 later in the morning, and finally O_3 in the afternoon, a pattern that has been observed since the earliest research on O_3 formation chemistry (Finlayson-Pitts and Pitts, 2000). The result is a complex dynamic, with the same data showing positive associations between maximum daily NO_2 and O_3 concentrations and negative associations between hourly NO_2 and O_3 concentrations.

National scale associations between 1-hour maximum NO_2 concentrations, eight-hour daily maximum O_3, and daily average $PM_{2.5}$ concentrations from mostly urban locations were described in detail in the 2013 ISA for Ozone (U.S. EPA, 2013b) and the 2009 ISA for PM (U.S. EPA, 2009). A wide range of correlations was observed, but clearer patterns emerged when data were stratified by season. There was considerable spread in the copollutant correlations in all seasons, but on average positive associations (Pearson correlation coefficient, $\rho>0.3$) were reported between $PM_{2.5}$ and NO_2 in all seasons (U.S. EPA, 2009), and between O_3 and NO_2 in summer (U.S. EPA, 2013b). Positive associations with NO_2 were strongest in winter for $PM_{2.5}$ (Pearson $\rho>0.6$) (U.S. EPA, 2013b), but positive associations between NO_2 and O_3 only occurred in summer (Pearson $\rho>0.3$) and were negative in winter (Pearson $\rho<-0.3$). These observations are consistent with the characteristics of cold season and warm season air pollution mixtures, with the strongest positive associations between NO_2 and $PM_{2.5}$ under cold season conditions with fresh emissions sources, but positive associations between NO_2 and both O_3 and $PM_{2.5}$ under warm season conditions with high oxidant levels. These trends result from an increased number of stagnation events in colder months, as well as potential concurrent increases in NO_2 and $PM_{2.5}$ emissions from motor vehicles at colder temperatures (U.S. EPA, 2009). As explained in the 2013 Ozone ISA (U.S. EPA, 2013b), photochemical production of O_3 during winter is much lower than during summer and O_3 comes mainly from stratospheric intrusions higher up in the atmosphere, where $PM_{2.5}$ concentrations are much lower. On days with relatively low pollution, this can lead to high concentrations of O_3 and lower concentrations of primary pollutants such as NO, particularly at higher elevations where stratospheric intrusions occur more frequently. On days with elevated NO and $PM_{2.5}$, the intruding O_3 is readily titrated

by NO near the surface. These processes result in negative correlations between O_3 and primary pollutants like $PM_{2.5}$ and NO_X during the winter.

In the 2016 Oxides of Nitrogen ISA that followed these documents, ambient copollutant data were not analyzed by comparing NAAQS indicators. Instead, NO_2 copollutant associations were more thoroughly explored in a body of exposure studies relevant for understanding confounding, and copollutant information was covered in the Exposure Chapter of the 2016 Oxides of Nitrogen ISA. A literature synthesis of more than 50 short-term exposure studies indicated that NO_2 was more strongly associated with various PM metrics or components averaged over periods of less than a day than for longer periods but was often negatively associated with O_3 (U.S. EPA, 2016). However, stronger associations between NO_2 and O_3 were observed in summer than in other seasons (U.S. EPA, 2016). Table 1-8 provides an update of seasonally stratified associations between daily maximum 1-hour average NO_2 and maximum daily average eight-hour O_3 on the same day for the Los Angeles, CA Main Street AQS monitoring results.

Table 1-88 Association between maximum daily 1-hour average NO_2 concentrations and maximum daily average 8-hour O_3, July 2022 to June 2023

Season	Pearson correlation coefficient
July, August, September 2022	0.52
October, November, December 2022	-0.14
January, February, March 2023	-0.06
April, May, June 2023	0.49

List of abbreviations in alphabetical order: NO_2 = nitrogen dioxide; O_3 = ozone.
Note: Concentrations reported at the Los Angeles, CA, U.S., Main Street air monitoring station.
Source: Data from monitoring station #6-37-1103 (https://www.epa.gov/aqs).

Recent U.S. studies are generally consistent with earlier national scale observations of associations between NO_2 and its copollutants. For example, similar to national patterns reported in the 2009 ISA for PM (U.S. EPA, 2009), a comparison of NO_2 and copollutant concentrations between November 2013 to May 2019 in Fairbanks, AK resulted in positive associations between NO_2 and $PM_{2.5}$ in all seasons and a year-round Spearman correlation coefficient of 0.72 (Ye and Wang, 2020). Similar to national scale O_3 statistics in the 2013 ISA for Ozone (U.S. EPA, 2013b), associations between O_3 and NO_2 varied with season, with a positive association occurring only in summer (Spearman $\rho = 0.41$). Negative associations occurred in all other seasons (Spearman $\rho = -0.35$ to -0.25), instead of just winter as observed in the 2013 ISA for Ozone national scale comparison, because Spring and Fall in Fairbanks, AK is more similar to winter in other regions of the United States. In the Cache Valley of Utah and Idaho—a region that has been in $PM_{2.5}$ nonattainment and that was discussed in detail in the 2020 Ozone ISA (U.S. EPA, 2020a) because it is prone to winter O_3 episodes—an even stronger association was observed between NO_2 and $PM_{2.5}$ based on hourly concentrations (Spearman $\rho = 0.75$) (Mukerjee et al., 2019).

Associations were stronger still between $PM_{2.5}$ and NO_X (Spearman $\rho = 0.80$) and $PM_{2.5}$ and NO_Y (Spearman $\rho = 0.88$) (Mukerjee et al., 2019).

These stronger associations between $PM_{2.5}$ and NO_2 relative to national patterns could reflect the proximity and predominance of the same source for both NO_X and $PM_{2.5}$. A strong negative association was observed between NO_2 and O_3 (Spearman $\rho = -0.92$), but there were no winter O_3 episodes during the study period, and O_3 concentrations were generally low and typical of winter levels in other U.S. regions. The strong negative association between hourly NO_2 and O_3 concentrations is consistent with typical diurnal patterns for concentrations of NO_2 and O_3 peaking at different times of day. It is also consistent with the positive associations observed for national scale results described in the previous paragraph, which compared daily maximum 8-hour O_3 concentrations with hourly maximum NO_2 concentrations.

Outside of the United States, there have been a few large-scale efforts to investigate relevant copollutant associations. Xie et al. (2015) compiled statistics on multiple pollutants from 286 monitoring stations across 31 Chinese provincial capital cities for a 12-month period in 2013 to 2014. Across all cities, they reported a mean Pearson correlation coefficient of 0.498 between NO_2 and $PM_{2.5}$, with higher means for the largest cities (e.g., 0.686 for Beijing, 0.594 for Shanghai). Eeftens et al. (2015) compared 2-year mean NO_2 concentrations to 2-year mean $PM_{2.5}$ concentrations for 40 stations in each of eight study areas in Switzerland, reporting a correlation coefficient of $r^2 = 0.42$ ($r = 0.65$). These results correspond with a previous study by Eeftens et al. (2012) that compared annual mean NO_2 and $PM_{2.5}$ concentrations for all of Europe, reporting a correlation coefficient of $r^2 = 0.51$ ($r = 0.71$). These results are similar to the results from Xie et al. (2015) for China, the winter data reported in the 2009 Particulate Matter ISA (U.S. EPA, 2009), and recent U.S. studies in Fairbanks, AK and the Cache Valley, UT-ID reported in this section.

Fires can contribute additional complexity to copollutant relationships. In the western United States, Kalashnikov et al. (2022) observed increasing co-occurrence of extreme O_3 and $PM_{2.5}$ concentrations associated with increasing prevalence of multi-day heat waves and wildfires. Across 18 U.S. cities, PM and O_3 were consistently elevated on days influenced by wildfire smoke. NO_X increases due to wildfire smoke were smaller and inconsistent, probably because (1) NO_X contributions from wildfire smoke are more modest in comparison to general urban variability than is the case for particulate matter, and (2) fire NO_X emissions are highly variable (Buysse et al., 2019). NO/NO_2 concentration ratios were also lower on days with wildfire smoke, possibly because of additional atmospheric oxidants present in the smoke (Buysse et al., 2019). As the number of days with fire influence increases, some changes in the statistical relationships between ambient concentrations of NO_2, O_3, and $PM_{2.5}$ could occur.

In addition to the long-term multipollutant comparison studies summarized here, worldwide COVID-19 lockdown periods provided a unique opportunity for a more intensive study of the relationships between NO_2 and copollutant concentrations at a variety of locations. The impact of COVID-19 lockdown periods on NO_2 concentrations is described in detail in Section 1.2.8. Relationships between copollutants during COVID-19 lockdown periods have also been studied, and there are

numerous reports of concurrent decreases in NO_2 and $PM_{2.5}$ concentrations but increases in O_3 concentrations (Sokhi et al., 2021).

Overall, there is considerable previous and more recent evidence for a moderate positive association between NO_2 and $PM_{2.5}$ that is stronger in winter than summer, as well as for a moderate association between NO_2 and O_3 that is positive in summer and negative in winter.

1.6 Conclusions

The research described in this chapter provides useful context for sources, characterization, quantification, and spatial extent of NO_2, additional oxides of nitrogen, and copollutants. Overall, anthropogenic NO_X emissions in the United States have decreased by roughly 70% since 2002, from approximately 25,000 kTon/year to approximately 7,000 kTon/year. Emissions decreases have been accompanied by changes in the relative contributions of different emissions sources. Although mobile sources and EGUs remain the greatest contributors to U.S. NO_X emissions, agricultural activities and fires are potentially responsible for an increasing fraction on a national scale and can dominate short-term and local scale emissions. Major developments in understanding chemical mechanisms since the 2016 Oxides of Nitrogen ISA (U.S. EPA, 2016) include particulate nitrate (pNO_3^-) as sources of HONO and NO_X. These updates, along with improved treatment of vertical mixing, have been incorporated into chemical transport models, which thus are more able to accurately estimate ambient NO_X concentrations. Other major developments include advancements in satellite technologies like TROPOMI and TEMPO that include better spatial and temporal variability resolution, to the point where it is now possible to identify neighborhood-scale sources and estimate specific point source emissions.

Ambient NO_2 concentrations also have decreased substantially since 2000. There were no monitoring stations with annual average NO_2 concentrations exceeding 53 ppb. The vast majority (74%) of monitoring stations had annual average NO_2 concentrations less than 10 ppb. Similarly, there were no monitoring stations exceeding 100 ppb. The five stations in the United States with the highest 1-hour concentrations (61 to 71 ppb) were in urban areas of Los Angeles and the Central Valley of California; Denver, CO; and Newark, NJ. NO_2 concentrations were highest in winter and lowest in summer for both MDA1 and DA24 metrics. Urban NO_X was generally higher on weekdays than weekends; hourly data also exhibited distinct patterns, with the highest NO_X concentrations during both morning and evening rush hours. There is some degree of copollutant association between NO_X and both $PM_{2.5}$ and O_3, though it can vary seasonally. Positive associations were reported between $PM_{2.5}$ and NO_2 in all seasons and between O_3 and NO_2 in summer, but associations were negative between NO_2 and O_3 in winter. Together, the information described in this chapter provides important context for the subsequent chapters of this ISA.

1.7 References

Alam, MS; Crilley, LR; Lee, JD; Kramer, LJ; Pfrang, C; Vázquez-Moreno, M; Ródenas, M; Muñoz, A; Bloss, WJ. (2020). Interference from alkenes in chemiluminescent NOx measurements. Atmos Meas Tech 13: 5977-5991. http://dx.doi.org/10.5194/amt-13-5977-2020

Alexander, B; Hastings, MG; Allman, DJ; Dachs, J; Thornton, JA; Kunasek, SA. (2009). Quantifying atmospheric nitrate formation pathways based on a global model of the oxygen isotopic composition (Δ17O) of atmospheric nitrate. Atmos Chem Phys 9: 5043-5056. http://dx.doi.org/10.5194/acp-9-5043-2009

Alexander, B; Sherwen, T; Holmes, CD; Fisher, JA; Chen, Q; Evans, MJ; Kasibhatla, P. (2020). Global inorganic nitrate production mechanisms: comparison of a global model with nitrate isotope observations. Atmos Chem Phys 20: 3859-3877. http://dx.doi.org/10.5194/acp-20-3859-2020

Almaraz, M; Bai, E; Wang, C; Trousdell, J; Conley, S; Faloona, I; Houlton, BZ. (2018). Agriculture is a major source of NOx pollution in California. Sci Adv 4: eaao3477. http://dx.doi.org/10.1126/sciadv.aao3477

Andersen, ST; Carpenter, LJ; Reed, C; Lee, JD; Chance, R; Sherwen, T; Vaughan, AR; Stewart, J; Edwards, PM; Bloss, WJ; Sommariva, R; Crilley, LR; Nott, GJ; Neves, L; Read, K; Heard, DE; Seakins, PW; Whalley, LK; Boustead, GA; Fomba, KW. (2023). Extensive field evidence for the release of HONO from the photolysis of nitrate aerosols. Sci Adv 9: eadd6266. http://dx.doi.org/10.1126/sciadv.add6266

Anderson, DC; Loughner, CP; Diskin, G; Weinheimer, A; Canty, TP; Salawitch, RJ; Worden, HM; Fried, A; Mikoviny, T; Wisthaler, A; Dickerson, RR. (2014). Measured and modeled CO and NOy in DISCOVER-AQ: An evaluation of emissions and chemistry over the eastern US. Atmos Environ 96: 78-87. http://dx.doi.org/10.1016/j.atmosenv.2014.07.004

Anenberg, SC; Mohegh, A; Goldberg, DL; Kerr, GH; Brauer, M; Burkart, K; Hystad, P; Larkin, A; Wozniak, S; Lamsal, L. (2022). Long-term trends in urban NO2 concentrations and associated paediatric asthma incidence: estimates from global datasets. The Lancet Planetary Health 6: e49-e58. http://dx.doi.org/10.1016/S2542-5196(21)00255-2

Anonymous. (2024). Appendix E to Part 58—Probe and Monitoring Path Siting Criteria for Ambient Air Quality Monitoring.

Appel, KW; Bash, JO; Fahey, KM; Foley, KM; Gilliam, RC; Hogrefe, C; Hutzell, WT; Kang, D; Mathur, R; Murphy, BN; Napelenok, SL; Nolte, CG; Pleim, JE; Pouliot, GA; Pye, HOT; Ran, L; Roselle, SJ; Sarwar, G; Schwede, DB; Wong, DC. (2021). The Community Multiscale Air Quality (CMAQ) model versions 5.3 and 5.3.1: System updates and evaluation. GMD 14: 2867-2897. http://dx.doi.org/10.5194/gmd-14-2867-2021

Apte, JS; Messier, KP; Gani, S; Brauer, M; Kirchstetter, TW; Lunden, MM; Marshall, JD; Portier, CJ; Vermeulen, RCH; Hamburg, SP. (2017). High-resolution air pollution mapping with Google street view cars: Exploiting big data [Abstract]. Environ Sci Technol 51: 6999-7008. http://dx.doi.org/10.1021/acs.est.7b00891

Archer C, L; Cervone, G; Golbazi, M; Al Fahel, N; Hultquist, C. (2020). Changes in air quality and human mobility in the USA during the COVID-19 pandemic. Bulletin of atmospheric science and technology 1: 491-514. http://dx.doi.org/10.1007/s42865-020-00019-0

Ayres, BR; Allen, HM; Draper, DC; Brown, SS; Wild, RJ; Jimenez, JL; Day, DA; Campuzano-Jost, P; Hu, W; de Gouw, J; Koss, A; Cohen, RC; Duffey, KC; Romer, P; Baumann, K; Edgerton, E; Takahama, S; Thornton, JA; Lee, BH; Lopez-Hilfiker, FD; Mohr, C; Wennberg, PO; Nguyen, TB; Teng, A; Goldstein, AH; Olson, K; Fry, JL. (2015). Organic nitrate aerosol formation via NO3 + biogenic volatile organic compounds in the southeastern United States. Atmos Chem Phys 15: 13377-13392. http://dx.doi.org/10.5194/acp-15-13377-2015

Baldwin, N; Gilani, O; Raja, S; Batterman, S; Ganguly, R; Hopke, P; Berrocal, V; Robins, T; Hoogterp, S. (2015). Factors affecting pollutant concentrations in the near-road environment. Atmos Environ 115: 223-235. http://dx.doi.org/10.1016/j.atmosenv.2015.05.024

Barrett, SRH; Speth, RL; Eastham, SD; Dedoussi, IC; Ashok, A; Malina, R; Keith, DW. (2015). Impact of the Volkswagen emissions control defeat device on US public health. Environ Res Lett 10: 114005. http://dx.doi.org/10.1088/1748-9326/10/11/114005

Benedict, KB; Prenni, AJ; Carrico, CM; Sullivan, A; Schichtel, BA; Collett, JL, Jr. (2017). Enhanced concentrations of reactive nitrogen species in wildfire smoke. Atmos Environ 148: 8-15. http://dx.doi.org/10.1016/j.atmosenv.2016.10.030

Benish, SE; Bash, JO; Foley, KM; Appel, KW; Hogrefe, C; Gilliam, R; Pouliot, G. (2022). Long-term regional trends of nitrogen and sulfur deposition in the United States from 2002 to 2017. Atmos Chem Phys 22: 12749-12767. http://dx.doi.org/10.5194/acp-22-12749-2022

Berman, JD; Ebisu, K. (2020). Changes in U.S. air pollution during the COVID-19 pandemic. Sci Total Environ 739: 139864. http://dx.doi.org/10.1016/j.scitotenv.2020.139864

Bindle, L; Martin, RV; Cooper, MJ; Lundgren, EW; Eastham, SD; Auer, BM; Clune, TL; Weng, H; Lin, J; Murray, LT; Meng, J; Keller, CA; Putman, WM; Pawson, S; Jacob, DJ. (2021). Grid-stretching capability for the GEOS-Chem 13.0.0 atmospheric chemistry model. GMD 14: 5977-5997. http://dx.doi.org/10.5194/gmd-14-5977-2021

Bishop, GA; Haugen, MJ. (2018). The story of ever diminishing vehicle tailpipe emissions as observed in the Chicago, Illinois area. Environ Sci Technol 52: 7587-7593. http://dx.doi.org/10.1021/acs.est.8b00926

Bishop, GA; Haugen, MJ; McDonald, BC; Boies, AM. (2022). Utah Wintertime Measurements of Heavy-Duty Vehicle Nitrogen Oxide Emission Factors. Environ Sci Technol 56: 1885-1893. http://dx.doi.org/10.1021/acs.est.1c06428

Bishop, GA; Stedman, DH. (2015). Reactive nitrogen species emission trends in three light-/medium-duty United States fleets. Environ Sci Technol 49: 11234-11240. http://dx.doi.org/10.1021/acs.est.5b02392

Boersma, KF; Eskes, HJ; Brinksma, EJ. (2004). Error analysis for tropospheric NO2 retrieval from space. J Geophys Res 109: D04311. http://dx.doi.org/10.1029/2003JD003962

Boersma, KF; Eskes, HJ; Dirksen, RJ; van der A, RJ; Veefkind, JP; Stammes, P; Huijnen, V; Kleipool, QL; Sneep, M; Claas, J; Leitão, J; Richter, A; Zhou, Y; Brunner, D. (2011). An improved tropospheric NO2 column retrieval algorithm for the Ozone Monitoring Instrument. Atmos Meas Tech 4: 1905-1928. http://dx.doi.org/10.5194/amt-4-1905-2011

Bourgeois, I; Peischl, J; Neuman, JA; Brown, SS; Allen, HM; Campuzano-Jost, P; Coggon, MM; Digangi, JP; Diskin, GS; Gilman, JB; Gkatzelis, G; Guo, H; Halliday, HA; Hanisco, TF; Holmes, CD; Huey, LG; Jimenez, JL; Lamplugh, AD; Lee, YR; Ryerson, TB. (2022). Comparison of airborne measurements of NO, NO2, HONO, NOy, and CO during FIREX-AQ. Atmos Meas Tech 15: 4901-4930. http://dx.doi.org/10.5194/amt-15-4901-2022

Bowling, DR; Crosman, ET; Ehleringer, JR; Fasoli, B; Horel, J; Jacques, AA; Leclair-Marzolf, L; Lin, JC; Mitchell, LE. (2018). Monitoring of greenhouse gases and pollutants across an urban area using a light-rail public transit platform. Atmos Environ 187: 9-23. http://dx.doi.org/10.1016/j.atmosenv.2018.05.044

Brandt, RE; Schwab, JJ; Casson, PW; Roychowdhury, UK; Wolfe, D; Demerjian, KL; Civerolo, KL; Rattigan, OV; Felton, HD. (2016). Atmospheric chemistry measurements at Whiteface Mountain, NY: Ozone and reactive trace gases. Aerosol Air Qual Res 16: 873-884. http://dx.doi.org/10.4209/aaqr.2015.05.0376

Bray, CD; Battye, WH; Aneja, VP; Schlesinger, WH. (2021). Global emissions of NH3, NOx, and N2O from biomass burning and the impact of climate change. J Air Waste Manag Assoc 71: 102-114. http://dx.doi.org/10.1080/10962247.2020.1842822

Breuer, MA; Burgard, DA. (2019). Bridge-based remote sensing of NOx emissions from locomotives. Atmos Environ 198: 77-82. http://dx.doi.org/10.1016/j.atmosenv.2018.10.046

Brown, D; Sadiq, R; Hewage, K. (2014). An overview of air emission intensities and environmental performance of grey cement manufacturing in Canada. Clean Tech Environ Pol 16: 1119-1131. http://dx.doi.org/10.1007/s10098-014-0714-y

Burgard, DA; Bria, CRM. (2016). Bridge-based sensing of NOX and SO2 emissions from ocean-going ships. Atmos Environ 136: 54-60. http://dx.doi.org/10.1016/j.atmosenv.2016.04.014

Burley, JD; Bytnerowicz, A; Buhler, M; Zielinska, B; Schweizer, D; Cisneros, R; Schilling, S; Varela, JC; McDaniel, M; Horn, M; Dulen, D. (2016). Air quality at Devils Postpile National Monument, Sierra Nevada Mountains, California, USA. Aerosol Air Qual Res 16: 2315-2332. http://dx.doi.org/10.4209/aaqr.2016.02.0069

Burling, IR; Yokelson, RJ; Akagi, SK; Urbanski, SP; Wold, CE; Griffith, DWT; Johnson, TJ; Reardon, J; Weise, DR. (2011). Airborne and ground-based measurements of the trace gases and particles emitted by prescribed fires in the United States. Atmos Chem Phys 11: 12197-12216. http://dx.doi.org/10.5194/acp-11-12197-2011

Burling, IR; Yokelson, RJ; Griffith, DWT; Johnson, TJ; Veres, P; Roberts, JM; Warneke, C; Urbanski, SP; Reardon, J; Weise, DR; Hao, WM; De Gouw, J. (2010). Laboratory measurements of trace gas emissions from biomass burning of fuel types from the southeastern and southwestern United States. Atmos Chem Phys 10: 11115-11130. http://dx.doi.org/10.5194/acp-10-11115-2010

Burrows, JP; Weber, M; Buchwitz, M; Rozanov, V; Ladstatter-Weissenmayer, A; Richter, A; Debeek, R; Hoogen, R; Bramstedt, K; Eichmann, KU; Eisinger, M. (1999). The Global Ozone Monitoring Experiment (GOME): mission concept and first scientific results. J Atmos Sci 56: 151-175. http://dx.doi.org/10.1175/1520-0469(1999)056<0151:TGOMEG>2.0.CO;2

Buysse, CE; Kaulfus, A; Nair, U; Jaffe, DA. (2019). Relationships between particulate matter, ozone, and nitrogen oxides during urban smoke events in the western US. Environ Sci Technol 53: 12519-12528. http://dx.doi.org/10.1021/acs.est.9b05241

Byun, D; Schere, KL. (2006). Review of the governing equations, computational algorithms, and other components of the models-3 community multiscale air quality (CMAQ) modeling system [Review]. Appl Mech Rev 59: 51-77. http://dx.doi.org/10.1115/1.2128636

Cai, C; Kulkarni, S; Zhao, Z; Kaduwela, AP; Avise, JC; Damassa, JA; Singh, HB; Weinheimer, AJ; Cohen, RC; Diskin, GS; Wennberg, P; Dibb, JE; Huey, G; Wisthaler, A; Jimenez, JL; Cubison, MJ. (2016). Simulating reactive nitrogen, carbon monoxide, and ozone in California during ARCTAS-CARB 2008 with high wildfire activity. Atmos Environ 128: 28-44. http://dx.doi.org/10.1016/j.atmosenv.2015.12.031

Callies; Corpaccioli, E; Eisinger, M; Hahne, A; Lefebvre, A. (2000). GOME-2 – Metop's second-generation sensor for operational ozone monitoring. ESA Bull 102: 28-36.

Campbell, PC; Tong, D; Saylor, R; Li, Y; Ma, S; Zhang, X; Kondragunta, S; Li, F. (2022). Pronounced increases in nitrogen emissions and deposition due to the historic 2020 wildfires in the western US. Sci Total Environ 839: 156130. http://dx.doi.org/10.1016/j.scitotenv.2022.156130

Canty, TP; Hembeck, L; Vinciguerra, TP; Anderson, DC; Goldberg, DL; Carpenter, SF; Allen, DJ; Loughner, CP; Salawitch, RJ; Dickerson, RR. (2015). Ozone and NOx chemistry in the eastern US: evaluation of CMAQ/CB05 with satellite (OMI) data. Atmos Chem Phys 15: 10965-10982. http://dx.doi.org/10.5194/acp-15-10965-2015

Cao, T; Durbin, TD; Russell, RL; Cocker, DR, III; Scora, G; Maldonado, H; Johnson, KC. (2016). Evaluations of in-use emission factors from off-road construction equipment. Atmos Environ 147: 234-245. http://dx.doi.org/10.1016/j.atmosenv.2016.09.042

Carruthers, DJ; Stocker, JR; Ellis, A; Seaton, MD; Smith, SE. (2017). Evaluation of an explicit NOx chemistry method in AERMOD. J Air Waste Manag Assoc 67: 702-712. http://dx.doi.org/10.1080/10962247.2017.1280096

Carslaw, DC; Beevers, SD; Ropkins, K; Bell, MC. (2006). Detecting and quantifying aircraft and other on-airport contributions to ambient nitrogen oxides in the vicinity of a large international airport. Atmos Environ 40: 5424-5434. http://dx.doi.org/10.1016/j.atmosenv.2006.04.062

Chai, J; Dibb, JE; Anderson, BE; Bekker, C; Blum, DE; Heim, E; Jordan, CE; Joyce, EE; Kaspari, JH; Munro, H; Walters, WW; Hastings, MG. (2021). Isotopic evidence for dominant secondary production of HONO in near-ground wildfire plumes. Atmos Chem Phys 21: 13077-13098. http://dx.doi.org/10.5194/acp-21-13077-2021

Chen, LWA; Chien, LC; Li, Y; Lin, G. (2020). Nonuniform impacts of COVID-19 lockdown on air quality over the United States. Sci Total Environ 745: 141105. http://dx.doi.org/10.1016/j.scitotenv.2020.141105

Chen, Q; Edebeli, J; McNamara, SM; Kulju, KD; May, NW; Bertman, SB; Thanekar, S; Fuentes, JD; Pratt, KA. (2019). HONO, particulate nitrite, and snow nitrite at a midlatitude urban site during wintertime. ACS Earth Space Chem 3: 811-822. http://dx.doi.org/10.1021/acsearthspacechem.9b00023

Choi, Y. (2014). The impact of satellite-adjusted NOx emissions on simulated NOx and O-3 discrepancies in the urban and outflow areas of the Pacific and Lower Middle US. Atmos Chem Phys 14: 675-690. http://dx.doi.org/10.5194/acp-14-675-2014

Choi, Y; Kim, H; Tong, D; Lee, P. (2012). Summertime weekly cycles of observed and modeled NOx and O3 concentrations as a function of satellite-derived ozone production sensitivity and land use types over the Continental United States. Atmos Chem Phys 12: 6291-6307. http://dx.doi.org/10.5194/acp-12-6291-2012

Civerolo, KL; Rattigan, OV; Felton, HD; Schwab, JJ. (2017). Changes in gas-phase air pollutants across New York State, USA. Aerosol Air Qual Res 17: 147-166. http://dx.doi.org/10.4209/aaqr.2016.04.0141

Coggon, MM; Veres, PR; Yuan, B; Koss, A; Warneke, C; Gilman, JB; Lerner, BM; Peischl, J; Aikin, KC; Stockwell, CE; Hatch, LE; Ryerson, TB; Roberts, JM; Yokelson, RJ; de Gouw, JA. (2016). Emissions of nitrogen-containing organic compounds from the burning of herbaceous and arboraceous biomass: Fuel composition dependence and the variability of commonly used nitrile tracers. Geophys Res Lett 43: 9903-9912. http://dx.doi.org/10.1002/2016GL070562

Cooper, MJ; Martin, RV; Hammer, MS; Levelt, PF; Veefkind, P; Lamsal, LN; Krotkov, NA; Brook, JR; McLinden, CA. (2022). Global fine-scale changes in ambient NO2 during COVID-19 lockdowns. Nature 601: 380-387. http://dx.doi.org/10.1038/s41586-021-04229-0

Cooper, MJ; Martin, RV; McLinden, CA; Brook, JR. (2020). Inferring ground-level nitrogen dioxide concentrations at fine spatial resolution applied to the TROPOMI satellite instrument. Environ Res Lett 15: 104013. http://dx.doi.org/10.1088/1748-9326/aba3a5

Corbett, JJ; Fischbeck, PS; Pandis, SN. (1999). Global nitrogen and sulfur inventories for oceangoing ships. J Geophys Res Atmos 104: 3457-3470. http://dx.doi.org/10.1029/1998JD100040

Dang, RJ; Jacob, DJ; Shah, VR; Eastham, SD; Fritz, TM; Mickley, LJ; Liu, TJ; Wang, Y; Wang, J. (2023). Background nitrogen dioxide (NO2) over the United States and itsimplications for satellite observations and trends: effects of nitratephotolysis, aircraft, and open fires. Atmos Chem Phys 23: 6271-6284. http://dx.doi.org/10.5194/acp-23-6271-2023

Day, M; Pouliot, G; Hunt, S; Baker, KR; Beardsley, M; Frost, G; Mobley, D; Simon, H; Henderson, BB; Yelverton, T; Rao, V. (2019). Reflecting on progress since the 2005 NARSTO emissions inventory report [Review]. J Air Waste Manag Assoc 69: 1023-1048. http://dx.doi.org/10.1080/10962247.2019.1629363

de Foy, B. (2018). City-level variations in NOx emissions derived from hourly monitoring data in Chicago. Atmos Environ 176: 128-139. http://dx.doi.org/10.1016/j.atmosenv.2017.12.028

de Foy, B; Brune, WH; Schauer, JJ. (2020). Changes in ozone photochemical regime in Fresno, California from 1994 to 2018 deduced from changes in the weekend effect. Environ Pollut 263: 114380. http://dx.doi.org/10.1016/j.envpol.2020.114380

de Foy, B; Lu, Z; Streets, DG. (2016). Impacts of control strategies, the Great Recession and weekday variations on NO2 columns above North American cities. Atmos Environ 138: 74-86. http://dx.doi.org/10.1016/j.atmosenv.2016.04.038

de Foy, B; Lu, Z; Streets, DG; Lamsal, L; Duncan, BN. (2015). Estimates of power plant NOx emissions and lifetimes from OMI NO2 satellite retrievals. Atmos Environ 116: 1-11. http://dx.doi.org/10.1016/j.atmosenv.2015.05.056

de Foy, B; Schauer, JJ. (2019). Changes in speciated PM2.5 concentrations in Fresno, California, due to NOx reductions and variations in diurnal emission profiles by day of week. Elementa Sci Anthropocene 7: 45. http://dx.doi.org/10.1525/elementa.384

de Gouw, JA; McKeen, SA; Aikin, KC; Brock, CA; Brown, SS; Gilman, JB; Graus, M; Hanisco, T; Holloway, JS; Kaiser, J; Keutsch, FN; Lerner, BM; Liao, J; Markovic, MZ; Middlebrook, AM; Min, KE; Neuman, JA; Nowak, JB; Peischl, J; Wolfe, GM. (2015). Airborne measurements of the atmospheric emissions from a fuel ethanol refinery. J Geophys Res Atmos 120: 4385-4397. http://dx.doi.org/10.1002/2015JD023138

de Gouw, JA; Parrish, DD; Frost, GJ; Trainer, M. (2014). Reduced emissions of CO2, NOx, and SO2 from US power plants owing to switch from coal to natural gas with combined cycle technology. Earths Future 2: 75-82. http://dx.doi.org/10.1002/2013EF000196

Decker, ZCJ; Zarzana, KJ; Coggon, M; Min, KE; Pollack, I; Ryerson, TB; Peischl, J; Edwards, P; Dubé, WP; Markovic, MZ; Roberts, JM; Veres, PR; Graus, M; Warneke, C; de Gouw, J; Hatch, LE; Barsanti, KC; Brown, SS. (2019). Nighttime chemical transformation in biomass burning plumes: A box model analysis initialized with aircraft observations. Environ Sci Technol 53: 2529-2538. http://dx.doi.org/10.1021/acs.est.8b05359

Denman, KL; Brasseur, G; Chidthaisong, A; Ciais, P; Cox, PM; Dickinson, RE; Hauglustaine, D; Heinze, C; Holland, E; Jacob, D; Lohmann, U; Ramachandran, S; da Silva Dias, PL; Wofsy, SC; Zhang, X. (2007). Couplings between changes in the climate system and biogeochemistry. In Climate change 2007: The physical science basis (pp. 499-587). New York, NY: Cambridge University Press. http://www.ipcc.ch/publications_and_data/publications_ipcc_fourth_assessment_report_wg1_report_the_physical_science_basis.htm

DeWinter, JL; Brown, SG; Seagram, AF; Landsberg, K; Eisinger, DS. (2018). A national-scale review of air pollutant concentrations measured in the US near-road monitoring network during 2014 and 2015. Atmos Environ 183: 94-105. http://dx.doi.org/10.1016/j.atmosenv.2018.04.003

Di, Q; Amini, H; Shi, L; Kloog, I; Silvern, R; Kelly, J; Sabath, MB; Choirat, C; Koutrakis, P; Lyapustin, A; Wang, Y; Mickley, LJ; Schwartz, J. (2020). Assessing NO2 concentration and model uncertainty with high spatiotemporal resolution across the contiguous United States using ensemble model averaging. Environ Sci Technol 54: 1372-1384. http://dx.doi.org/10.1021/acs.est.9b03358

Diao, L; Roy, A; Czader, B; Pan, S; Jeon, W; Souri, AH; Choi, Y. (2016). Modeling the effect of relative humidity on nitrous acid formation in the Houston area. Atmos Environ 131: 78-82. http://dx.doi.org/10.1016/j.atmosenv.2016.01.053

Dix, B; de Bruin, J; Roosenbrand, E; Vlemmix, T; Francoeur, C; Gorchov-Negron, A; McDonald, B; Zhizhin, MN; Elvidge, C; Veefkind, P; Levelt, P; de Gouw, J. (2020). Nitrogen oxide emissions from US oil and gas production: Recent trends and source attribution. Geophys Res Lett 47: e2019GL085866. http://dx.doi.org/10.1029/2019GL085866

Dix, B; Francoeur, C; Li, M; Serrano-Calvo, R; Levelt, PF; Veefkind, JP; McDonald, BC; de Gouw, J. (2022). Quantifying NOx emissions from US oil and gas production regions using TROPOMI NO2. ACS Earth Space Chem 6: 403-414. http://dx.doi.org/10.1021/acsearthspacechem.1c00387

Doval Miñarro, M; Ballesta, PP; Barberá Rico, J; González Ferradás, E. (2013). Uncertainty models and influence of the calibration span on ambient air measurements of NO2 by chemiluminescence. Environ Sci Process Impacts 15: 512-523. http://dx.doi.org/10.1039/c2em30395g

DSDTT (NIOSH Division of Standards Development and Technology Transfer). (1988). Criteria for a recommended standard: Welding, brazing, and thermal cutting. (DHHS Pub Ser. : No. 88-110). Washington, DC: U.S. Department of Health and Human Services. https://stacks.cdc.gov/view/cdc/19474

Dufour, G; Eremenko, M; Siour, G; Sellitto, P; Cuesta, J; Perrin, A; Beekmann, M. (2022). 24 h evolution of an exceptional HONO plume emitted by the record-breaking 2019/2020 Australian wildfire tracked from space. Atmosphere (Basel) 13: 1485. http://dx.doi.org/10.3390/atmos13091485

Duncan, BN; Lamsal, LN; Thompson, AM; Yoshida, Y; Lu, Z; Streets, DG; Hurwitz, MM; Pickering, KE. (2016). A space-based, high-resolution view of notable changes in urban NOx pollution around the world (2005-2014). J Geophys Res Atmos 121: 976-996. http://dx.doi.org/10.1002/2015JD024121

Duncan, BN; Prados, AI; Lamsal, LN; Liu, Y; Streets, DG; Gupta, P; Hilsenrath, E; Kahn, RA; Nielsen, JE; Beyersdorf, AJ; Burton, SP; Fiore, AM; Fishman, J; Henze, DK; Hostetler, CA; Krotkov, NA; Lee, P; Lin, M; Pawson, S; Ziemba, LD. (2014). Satellite data of atmospheric pollution for US air quality applications: Examples of applications, summary of data end-user resources, answers to FAQs, and common mistakes to avoid. Atmos Environ 94: 647-662. http://dx.doi.org/10.1016/j.atmosenv.2014.05.061

Dunlea, EJ; Herndon, SC; Nelson, DD; Volkamer, RM; San Martini, F; Sheehy, PM; Zahniser, MS; Shorter, JH; Wormhoudt, JC; Lamb, BK; Allwine, EJ; Gaffney, JS; Marley, NA; Grutter, M; Marquez, C; Blanco, S; Cardenas, B; Retama, A; Ramon Villegas, CR; Kolb, CE; Molina, LT; Molina, MJ. (2007). Evaluation of nitrogen dioxide chemiluminescence monitors in a polluted urban environment. Atmos Chem Phys 7: 2691-2704. http://dx.doi.org/10.5194/acp-7-2691-2007

Durmaz, M; Kalender, SS; Ergin, S. (2017). Experimental study on the effects of ultra-low sulfur diesel fuel to the exhaust emissions of a ferry. Fresen Environ Bull 26: 5833-5840.

East, JD; Henderson, BH; Napelenok, SL; Koplitz, SN; Sarwar, G; Gilliam, R; Lenzen, A; Tong, DQ; Pierce, RB; Garcia-Menendez, F. (2022). Inferring and evaluating satellite-based constraints on NOx emissions estimates in air quality simulations. Atmos Chem Phys 22: 15981-16001. http://dx.doi.org/10.5194/acp-22-15981-2022

EC (European Commission). (2024). Global air pollutant emissions - EDGAR v8.1. Brussels, Belgium: Joint Research Centre. Retrieved from https://edgar.jrc.ec.europa.eu/dataset_ap81

Eeftens, M; Phuleria, HC; Meier, R; Aguilera, I; Corradi, E; Davey, M; Ducret-Stich, R; Fierz, M; Gehrig, R; Ineichen, A; Keidel, D; Probst-Hensch, N; Ragettli, MS; Schindler, C; Künzli, N; Tsai, MY. (2015). Spatial and temporal variability of ultrafine particles, NO2, PM2.5, PM2.5 absorbance, PM10 and PMcoarse in Swiss study areas. Atmos Environ 111: 60-70. http://dx.doi.org/10.1016/j.atmosenv.2015.03.031

Eeftens, M; Tsai, MY; Ampe, C; Anwander, B; Beelen, R; Bellander, T; Cesaroni, G; Cirach, M; Cyrys, J; de Hoogh, K; De Nazelle, A; de Vocht, F; Declercq, C; Dėdelė, A; Eriksen, K; Galassi, C; Gražulevičienė, R; Grivas, G; Heinrich, J; Hoek, G. (2012). Spatial variation of PM2.5, PM10, PM2.5 absorbance and PMcoarse concentrations between and within 20 European study areas and the relationship with NO2 - Results of the ESCAPE project. Atmos Environ 62: 303-317. http://dx.doi.org/10.1016/j.atmosenv.2012.08.038

Ekici, S; Sevinc, H. (2022). Understanding a commercial airline company: A case study on emissions and air quality costs. Int J Environ Sci Tech 19: 5139-5154. http://dx.doi.org/10.1007/s13762-021-03471-3

Filigrana, P; Milando, C; Batterman, S; Levy, JI; Mukherjee, B; Adar, SD. (2020). Spatiotemporal variations in traffic activity and their influence on air pollution levels in communities near highways. Atmos Environ 242: 117758. http://dx.doi.org/10.1016/j.atmosenv.2020.117758

Filonchyk, M; Peterson, MP. (2023). NO2 emissions from oil refineries in the Mississippi Delta. Sci Total Environ 898: 165569. http://dx.doi.org/10.1016/j.scitotenv.2023.165569

Finlayson-Pitts, BJ; Pitts, JN, Jr. (2000). Chemistry of the upper and lower atmosphere: Theory, experiments and applications. In Elsevier. San Diego, CA: Academic Press. http://dx.doi.org/10.1016/B978-0-12-257060-5.X5000-X

Finney, DL; Doherty, RM; Wild, O; Young, PJ; Butler, A. (2016). Response of lightning NOx emissions and ozone production to climate change: Insights from the Atmospheric Chemistry and Climate

Model Intercomparison Project. Geophys Res Lett 43: 5492-5500. http://dx.doi.org/10.1002/2016GL068825
Fischer, EV; Jacob, DJ; Yantosca, RM; Sulprizio, MP; Millet, DB; Mao, J; Paulot, F; Singh, HB; Roiger, A; Ries, L; Talbot, RW; Dzepina, K; Pandey Deolal, S. (2014). Atmospheric peroxyacetyl nitrate (PAN): A global budget and source attribution. Atmos Chem Phys 14: 2679-2698. http://dx.doi.org/10.5194/acp-14-2679-2014
Foley, KM; Pouliot, GA; Eyth, A; Aldridge, MF; Allen, C; Appel, KW; Bash, JO; Beardsley, M; Beidler, J; Choi, D; Farkas, C; Gilliam, RC; Godfrey, J; Henderson, BH; Hogrefe, C; Koplitz, SN; Mason, R; Mathur, R; Misenis, C; Possiel, N; Pye, HOT; Reynolds, L; Roark, M; Roberts, S; Schwede, DB; Seltzer, KM; Sonntag, D; Talgo, K; Toro, C; Vukovich, J; Xing, J; Adams, E. (2023). 2002-2017 anthropogenic emissions data for air quality modeling over the United States. Data in Brief 47: 109022. http://dx.doi.org/10.1016/j.dib.2023.109022
Fox, GA. (1995). Tinkering with the tinkerer: pollution versus evolution. Environ Health Perspect 103: 93-100. http://dx.doi.org/10.2307/3432418
Frederickson, LB; Sidaraviciute, R; Schmidt, JA; Hertel, O; Johnson, MS. (2022). Are dense networks of low-cost nodes really useful for monitoring air pollution? A case study in Staffordshire. Atmos Chem Phys 22: 13949-13965. http://dx.doi.org/10.5194/acp-22-13949-2022
Galib, M; Limmer, DT. (2021). Reactive uptake of N2O5 by atmospheric aerosol is dominated by interfacial processes. Science 371: 921-925. http://dx.doi.org/10.1126/science.abd7716
Gantt, B; Owen, RC; Watkins, N. (2021). Characterizing nitrogen oxides and fine particulate matter near major highways in the United States using the national near-road monitoring network. Environ Sci Technol 55: 2831-2838. http://dx.doi.org/10.1021/acs.est.0c05851
Gaston, CaJ; Prospero, JoM; Foley, Kr; Pye, HaOT; Custals, Li; Blades, Ed; Sealy, Pe; Christie, JaA. (2024). Diverging trends in aerosol sulfate and nitrate measured in the remote North Atlantic in Barbados are attributed to clean air policies, African smoke, and anthropogenic emissions. Atmos Chem Phys 24. http://dx.doi.org/10.5194/acp-24-8049-2024
Gaston, CJ; Thornton, JA. (2016). Reacto-diffusive length of N2O5 in aqueous sulfate- and chloride-containing aerosol particles. J Phys Chem A 120: 1039-1045. http://dx.doi.org/10.1021/acs.jpca.5b11914
Gaston, CJ; Thornton, JA; Ng, NL. (2014). Reactive uptake of N2O5 to internally mixed inorganic and organic particles: The role of organic carbon oxidation state and inferred organic phase separations. Atmos Chem Phys 14: 5693-5707. http://dx.doi.org/10.5194/acp-14-5693-2014
Gately, CK; Hutyra, LR; Peterson, S; Wing, IS. (2017). Urban emissions hotspots: Quantifying vehicle congestion and air pollution using mobile phone GPS data. Environ Pollut 229: 496-504. http://dx.doi.org/10.1016/j.envpol.2017.05.091
Geddes, JA; Martin, RV; Boys, BL; van Donkelaar, A. (2015). Long-Term Trends Worldwide in Ambient NO2 Concentrations Inferred from Satellite Observations. Environ Health Perspect 124: 281-289. http://dx.doi.org/10.1289/ehp.1409567
Geddes, JA; Pusede, SE; Wong, AYH. (2022). Changes in the relative importance of biogenic isoprene and soil NOx emissions on ozone concentrations in nonattainment areas of the United States. J Geophys Res Atmos 127: e2021JD036361. http://dx.doi.org/10.1029/2021JD036361
Gingerysty, NJ; Odame-Ankrah, CA; Jordan, N; Osthoff, HD. (2021). Interference from HONO in the measurement of ambient air NO2 via photolytic conversion and quantification of NO. J Environ Sci 107: 184-193. http://dx.doi.org/10.1016/j.jes.2020.12.011
Goldberg, DL; Anenberg, SC; Griffin, D; McLinden, CA; Lu, Z; Streets, DG. (2020). Disentangling the impact of the COVID-19 lockdowns on urban NO(2)from natural variability. Geophys Res Lett 47: e2020GL089269. http://dx.doi.org/10.1029/2020GL089269
Goldberg, DL; Anenberg, SC; Kerr, GH; Mohegh, A; Lu, Z; Streets, DG. (2021a). TROPOMI NO2 in the United States: A detailed look at the annual averages, weekly cycles, effects of temperature, and correlation with surface NO2 concentrations. Earths Future 9: e2020EF001665. http://dx.doi.org/10.1029/2020EF001665

Goldberg, DL; Anenberg, SC; Lu, Z; Streets, DG; Lamsal, LN; McDuffie, EE; Smith, SJ. (2021b). Urban NOx emissions around the world declined faster than anticipated between 2005 and 2019. Environ Res Lett 16: 115004. http://dx.doi.org/10.1088/1748-9326/ac2c34

Goldberg, DL; Lamsal, L; Loughner, CP; Swartz, WH; Lu, Z; Streets, DG. (2017). A high-resolution and observationally constrained OMI NO2 satellite retrieval. Atmos Chem Phys 17: 11403-11421. http://dx.doi.org/10.5194/acp-17-11403-2017

Goldberg, DL; Lu, Z; Streets, DG; de Foy, B; Griffin, D; McLinden, CA; Lamsal, LN; Krotkov, NA; Eskes, H. (2019). Enhanced capabilities of TROPOMI NO2: Estimating NOx from North American cities and power plants. Environ Sci Technol 53: 12594-12601. http://dx.doi.org/10.1021/acs.est.9b04488

Goldberg, DL; Tao, M; Kerr, GH; Ma, S; Tong, DQ; Fiore, AM; Dickens, AF; Adelman, ZE; Anenberg, SC. (2024). Evaluating the spatial patterns of US urban NOx emissions using TROPOMI NO2. Rem Sens Environ 300: 113917. http://dx.doi.org/10.1016/j.rse.2023.113917

Goldberg, DL; Vinciguerra, TP; Anderson, DC; Hembeck, L; Canty, TP; Ehrman, SH; Martins, DK; Stauffer, RM; Thompson, AM; Salawitch, RJ; Dickerson, RR. (2016). CAMx ozone source attribution in the eastern United States using guidance from observations during DISCOVER-AQ Maryland. Geophys Res Lett 43: 2249-2258. http://dx.doi.org/10.1002/2015GL067332

Gonzalez, DJX; Francis, CK; Shaw, GM; Cullen, MR; Baiocchi, M; Burke, M. (2022). Upstream oil and gas production and ambient air pollution in California. Sci Total Environ 806: 150298. http://dx.doi.org/10.1016/j.scitotenv.2021.150298

Government of Canada. (2024). Canada's Air Pollutant Emissions Inventory Report 2024: chapter 2.3. In Canada's Air Pollutant Emissions Inventory Report 2024. Gatineau, QC: Environment and Climate Change Canada. https://www.canada.ca/en/environment-climate-change/services/air-pollution/publications/emissions-inventory-report-2024/chapter-2-3.html#chapter-2-3

Grange, SK; Farren, NJ; Vaughan, AR; Rose, RA; Carslaw, DC. (2019). Strong temperature dependence for light-duty diesel vehicle NOx emissions. Environ Sci Technol 53: 6587-6596. http://dx.doi.org/10.1021/acs.est.9b01024

Gressent, A; Sauvage, B; Defer, E; Pätz, HW; Thomas, K; Holle, R; Cammas, JP; Nédélec, P; Boulanger, D; Thouret, V; Volz-Thomas, A. (2014). Lightning NOx influence on large-scale NOy and O3 plumes observed over the northern mid-latitudes. Tellus B Chem Phys Meteorol 66: 25544. http://dx.doi.org/10.3402/tellusb.v66.25544

Gritsch, C; Egger, F; Zehetner, F; Zechmeister-Boltenstern, S. (2016). The effect of temperature and moisture on trace gas emissions from deciduous and coniferous leaf litter. Jour Geo Res: Biog 121: 1339-1351. http://dx.doi.org/10.1002/2015JG003223

Gržinić, G; Bartels-Rausch, T; Berkemeier, T; Türler, A; Ammann, M. (2015). Viscosity controls humidity dependence of N2O5 uptake to citric acid aerosol. Atmos Chem Phys 15: 13615-13625. http://dx.doi.org/10.5194/acp-15-13615-2015

Gu, B; Chang, J; Min, Y; Ge, Y; Zhu, Q; Galloway, JN; Peng, C. (2013). The role of industrial nitrogen in the global nitrogen biogeochemical cycle. Sci Rep 3: 2579. http://dx.doi.org/10.1038/srep02579

Gu, J; Chen, L; Yu, C; Li, S; Tao, J; Fan, M; Xiong, X; Wang, Z; Shang, H; Su, L, in. (2017). Ground-Level NO2 Concentrations over China Inferred from the Satellite OMI and CMAQ Model Simulations. Remote Sensing 9: 519. http://dx.doi.org/10.3390/rs9060519

Guaman, M; Roberts-Semple, D; Aime, C; Shin, J; Akinremi, A. (2022). Traffic density and air pollution: Spatial and seasonal variations of nitrogen dioxide and ozone in Jamaica, New York. Atmosphere (Basel) 13: 2042. http://dx.doi.org/10.3390/atmos13122042

Guo, L; Chen, J; Luo, D; Liu, S; Lee, HJ; Motallebi, N; Fong, A; Deng, J; Rasool, QZ; Avise, JC; Kuwayama, T; Croes, BE; FitzGibbon, M. (2020). Assessment of nitrogen oxide emissions and San Joaquin Valley PM2.5 impacts from soils in California. J Geophys Res Atmos 125: e2020JD033304. http://dx.doi.org/10.1029/2020JD033304

Han, C; Yang, W; Wu, Q; Yang, H; Xue, X. (2016). Heterogeneous photochemical conversion of NO2 to HONO on the humic acid surface under simulated sunlight. Environ Sci Technol 50: 5017-5023. http://dx.doi.org/10.1021/acs.est.5b05101

Haugen, MJ; Bishop, GA; Thiruvengadam, A; Carder, DK. (2018). Evaluation of heavy- and medium-duty on-road vehicle emissions in California's south coast air basin. Environ Sci Technol 52: 13298-13305. http://dx.doi.org/10.1021/acs.est.8b03994

He, C; Hong, S; Zhang, L; Mu, H; Xin, AX; Zhou, YQ; Liu, JK; Liu, NJ; Su, YM; Tian, Y; Ke, BQ; Wang, YW; Yang, L. (2021). Global, continental, and national variation in PM2.5, O3, and NO2 concentrations during the early 2020 COVID-19 lockdown. Atmos Pollut Res 12: 136-145. http://dx.doi.org/10.1016/j.apr.2021.02.002

Heland, J; Schlager, H; Richter, A; Burrows, JP. (2002). First comparison of tropospheric NO2 column densities retrieved from GOME measurements and in situ aircraft profile measurements. Geophys Res Lett 29. http://dx.doi.org/10.1029/2002GL015528

Herman, J; Abuhassan, M; Kim, J; Kim, T, uomo; Dubey, M; Raponi, M; Tzortziou, M. (2019a). Underestimation of column NO2 amounts from the OMI satellite compared to diurnally varying ground-based retrievals from multiple PANDORA spectrometer instruments. Atmos Meas Tech 12: 5593-5612. http://dx.doi.org/10.5194/amt-12-5593-2019

Herman, J; Abuhassan, M; Kim, J; Kim, Tu; Dubey, M; Raponi, M; Tzortziou, M. (2019b). Underestimation of column NO2 amounts from the OMI satellite compared to diurnally varying ground-based retrievals from multiple PANDORA spectrometer instruments. Atmos Meas Tech 12: 5593-5612. http://dx.doi.org/10.5194/amt-12-5593-2019

Herman, J; Cede, A; Spinei, E; Mount, G; Tzortziou, M; Abuhassan, N. (2009). NO 2 column amounts from ground-based Pandora and MFDOAS spectrometers using the direct-sun DOAS technique: Intercomparisons and application to OMI validation. J Geophys Res 114: D13307. http://dx.doi.org/10.1029/2009JD011848

Hickman, JE; Wu, SL; Mickley, LJ; Lerdau, MT. (2010). Kudzu (Pueraria montana) invasion doubles emissions of nitric oxide and increases ozone pollution. Proc Natl Acad Sci USA 107: 10115-10119. http://dx.doi.org/10.1073/pnas.0912279107

Hoffman, Al; Bertram, TiH; Holloway, Tr; Harkey, Mo. (2024). Assessment of Nocturnal NO_x Heterogeneous Reaction Mechanisms in the Community Multiscale Air Quality (CMAQ) Model. J Geophys Res Atmos 129. http://dx.doi.org/10.1029/2023jd040290

Hsu, CH; Chan Miller, C; Pierce, RB; Johnson, MS; McDonald, BC; Henze, DK; Mizzi, AP; Abad, GG; He, J; Harkins, C; Naeger, AR; Lyu, C; Liu, X. (2024). An observing system simulation experiment analysis of how well geostationary satellite trace-gas observations constrain NOx emissions in the US. J Geophys Res Atmos 129: e2023JD039323. http://dx.doi.org/10.1029/2023JD039323

Huang, G; Ponder, R; Bond, A; Brim, H; Temeng, A; Naeger, AR; Zhu, L. (2021). Unexpected impact of COVID-19 lockdown on the air quality in the metro Atlanta, USA using ground-based and satellite observations. Aerosol Air Qual Res 21: 210153. http://dx.doi.org/10.4209/aaqr.210153

Huang, Mi; Bowman, KW; Carmichael, GR; Chai, T; Pierce, RB; Worden, JR; Luo, M; Pollack, IB; Ryerson, TB; Nowak, JB; Neuman, JA; Roberts, JM; Atlas, EL; Blake, DR. (2014). Changes in nitrogen oxides emissions in California during 2005-2010 indicated from top-down and bottom-up emission estimates. J Geophys Res Atmos 119: 12928-12952. http://dx.doi.org/10.1002/2014JD022268

Huang, X; Yang, K; Kondragunta, S; Wei, Z; Valin, L; Szykman, J; Goldberg, M. (2022) NO2 retrievals from NOAA-20 OMPS: Algorithm, evaluation, and observations of drastic changes during COVID-19. Atmos Environ 290: 119367. http://dx.doi.org/10.1016/j.atmosenv.2022.119367

Huber, DE; Kort, EA; Steiner, AL. (2024). Soil moisture, soil NOx and regional air quality in the agricultural central United States. J Geophys Res Atmos 129: e2024JD041015. http://dx.doi.org/10.1029/2024jd041015

Huber, DE; Steiner, AL; Kort, EA. (2020). Daily cropland soil NOx emissions identified by TROPOMI and SMAP. Geophys Res Lett 47: e2020GL089949. http://dx.doi.org/10.1029/2020GL089949
Huber, DE; Steiner, AL; Kort, EA. (2023). Sensitivity of modeled soil NOx emissions to soil moisture. J Geophys Res Atmos 128: e2022JD037611. http://dx.doi.org/10.1029/2022JD037611
Hudman, RC; Moore, NE; Mebust, AK; Martin, RV; Russell, AR; Valin, LC; Cohen, RC. (2012). Steps towards a mechanistic model of global soil nitric oxide emissions: Implementation and space based-constraints. Atmos Chem Phys 12: 7779-7795. http://dx.doi.org/10.5194/acp-12-7779-2012
Hudman, RC; Russell, AR; Valin, LC; Cohen, RC. (2010). Interannual variability in soil nitric oxide emissions over the United States as viewed from space. Atmos Chem Phys 10: 9943-9952. http://dx.doi.org/10.5194/acp-10-9943-2010
Islam, SMN; Jackson, PL; Kharol, SK; McLinden, CA. (2020). Impact of natural gas production on nitrogen dioxide and sulphur dioxide over Northeast British Columbia, Canada. Atmos Environ 223: 117231. http://dx.doi.org/10.1016/j.atmosenv.2019.117231
Jaeglé, L; Shah, V; Thornton, JA; Thornton, JA; Lopez-Hilfiker, FD; Lee, BH; McDuffie, EE; Fibiger, D; Brown, SS; Veres, P; Sparks, TL; Ebben, CJ; Wooldridge, PJ; Kenagy, HS; Cohen, RC; Weinheimer, AJ; Campos, TL; Montzka, DD; Digangi, JP; Wolfe, GM; Hanisco, T; Schroder, JC; Campuzano-Jost, P; Day, DA; Jimenez, JL; Sullivan, AP; Guo, H; Weber, RJ. (2018). Nitrogen oxides emissions, chemistry, deposition, and export over the northeast united states during the WINTER aircraft campaign. J Geophys Res Atmos 123: 12368-12393. http://dx.doi.org/10.1029/2018JD029133
Jaffe, DA; Ninneman, M; Chan, HC. (2022). NOx and O3 trends at U.S. non-attainment areas for 1995-2020: influence of COVID-19 reductions and wildland fires on policy-relevant concentrations. J Geophys Res Atmos 127: e2021JD036385. http://dx.doi.org/10.1029/2021JD036385
Jamali, S; Klingmyr, D; Tagesson, T. (2020). Global-scale patterns and trends in tropospheric NO2 concentrations, 2005-2018. Remote Sensing 12: 3526. http://dx.doi.org/10.3390/rs12213526
Jiang, Y; Xue, LK; Shen, HQ; Dong, C; Xiao, ZS; Wang, WX. (2022a). Dominant processes of HONO derived from multiple field observations in contrasting environments. Environ Sci Technol Lett 9: 258-264. http://dx.doi.org/10.1021/acs.estlett.2c00004
Jiang, Z; McDonald, BC; Worden, H; Worden, JR; Miyazaki, K; Qu, Z; Henze, DK; Jones, DBA; Arellano, AF; Fischer, EV; Zhu, LY; Boersma, KF. (2018). Unexpected slowdown of US pollutant emission reduction in the past decade. Proc Natl Acad Sci USA 115: 5099-5104. http://dx.doi.org/10.1073/pnas.1801191115
Jiang, Z; Zhu, R; Miyazaki, K; McDonald, BC; Klimont, Z; Zheng, B; Boersma, KF; Zhang, Q; Worden, H; Worden, JR; Henze, DK; Jones, DBA; Denier van der Gon, HAC; Eskes, H. (2022b). Decadal variabilities in tropospheric nitrogen oxides over United States, Europe, and China. J Geophys Res Atmos 127: e2021JD035872. http://dx.doi.org/10.1029/2021JD035872
Jiao, W; Hagler, G; Williams, R; Sharpe, R; Brown, R; Garver, D; Judge, R; Caudill, M; Rickard, J; Davis, M; Weinstock, L; Zimmer-Dauphinee, S; Buckley, K. (2016). Community Air Sensor Network (CAIRSENSE) project: Evaluation of low-cost sensor performance in a suburban environment in the southeastern United States. Atmos Meas Tech 9: 5281-5292. http://dx.doi.org/10.5194/amt-9-5281-2016
Jin, X; Fiore, AM; Cohen, RC. (2023). Space-based observations of ozone precursors within california wildfire plumes and the impacts on ozone-NOx-VOC chemistry. Environ Sci Technol 57: 14648-14660. http://dx.doi.org/10.1021/acs.est.3c04411
Jin, X; Zhu, Q; Cohen, RC. (2021). Direct estimates of biomass burning NOx emissions and lifetimes using daily observations from TROPOMI. Atmos Chem Phys 21: 15569-15587. http://dx.doi.org/10.5194/acp-21-15569-2021
Johansson, JKE; Mellqvist, J; Samuelsson, J; Offerle, B; Lefer, B; Rappenglück, B; Flynn, J; Yarwood, G. (2014). Emission measurements of alkenes, alkanes, SO2, and NO2 from stationary sources in southeast Texas over a 5 year period using SOF and mobile DOAS. J Geophys Res Atmos 119: 1973-1991. http://dx.doi.org/10.1002/2013JD020485

Jordan, N; Garner, NM; Matchett, LC; Tokarek, TW; Osthoff, HD; Odame-Ankrah, CA; Grimm, CE; Pickrell, KN; Swainson, C; Rosentreter, BW. (2020). Potential interferences in photolytic nitrogen dioxide converters for ambient air monitoring: Evaluation of a prototype. J Air Waste Manag Assoc 70: 753-764. http://dx.doi.org/10.1080/10962247.2020.1769770

Judd, LM; Al-Saadi, JA; Janz, SJ; Kowalewski, MG; Pierce, RB; Szykman, JJ; Valin, LC; Swap, R; Cede, A; Mueller, M; Tiefengraber, M; Abuhassan, N; Williams, D. (2019). Evaluating the impact of spatial resolution on tropospheric NO2 column comparisons within urban areas using high-resolution airborne data. Atmos Meas Tech 12: 6091-6111. http://dx.doi.org/10.5194/amt-12-6091-2019

Judd, LM; Al-Saadi, JA; Szykman, JJ; Valin, LC; Janz, SJ; Kowalewski, MG; Eskes, HJ; Veefkind, JP; Cede, A; Mueller, M; Gebetsberger, M; Swap, R; Pierce, RB; Nowlan, CR; Abad, GG; Nehrir, A; Williams, D. (2020). Evaluating Sentinel-5P TROPOMI tropospheric NO2 column densities with airborne and Pandora spectrometers near New York City and Long Island Sound. Atmos Meas Tech 13: 6113-6140. http://dx.doi.org/10.5194/amt-13-6113-2020

Juncosa Calahorrano, JF; Lindaas, J; O'Dell, K; Palm, BB; Peng, Q; Flocke, F; Pollack, IB; Garofalo, LA; Farmer, DK; Pierce, JR; Collett, JL, Jr.; Weinheimer, A; Campos, T; Hornbrook, RS; Hall, SR; Ullmann, K; Pothier, MA; Apel, EC; Permar, W; Fischer, EV. (2021). Daytime oxidized reactive nitrogen partitioning in western U.S. wildfire smoke plumes. J Geophys Res Atmos 126: e2020JD033484. http://dx.doi.org/10.1029/2020JD033484

Jung, J; Lee, J; Kim, B; Oh, S. (2017). Seasonal variations in the NO2 artifact from chemiluminescence measurements with a molybdenum converter at a suburban site in Korea (downwind of the Asian continental outflow) during 2015-2016. Atmos Environ 165: 290-300. http://dx.doi.org/10.1016/j.atmosenv.2017.07.010

Kalashnikov, DA; Schnell, JL; Abatzoglou, JT; Swain, DL; Singh, D. (2022). Increasing co-occurrence of fine particulate matter and ground-level ozone extremes in the western United States. Sci Adv 8: eabi9386. http://dx.doi.org/10.1126/sciadv.abi9386

Karamchandani, P; Emery, C; Yarwood, G; Lefer, B; Stutz, J; Couzo, E; Vizuete, W. (2015). Implementation and refinement of a surface model for heterogeneous HONO formation in a 3-D chemical transport model. Atmos Environ 112: 356-368. http://dx.doi.org/10.1016/j.atmosenv.2015.01.046

Karner, AA; Eisinger, DS; Niemeier, DA. (2010). Near-roadway air quality: Synthesizing the findings from real-world data. Environ Sci Technol 44: 5334-5344. http://dx.doi.org/10.1021/es100008x

Kaulfus, AS; Nair, U; Jaffe, D; Christopher, SA; Goodrick, S. (2017). Biomass Burning Smoke Climatology of the United States: Implications for Particulate Matter Air Quality. Environ Sci Technol 51: 11731-11741. http://dx.doi.org/10.1021/acs.est.7b03292

Kebabian, PL; Wood, EC; Herndon, SC; Freedman, A. (2008). A practical alternative to chemiluminescence-based detection of nitrogen dioxide: Cavity attenuated phase shift spectroscopy. Environ Sci Technol 42: 6040-6045. http://dx.doi.org/10.1021/es703204j

Kenagy, HS; Sparks, TL; Ebben, CJ; Wooldrige, PJ; Lopez-Hilfiker, FD; Lee, BH; Thornton, JA; McDuffie, EEFDL; Brown, SSMDD; Weinheimer, AJ; Schroder, JC; Campuzano-Jost, P; Day, DA; Jimenez, JL; Dibb, JE; Campos, T; Shah, V; Jaeglé, L; Coehn, RC. (2018). NO(x) lifetime and NO(y) partitioning during WINTER. J Geophys Res Atmos 123: 9813-9827. http://dx.doi.org/10.1029/2018JD028736

Kerr, GH; Goldberg, DL; Harris, MH; Henderson, BH; Hystad, P; Roy, A; Anenberg, SC. (2023). Ethnoracial Disparities in Nitrogen Dioxide Pollution in the United States: Comparing Data Sets from Satellites, Models, and Monitors. Environ Sci Technol 57: 19532-19544. http://dx.doi.org/10.1021/acs.est.3c03999

Kiliç, A; Karabulut, UC; Akdamar, E; Bilgili, L. (2022). Determination of NOx emission factor for diesel engines of recreational boats by on-board measurement. Int J Marit Eng 164: A257-A267. http://dx.doi.org/10.5750/ijme.v164iA3.784

Kim, SW; Heckel, A; Frost, GJ; Richter, A; Gleason, J; Burrows, JP; McKeen, S; Hsie, EY; Granier, C; Trainer, M. (2009). NO2 columns in the western United States observed from space and simulated by a regional chemistry model and their implications for NOx emissions. J Geophys Res Atmos 114: D11301. http://dx.doi.org/10.1029/2008jd011343

Kim, SW; Heckel, A; McKeen, SA; Frost, GJ; Hsie, EY; Trainer, MK; Richter, A; Burrows, JP; Peckham, SE; Grell, GA. (2006). Satellite-observed U.S. power plant NOx emission reductions and their impact on air quality. Geophys Res Lett 33: L22812. http://dx.doi.org/10.1029/2006GL027749

Kim, SW; McKeen, SA; Frost, GJ; Lee, SH; Trainer, M; Richter, A; Angevine, WM; Atlas, E; Bianco, L; Boersma, KF; Brioude, J; Burrows, JP; de Gouw, J; Fried, A; Gleason, J; Hilboll, A; Mellqvist, J; Peischl, J; Richter, D; Rivera, C; Ryerson, T; Te Lintel Hekkert, S; Walega, J; Warneke, C; Weibring, P; Williams, E. (2011). Evaluations of NOx and highly reactive VOC emission inventories in Texas and their implications for ozone plume simulations during the Texas Air Quality Study 2006. Atmos Chem Phys 11: 11361-11386. http://dx.doi.org/10.5194/acp-11-11361-2011

Kleffmann, J; Tapia, GV; Bejan, I; Kurtenbach, R; Wiesen, P. (2013). NO2 measurement techniques: Pitfalls and new developments. In I Barnes; KJ Rudzin'ski (Eds.), Disposal of dangerous chemicals in urban areas and mega cities (pp. 15-28). New York, NY: Springer. http://dx.doi.org/10.1007/978-94-007-5034-0_2

Knowland, KE; Keller, CA; Wales, PA; Wargan, K; Coy, L; Johnson, MS; Liu, J; Lucchesi, RA; Eastham, SD; Fleming, E; Liang, Q; Leblanc, T; Livesey, NJ; Walker, KA; Ott, LE; Pawson, S. (2022). NASA GEOS Composition Forecast Modeling System GEOS-CF v1.0: Stratospheric Composition. J Adv Model Earth Syst 14: e2021MS002852. http://dx.doi.org/10.1029/2021MS002852

Kondragunta, S; Wei, Z; McDonald, BC; Goldberg, DL; Tong, DQ. (2021). COVID-19 induced fingerprints of a new normal urban air quality in the United States. J Geophys Res Atmos 126: e2021JD034797. http://dx.doi.org/10.1029/2021JD034797

Koshak, W; Peterson, H; Biazar, A; Khan, M; Wang, L. (2014). The NASA Lightning Nitrogen Oxides Model (LNOM): Application to air quality modeling. Atmos Res 135: 363-369. http://dx.doi.org/10.1016/j.atmosres.2012.12.015

Krotkov, NA; McLinden, CA; Li, C; Lamsal, LN; Celarier, EA; Marchenko, SV; Swartz, WH; Bucsela, EJ; Joiner, J; Duncan, BN; Boersma, KF; Veefkind, JP; Levelt, PF; Fioletov, VE; Dickerson, RR; He, H; Lu, Z; Streets, DG. (2016). Aura OMI observations of regional SO2 and NO2 pollution changes from 2005 to 2015. Atmos Chem Phys 16: 4605-4629. http://dx.doi.org/10.5194/acp-16-4605-2016

Kuhn, Le; Beirle, St; Kumar, Vi; Osipov, Se; Pozzer, An; Boesch, Ti; Kumar, Ra; Wagner, Th. (2024). On the influence of vertical mixing, boundary layer schemes, and temporal emission profiles on tropospheric NO2 in WRF-Chem - comparisons to in situ, satellite, and MAX-DOAS observations. Atmos Chem Phys 24. http://dx.doi.org/10.5194/acp-24-185-2024

Lal, RM; Ramaswami, A; Russell, AG. (2020). Assessment of the Near-Road (monitoring) Network including comparison with nearby monitors within US cities. Environ Res Lett 15: 114026. http://dx.doi.org/10.1088/1748-9326/ab8156

Lamsal, LN; Duncan, BN; Yoshida, Y; Krotkov, NA; Pickering, KE; Streets, DG; Lu, Z. (2015). U.S. NO2 trends (2005-2013): EPA Air Quality System (AQS) data versus improved observations from the Ozone Monitoring Instrument (OMI). Atmos Environ 110: 130-143. http://dx.doi.org/10.1016/j.atmosenv.2015.03.055

Lamsal, LN; Martin, RV; van Donkelaar, A; Steinbacher, M; Celarier, EA; Bucsela, E; Dunlea, EJ; Pinto, JP. (2008). Ground-level nitrogen dioxide concentrations inferred from the satellite-borne ozone monitoring instrument. J Geophys Res 113: D16308. http://dx.doi.org/10.1029/2007JD009235

Larkin, A; Anenberg, S; Goldberg, DL; Mohegh, A; Brauer, M; Hystad, P. (2023). A global spatial-temporal land use regression model for nitrogen dioxide air pollution. Frontiers in Environmental Science 11: 1125979. http://dx.doi.org/10.3389/fenvs.2023.1125979

Larkin, A; Geddes, JA; Martin, RV; Xiao, Q; Liu, Y; Marshall, JD; Brauer, M; Hystad, P. (2017). Global land use regression model for nitrogen dioxide air pollution. Environ Sci Technol 51: 6957-6964. http://dx.doi.org/10.1021/acs.est.7b01148

Larson, T; Gould, T; Riley, EA; Austin, E; Fintzi, J; Sheppard, L; Yost, M; Simpson, C. (2017). Ambient air quality measurements from a continuously moving mobile platform: Estimation of area-wide, fuel-based, mobile source emission factors using absolute principal component scores. Atmos Environ 152: 201-211. http://dx.doi.org/10.1016/j.atmosenv.2016.12.037

Lassiter, MG; Lin, JJ; Compton, JE; Phelan, J; Sabo, RD; Stoddard, JL; McDow, SR; Greaver, TL. (2023). Shifts in the composition of nitrogen deposition in the conterminous United States are discernable in stream chemistry. Sci Total Environ 881: 163409. http://dx.doi.org/10.1016/j.scitotenv.2023.163409

Laughner, JL; Cohen, RC. (2019). Direct observation of changing NOx lifetime in North American cities. Science 366: 723-727. http://dx.doi.org/10.1126/science.aax6832

Laughner, JL; Zare, A; Cohen, RC. (2016). Effects of daily meteorology on the interpretation of space-based remote sensing of NO2. Atmos Chem Phys 16: 15247-15264. http://dx.doi.org/10.5194/acp-16-15247-2016

Laughner, JL; Zhu, Q; Cohen, RC. (2019). Evaluation of version 3.0B of the BEHR OMI NO2 product. Atmos Meas Tech 12: 129-146. http://dx.doi.org/10.5194/amt-12-129-2019

Lauster, B; Dörner, S; Beirle, S; Donner, S; Gromov, S; Uhlmannsiek, K; Wagner, T. (2021). Estimating real driving emissions from multi-axis differential optical absorption spectroscopy (MAX-DOAS) measurements at the A60 motorway near Mainz, Germany. Atmos Meas Tech 14: 769-783. http://dx.doi.org/10.5194/amt-14-769-2021

Lee, HJ; Koutrakis, P. (2014). Daily Ambient NO^sub 2^ Concentration Predictions Using Satellite Ozone Monitoring Instrument NO^sub 2^ Data and Land Use Regression. Environ Sci Technol 48: 2305.

Lee, HJ; Liu, Y; Chat, RB. (2023). Neighborhood-scale ambient NO2 concentrations using TROPOMI NO2 data: Applications for spatially comprehensive exposure assessment. Sci Total Environ 857: 159342. http://dx.doi.org/10.1016/j.scitotenv.2022.159342

Levelt, PF; Hilsenrath, E; Leppelmeier, GW; Van Den Oord, GHJ; Bhartia, PK; Tamminen, J; De Haan, JF; Veefkind, JP. (2006a). Science objectives of the ozone monitoring instrument. IEEE Trans Geosci Remote Sens 44: 1199-1208. http://dx.doi.org/10.1109/TGRS.2006.872336

Levelt, PF; Ven Den Oord, GHJ; Dobber, MR; Malkki, A; Visser, H; De Vries, J; Stammes, P; Lundell, JOV; Saari, H. (2006b). The ozone monitoring instrument. IEEE Trans Geosci Remote Sens 44: 1093-1101. http://dx.doi.org/10.1109/TGRS.2006.872333

Levy, M; Zhang, R; Zheng, J; Zhang, AL; Xu, We; Gomez-Hernandez, M; Wang, Y; Olaguer, E. (2014). Measurements of nitrous acid (HONO) using ion drift-chemical ionization mass spectrometry during the 2009 SHARP field campaign. Atmos Environ 94: 231-240. http://dx.doi.org/10.1016/j.atmosenv.2014.05.024

Li, CG; Dixit, P; Welch, B; Nigam, A; Soriano, B; Lee, J; Russell, RL; Jiang, Yu; Zhu, HW; Karavalakis, G; Johnson, KC; Cocker, DR; Durbin, TD; Miller, JW. (2021a). Yard tractors: Their path to zero emissions. Transport Res Transport Environ 98: 102972. http://dx.doi.org/10.1016/j.trd.2021.102972

Li, JF; Wang, YH; Zhang, RX; Smeltzer, C; Weinheimer, A; Herman, J; Boersma, KF; Celarier, EA; Long, RW; Szykman, JJ; Delgado, R; Thompson, AM; Knepp, TN; Lamsal, LN; Janz, SJ; Kowalewski, MG; Liu, X; Nowlan, CR. (2021b). Comprehensive evaluations of diurnal NO2 measurements during DISCOVER-AQ 2011: Effects of resolution-dependent representation of NOx emissions. Atmos Chem Phys 21: 11133-11160. http://dx.doi.org/10.5194/acp-21-11133-2021

Li, M; McDonald, BC; McKeen, SA; Eskes, H; Levelt, P; Francoeur, C; Harkins, C; He, J; Barth, M; Henze, DK; Bela, MM; Trainer, M; de Gouw, JA; Frost, GJ. (2021c). Assessment of updated fuel-based emissions inventories over the contiguous United States using TROPOMI NO2 retrievals. J Geophys Res Atmos 126: e2021JD035484. http://dx.doi.org/10.1029/2021JD035484

Li, X; Dallmann, TR; May, AA; Presto, AA. (2020). Seasonal and long-term trend of on-road gasoline and diesel vehicle emission factors measured in traffic tunnels. Appl Sci 10: 2458. http://dx.doi.org/10.3390/app10072458

Lin, M, eiyun; Horowitz, L, arry W.; Hu, L, u; Permar, W, ade. (2024). Reactive nitrogen partitioning enhances the contribution of canadian wildfire plumes to us ozone air quality. Geophys Res Lett 51. http://dx.doi.org/10.1029/2024gl109369

Liu, B; Frey, HC. (2015). Variability in light-duty gasoline vehicle emission factors from trip-based real-world measurements. Environ Sci Technol 49: 12525-12534. http://dx.doi.org/10.1021/acs.est.5b00553

Liu, F; Duncan, BN; Krotkov, NA; Lamsal, LN; Beirle, S; Griffin, D; McLinden, CA; Goldberg, DL; Lu, Z. (2020). A methodology to constrain carbon dioxide emissions from coal-fired power plants using satellite observations of co-emitted nitrogen dioxide. Atmos Chem Phys 20: 99-116. http://dx.doi.org/10.5194/acp-20-99-2020

Liu, J; Lipsitt, J; Jerrett, M; Zhu, Y. (2021a). Decreases in near-road NO and NO2 concentrations during the COVID-19 pandemic in California. Environ Sci Technol Lett 8: 161-167. http://dx.doi.org/10.1021/acs.estlett.0c00815

Liu, S; Valks, P; Beirle, S; Loyola, DG. (2021b). Nitrogen dioxide decline and rebound observed by GOME-2 and TROPOMI during COVID-19 pandemic. Air Qual Atmos Health 14: 1737-1755. http://dx.doi.org/10.1007/s11869-021-01046-2

Liu, SV; Chen, FL; Xue, J. (2019). A meta-analysis of selected near-road air pollutants based on concentration decay rates. Heliyon 5: e02236. http://dx.doi.org/10.1016/j.heliyon.2019.e02236

Liu, X; Huey, LG; Yokelson, RJ; Selimovic, V; Simpson, IJ; Müller, M; Jimenez, JL; Campuzano-Jost, P; Beyersdorf, AJ; Blake, DR; Butterfield, Z; Choi, Y; Crounse, JD; Day, DA; Diskin, GS; Dubey, MK; Fortner, E; Hanisco, TF; Hu, W; Wolfe, GM. (2017a). Airborne measurements of western US wildfire emissions: Comparison with prescribed burning and air quality implications. J Geophys Res Atmos 122: 6108-6129. http://dx.doi.org/10.1002/2016JD026315

Liu, X; Mizzi, AP; Anderson, JL; Fung, IY; Cohen, RC. (2017b). Assimilation of satellite NO2 observations at high spatial resolution using OSSEs. Atmos Chem Phys 17: 7067-7081. http://dx.doi.org/10.5194/acp-17-7067-2017

Lloret, J; Valiela, I. (2016). Unprecedented decrease in deposition of nitrogen oxides over North America: The relative effects of emission controls and prevailing air-mass trajectories. Biogeochemistry 129: 165-180. http://dx.doi.org/10.1007/s10533-016-0225-5

Long, CM; Briggs, NL; Bamgbose, IA. (2019). Synthesis and health-based evaluation of ambient air monitoring data for the Marcellus Shale region [Review]. J Air Waste Manag Assoc 69: 527-547. http://dx.doi.org/10.1080/10962247.2019.1572551

Lorente, A; Boersma, KF; Yu, H; Doerner, S; Hilboll, A; Richter, A; Liu, M; Lamsal, L, okN; Barkley, M; De Smedt, I; Van Roozendael, M; Wang, Y; Wagner, T; Beirle, S; Lin, J, inTai; Krotkov, N; Stammes, P; Wang, P; Eskes, HJ; Krol, M. (2017). Structural uncertainty in air mass factor calculation for NO2 and HCHO satellite retrievals. Atmos Meas Tech 10: 759-782. http://dx.doi.org/10.5194/amt-10-759-2017

Lu, X; Wang, Y; Li, J; Shen, L; Fung, JCH. (2018). Evidence of heterogeneous HONO formation from aerosols and the regional photochemical impact of this HONO source. Environ Res Lett 13: 114002. http://dx.doi.org/10.1088/1748-9326/aae492

Lu, Z; Streets, DG; de Foy, B; Lamsal, LN; Duncan, BN; Xing, J. (2015). Emissions of nitrogen oxides from US urban areas: estimation from Ozone Monitoring Instrument retrievals for 2005-2014. Atmos Chem Phys 15: 10367-10383. http://dx.doi.org/10.5194/acp-15-10367-2015

Lurmann, F; Avol, Ed; Gilliland, F. (2015). Emissions reduction policies and recent trends in Southern California's ambient air quality. J Air Waste Manag Assoc 65: 324-335. http://dx.doi.org/10.1080/10962247.2014.991856

Ma, Q; Wang, T; Liu, C; He, H; Wang, Z; Wang, W; Liang, Y. (2017). SO2 initiates the efficient conversion of NO2 to HONO on MgO surface. Environ Sci Technol 51: 3767-3775. http://dx.doi.org/10.1021/acs.est.6b05724

Maljanen, M; Gondal, Z; Bhattarai, HR. (2016). Emissions of nitrous acid (HONO), nitric oxide (NO), and nitrous oxide (N2O) from horse dung. Agricultural and Food Science 25: 225-229. http://dx.doi.org/10.23986/afsci.59314

Martin, RV; Chance, K; Jacob, DJ; Kurosu, TP; Spurr, RJD; Bucsela, E; Gleason, JF; Palmer, PI; Bey, I; Fiore, AM; Li, Q; Yantosca, RM; Koelemeijer, RBA. (2002). An improved retrieval of tropospheric nitrogen dioxide from GOME. J Geophys Res 107: ACH 9-1-ACH 9-21. http://dx.doi.org/10.1029/2001JD001027

Martin, RV; Jacob, DJ; Chance, KV; Kurosu, TP; Palmer, PI; Evans, MJ. (2003). Global inventory of nitrogen oxide emissions constrained by space-based observations of NO2 columns. J Geophys Res 108D17: 4537. http://dx.doi.org/10.1029/2003JD003453

McDonald, BC; Mckeen, SA; Cui, YY; Ahmadov, R; Kim, SW; Frost, GJ; Pollack, IB; Peischl, J; Ryerson, TB; Holloway, JS; Graus, M; Warneke, C; Gilman, JB; de Gouw, JA; Kaiser, J; Keutsch, FN; Hanisco, TF; Wolfe, GM; Trainer, M. (2018). Modeling ozone in the eastern U.S. using a fuel-based mobile source emissions inventory. Environ Sci Technol 52: 7360-7370. http://dx.doi.org/10.1021/acs.est.8b00778

McDuffie, EE; Fibiger, DL; Dubé, WP; Hilfiker, FL; Lee, BH; Jaeglé, L; Guo, H; Weber, RJ; Reeves, JM; Weinheimer, AJ; Schroder, JC; Campuzano-Jost, P; Jimenez, JL; Dibb, JE; Veres, P; Ebben, C; Sparks, TL; Wooldridge, PJ; Cohen, RC; Brown, SS. (2018a). ClNO2 yields from aircraft measurements during the 2015 WINTER campaign and critical evaluation of the current parameterization. J Geophys Res Atmos 123: 12994-13015. http://dx.doi.org/10.1029/2018JD029358

McDuffie, EE; Fibiger, DL; Dubé, WP; Lopez-Hilfiker, F; Lee, B; Thornton, JA; Shah, V; Jaeglé, L; Guo, H; Weber, RJ; Reeves, JM; Weinheimer, AJ; Schroder, JC; Campuzano-Jost, P; Jimenez, JL; Dibb, JE; Veres, P; Ebben, C; Sparks, TL; Wooldridge, PJ; Cohen, RC; Hornbrook, RS; Apel, EC; Campos, T; Hall, SR; Ullmann, K; Brown, SS. (2018b). Heterogeneous N205 uptake during winter: Aircraft measurements during the 2015 winter campaign and critical evaluation of current parameterizations. J Geophys Res Atmos 123: 4345-4372. http://dx.doi.org/10.1002/2018JD028336

McNamara, SM; Kolesar, KR; Wang, SY; Kirpes, RM; May, NW; Gunsch, MJ; Cook, RD; Fuentes, JD; Hornbrook, RS; Apel, EC; China, S; Laskin, A; Pratt, KA. (2020). Observation of road salt aerosol driving inland wintertime atmospheric chlorine chemistry. ACS Cent Sci 6: 684-694. http://dx.doi.org/10.1021/acscentsci.9b00994

Messier, KP; Chambliss, SE; Gani, S; Alvarez, R; Brauer, M; Choi, JJ; Hamburg, SP; Kerckhoffs, J; LaFranchi, B; Lunden, MM; Marshall, JD; Portier, CJ; Roy, A; Szpiro, AA; Vermeulen, RCH; Apte, JS. (2018). Mapping air pollution with Google Street View cars: Efficient approaches with mobile monitoring and land use regression. Environ Sci Technol 52: 12563-12572. http://dx.doi.org/10.1021/acs.est.8b03395

Miller, SA; Moore, FC. (2020). Climate and health damages from global concrete production. Nat Clim Chang 10: 439-443. http://dx.doi.org/10.1038/s41558-020-0733-0

Miyazaki, K; Eskes, H; Sudo, K; Boersma, KF; Bowman, K; Kanaya, Y. (2017). Decadal changes in global surface NOx emissions from multi-constituent satellite data assimilation. Atmos Chem Phys 17: 807-837. http://dx.doi.org/10.5194/acp-17-807-2017

Monn, C; Carabias, V; Junker, M; Waeber, R; Karrer, M; Wanner, HU. (1997). Small-scale spatial variability of particulate matter <10 mu m (PM10) and nitrogen dioxide. Atmos Environ 31: 2243-2247. http://dx.doi.org/10.1016/S1352-2310(97)00030-7

Mukerjee, S; Smith, L; Long, R; Lonneman, W; Kaushik, S; Colon, M; Oliver, K; Whitaker, D. (2019). Particulate matter, nitrogen oxides, ozone, and select volatile organic compounds during a winter sampling period in Logan, Utah, USA. J Air Waste Manag Assoc 69: 778-788. http://dx.doi.org/10.1080/10962247.2019.1587553

Murray, LT. (2016). Lightning NO_x and Impacts on Air Quality (vol 2, pg 115, 2016). Curr Pollut Rep 2: 134-134. http://dx.doi.org/10.1007/s40726-016-0038-0

Nasem. (2022). Advancing the framework for assessing causality of health and welfare effects to inform National Ambient Air Quality Standards reviews. Washington, DC: National Academies Press. http://dx.doi.org/10.17226/26612

Nawaz, MO; Johnson, J; Yarwood, G; de Foy, B; Judd, L; Goldberg, LD. (2024). An intercomparison of satellite, airborne, and ground-level observations with WRF–CAMx simulations of NO2 columns over Houston, Texas, during the September 2021 TRACER-AQ campaign. Atmos Chem Phys 24. http://dx.doi.org/10.5194/acp-24-6719-2024

Neighbour, EA; Pearson, M; Paul, ND; Wood, WA; Smith, PJ; Johnston, GK; Caporn, SJM. (1990). A small-scale controlled environment chamber for the investigation of the effects of pollutant gases on plants growing at cool or sub-zero temperature. Environ Pollut 64: 155-168. http://dx.doi.org/10.1016/0269-7491(90)90112-P

Neuman, JA; Trainer, M; Brown, SS; Min, KE; Nowak, JB; Parrish, DD; Peischl, J; Pollack, IB; Roberts, JM; Ryerson, TB; Veres, PR. (2016). HONO emission and production determined from airborne measurements over the Southeast US. J Geophys Res Atmos 121: 9237-9250. http://dx.doi.org/10.1002/2016JD025197

Novotny, EV; Bechle, MJ; Millet, DB; Marshall, JD. (2011). National satellite-based land-use regression: NO2 in the United States. Environ Sci Technol 45: 4407-4414. http://dx.doi.org/10.1021/es103578x

Office of Transportation and Air Quality. (2021). Overview of EPA's MOtor Vehicle Emission Simulator (MOVES3) [EPA Report]. (EPA-420-R-21-004). https://www.epa.gov/sites/default/files/2021-03/documents/420r21004.pdf

Oikawa, PY; Ge, C; Wang, J; Eberwein, JR; Liang, LL; Allsman, LA; Grantz, DA; Jenerette, GD. (2015). Unusually high soil nitrogen oxide emissions influence air quality in a high-temperature agricultural region. Nat Commun 6: 8753. http://dx.doi.org/10.1038/ncomms9753

Pacsi, AP; Alhajeri, NS; Zavala-Araiza, D; Webster, MD; Allen, DT. (2013). Regional air quality impacts of increased natural gas production and use in Texas. Environ Sci Technol 47: 3521-3527. http://dx.doi.org/10.1021/es3044714

Pang, K; Zhang, K; Ma, S. (2021). Tailpipe emission characterizations of diesel-fueled forklifts under real-world operations using a portable emission measurement system. J Environ Sci 100: 34-42. http://dx.doi.org/10.1016/j.jes.2020.07.011

Park, JU; Park, JS; Diaz, DS; Gebetsberger, M; Mueller, M; Shalaby, L; Tiefengraber, M; Kim, HJ; Park, SS; Song, CK; Kim, SW. (2022). Spatiotemporal inhomogeneity of total column NO2 in a polluted urban area inferred from TROPOMI and Pandora intercomparisons. GIScience and Remote Sensing 59: 354-373. http://dx.doi.org/10.1080/15481603.2022.2026640

Peng, Q; Palm, BB; Fredrickson, CD; Lee, BH; Hall, SR; Ullmann, K; Campos, T; Weinheimer, AJ; Apel, EC; Flocke, F; Permar, W; Hu, L; Garofalo, LA; Pothier, MA; Farmer, DK; Ku, IT; Sullivan, AP; Collett, JL, Jr.; Fischer, E; Thornton, JA. (2021). Observations and modeling of NOx photochemistry and fate in fresh wildfire plumes. ACS Earth Space Chem 5: 2652-2667. http://dx.doi.org/10.1021/acsearthspacechem.1c00086

Peng, Q; Palm, BB; Fredrickson, CD; Lee, BH; Hall, SR; Ullmann, K; Weinheimer, AJ; Levin, E; DeMott, P; Garofalo, LA; Pothier, MA; Farmer, DK; Fischer, E; Thornton, JA. (2022). Direct constraints on secondary HONO production in aged wildfire smoke from airborne measurements over the western US. Geophys Res Lett 49: e2022GL098704. http://dx.doi.org/10.1029/2022GL098704

Pinardi, G; Van Roozendael, M; Hendrick, F; Theys, N; Abuhassan, N; Bais, A; Boersma, F; Cede, A; Chong, JY; Donner, S; Drosoglou, T; Dzhola, A; Eskes, H; Friess, U; Granville, J; Herman, JR; Holla, R; Hovila, J; Irie, H; Wittrock, F. (2020). Validation of tropospheric NO2 column measurements of GOME-2A and OMI using MAX-DOAS and direct sun network observations. Atmos Meas Tech 13: 6141-6174. http://dx.doi.org/10.5194/amt-13-6141-2020

Pinkerton, JE. (2014). Trends in pulp and paper mill emissions of SO2 and NOx, 1980-2010. TAPPI J 13: 9-14.

Pinto, JP; Dibb, J; Lee, BH; Rappenglück, B; Wood, EC; Levy, M; Zhang, RY; Lefer, B; Ren, XR; Stutz, J; Tsai, C; Ackermann, L; Golovko, J; Herndon, SC; Oakes, M; Meng, QY; Munger, JW; Zahniser, M; Zheng, J. (2014). Intercomparison of field measurements of nitrous acid (HONO) during the SHARP campaign. J Geophys Res Atmos 119: 5583-5601. http://dx.doi.org/10.1002/2013JD020287

Place, BK; Piletic, IR; D'Ambro, EL; Saunders, E; Simon, H; Torres-Vasquez, An; Pleim, J; Schwantes, RH; Coggon, MM; Xu, Lu; Stockwell, WR; Hutzell, WT; Pye, HOT; Appel, KW; Farrell, S; Valin, L; Murphy, BN; Seltzer, KM; Sarwar, G; Allen, C. (2023). Sensitivity of northeastern US surface ozone predictions to the representation of atmospheric chemistry in the Community Regional Atmospheric Chemistry Multiphase Mechanism (CRACMMv1.0). Atmos Chem Phys 23: 9173-9190. http://dx.doi.org/10.5194/acp-23-9173-2023

PNNL (Pacific Northwest National Laboratory). (2021). CEDS v_2021_04_21 gridded emissions data (0.1°). Richland, WA. Retrieved from https://data.pnnl.gov/group/nodes/dataset/13488

Polidori, A; Fine, PM. (2012). Ambient concentrations of criteria and air toxic pollutants in close proximity to a freeway with heavy-duty diesel traffic. Final report. South Coast Air Quality Management District. http://www.aqmd.gov/docs/default-source/air-quality/air-quality-monitoring-studies/near-roadway-study.pdf?sfvrsn=2

Pollack, IB; Ryerson, TB; Trainer, M; Parrish, DD; Andrews, AE; Atlas, EL; Blake, DR; Brown, SS; Commane, R; Daube, BC; De Gouw, JA; Dubé, WP; Flynn, J; Frost, GJ; Gilman, JB; Grossberg, N; Holloway, JS; Kofler, J; Kort, EA; Kuster, WC; Lang, PM; Lefer, B; Lueb, RA; Neuman, JA; Nowak, JB; Novelli, PC; Peischl, J; Perring, AE; Roberts, JM; Santoni, G; Schwarz, JP; Spackman, J. R.; Wagner, NL; Warneke, C; Washenfelder, RA; Wofsy, SC; Xiang, B. (2012). Airborne and ground-based observations of a weekend effect in ozone, precursors, and oxidation products in the California South Coast Air Basin. J Geophys Res 117: D00V05. http://dx.doi.org/10.1029/2011JD016772

Pouyaei, A; Mizzi, A; Choi, Y; Mousavinezhad, S; Khorshidian, N. (2023). Downwind ozone changes of the 2019 Williams Flats wildfire: Insights from WRF Chem/DART assimilation of OMI NO2, HCHO, and MODIS AOD retrievals. J Geophys Res Atmos 128: e2022JD038019. http://dx.doi.org/10.1029/2022JD038019

Present, PSR; Zare, A; Cohen, RC. (2020). The changing role of organic nitrates in the removal and transport of NOx. Atmos Chem Phys 20: 267-279. http://dx.doi.org/10.5194/acp-20-267-2020

Pusede, SE; Duffey, KC; Shusterman, AA; Saleh, A; Laughner, JL; Wooldridge, PJ; Zhang, Q; Parworth, CL; Kim, H; Capps, SL; Valin, LC; Cappa, CD; Fried, A; Walega, J; Nowak, JB; Weinheimer, AJ; Hoff, RM; Berkoff, TA; Beyersdorf, AJ; Cohen, RC. (2016). On the effectiveness of nitrogen oxide reductions as a control over ammonium nitrate aerosol. Atmos Chem Phys 16: 2575-2596. http://dx.doi.org/10.5194/acp-16-2575-2016

Pusede, SE; VandenBoer, TC; Murphy, JG; Markovic, MZ; Young, CJ; Veres, PR; Roberts, JM; Washenfelder, RA; Brown, SS; Ren, X; Tsai, C; Stutz, J; Brune, WH; Browne, EC; Wooldridge, PJ; Graham, AR; Weber, R; Goldstein, AH; Dusanter, S; Cohen, RC. (2015). An atmospheric constraint on the NO2 dependence of daytime near-surface nitrous acid (HONO). Environ Sci Technol 49: 12774-12781. http://dx.doi.org/10.1021/acs.est.5b02511

Pye, HOT; Coggon, MM; Saunders, E; Xu, L; Sarwar, G; Hutzell, WT; Foley, KM; Pouliot, G; Bash, J; Stockwell, WR; Place, BK; Murphy, BN; Seltzer, KM; D'Ambro, EL; Allen, C; Piletic, IR; Farrell, S; Schwantes, RH. (2023). Linking gas, particulate, and toxic endpoints to air emissions

in the Community Regional Atmospheric Chemistry Multiphase Mechanism (CRACMM). Atmos Chem Phys 23: 5043-5099. http://dx.doi.org/10.5194/acp-23-5043-2023
Qi, H; Zhang, G; Xu, L; Yang, L; Wang, Z; Xu, Y; Chen, K. (2024). High-precision photoacoustic nitrogen dioxide gas analyzer for fast dynamic measurement. Anal Chem 96: 1354-1361. http://dx.doi.org/10.1021/acs.analchem.3c05084
Qu, Z; Jacob, DJ; Silvern, RF; Shah, V; Campbell, PC; Valin, LC; Murray, LT. (2021). US COVID-19 shutdown demonstrates importance of background NO2 in inferring NOx emissions from satellite NO2 observations. Geophys Res Lett 48: e2021GL092783. http://dx.doi.org/10.1029/2021GL092783
Rasool, QZ; Zhang, R; Lash, B; Cohan, DS; Cooter, EJ; Bash, JO; Lamsal, LN. (2016). Enhanced representation of soil NO emissions in the Community Multiscale Air Quality (CMAQ) model version 5.0.2. GMD 9: 3177-3197. http://dx.doi.org/10.5194/gmd-9-3177-2016
Rattigan, OV; Carpenter, AC; Civerolo, KL; Felton, HD. (2020). Pollutant measurements at near road and urban background sites in New York, USA. Atmos Pollut Res 11: 859-870. http://dx.doi.org/10.1016/j.apr.2020.01.014
Rawat, P; Crawford, JH; Travis, KR; Judd, LM; Demetillo, MAG; Valin, LC; Szykman, JJ; Whitehill, A; Baumann, E; Hanisco, TF. (2025) Maximizing the use of Pandora data for scientific applications. Atmospheric Measurement Techniques Discussions. http://dx.doi.org/10.5194/amt-2024-114
Reed, C; Evans, MJ; Crilley, LR; Bloss, WJ; Sherwen, T; Read, KA; Lee, JD; Carpenter, LJ. (2017). Evidence for renoxification in the tropical marine boundary layer. Atmos Chem Phys 17: 4081-4092. http://dx.doi.org/10.5194/acp-17-4081-2017
Reed, C; Evans, MJ; Di Carlo, P; Lee, JD; Carpenter, LJ. (2016). Interferences in photolytic NO2 measurements: Explanation for an apparent missing oxidant? Atmos Chem Phys 16: 4707-4724. http://dx.doi.org/10.5194/acp-16-4707-2016
Richmond-Bryant, J; Owen, RC; Graham, S; Snyder, M; McDow, S; Oakes, M; Kimbrough, S. (2017). Estimation of on-road NO2 concentrations, NO2/NOX ratios, and related roadway gradients from near-road monitoring data. Air Qual Atmos Health 10: 611-625. http://dx.doi.org/10.1007/s11869-016-0455-7
Ricker, HM; Leonardi, A; Navea, JG. (2022). Reduction and photoreduction of NO2 in humic acid films as a source of HONO, ClNO, N2O, NO X , and organic nitrogen. ACS Earth Space Chem 6: 3066-3077. http://dx.doi.org/10.1021/acsearthspacechem.2c00282
Rogers, CM; Bowman, KP. (2001). Transport of smoke from the Central American fires of 1998. J Geophys Res Atmos 106: 28357-28368.
Romer, PS; Duffey, KC; Wooldridge, PJ; Allen, HM; Ayres, BR; Brown, SS; Brune, WH; Crounse, JD; de Gouw, J; Draper, DC; Feiner, PA; Fry, JL; Goldstein, AH; Koss, A; Misztal, PK; Nguyen, TB; Olson, K; Teng, AP; Wennberg, PO; Wild, RJ; Zhang, Li; Cohen, RC. (2016). The lifetime of nitrogen oxides in an isoprene-dominated forest. Atmos Chem Phys 16: 7623-7637. http://dx.doi.org/10.5194/acp-16-7623-2016
Romer, PS; Duffey, KC; Wooldridge, PJ; Edgerton, E; Baumann, K; Feiner, PA; Miller, DO; Brune, WH; Koss, AR; de Gouw, JA; Misztal, PK; Goldstein, AH; Cohen, RC. (2018). Effects of temperature-dependent NOx emissions on continental ozone production. Atmos Chem Phys 18: 2601-2614. http://dx.doi.org/10.5194/acp-18-2601-2018
Roy, AA; Adams, PJ; Robinson, AL. (2014). Air pollutant emissions from the development, production, and processing of Marcellus Shale natural gas. J Air Waste Manag Assoc 64: 19-37. http://dx.doi.org/10.1080/10962247.2013.826151
Russell, AR; Valin, LC; Bucsela, EJ; Wenig, MO; Cohen, RC. (2010). Space-based constraints on spatial and temporal patterns of NO(x) emissions in California, 2005-2008. Environ Sci Technol 44: 3608-3615. http://dx.doi.org/10.1021/es903451j
Russell, AR; Valin, LC; Cohen, RC. (2012). Trends in OMI NO2 observations over the United States: Effects of emission control technology and the economic recession. Atmos Chem Phys 12: 12197-12209. http://dx.doi.org/10.5194/acp-12-12197-2012

Russell, HS; Frederickson, LB; Kwiatkowski, S; Emygdio, APM; Kumar, P; Schmidt, JA; Hertel, O; Johnson, MS. (2022). Enhanced ambient sensing environment—A new method for calibrating low-cost gas sensors. Sensors 22: 7238. http://dx.doi.org/10.3390/s22197238

Sadanaga, Y; Takaji, R; Ishiyama, A; Nakajima, K; Matsuki, A; Bandow, H. (2016). Thermal dissociation cavity attenuated phase shift spectroscopy for continuous measurement of total peroxy and organic nitrates in the clean atmosphere. Rev Sci Instrum 87: 074102. http://dx.doi.org/10.1063/1.4958167

Saha, PK; Khlystov, A; Snyder, MG; Grieshop, AP. (2018). Characterization of air pollutant concentrations, fleet emission factors, and dispersion near a North Carolina interstate freeway across two seasons. Atmos Environ 177: 143-153. http://dx.doi.org/10.1016/j.atmosenv.2018.01.019

Sarwar, G; Hogrefe, C; Henderson, BH; Mathur, R; Gilliam, R; Callaghan, AB; Lee, J; Carpenter, LJ. (2024). Impact of particulate nitrate photolysis on air quality over the Northern Hemisphere. Sci Total Environ 917: 170406. http://dx.doi.org/10.1016/j.scitotenv.2024.170406

SCAQMD (South Coast Air Quality Management District). (2021). Air Quality Sensor Performance Evaluation Center (AQ-SPEC). Available online at http://www.aqmd.gov/aq-spec/ (accessed February 11, 2021).

Schoenhardt, A; Altube, P; Gerilowski, K; Krautwurst, S; Hartmann, J; Meier, AC; Richter, A; Burrows, JP. (2015). A wide field-of-view imaging DOAS instrument for two-dimensional trace gas mapping from aircraft. Atmos Meas Tech 8: 5113-5131. http://dx.doi.org/10.5194/amt-8-5113-2015

Sekiya, T; Miyazaki, K; Eskes, H; Sudo, K; Takigawa, M; Kanaya, Y. (2022). A comparison of the impact of TROPOMI and OMI tropospheric NO2 on global chemical data assimilation. Atmos Meas Tech 15: 1703-1728. http://dx.doi.org/10.5194/amt-15-1703-2022

Selimovic, V; Yokelson, RJ; McMeeking, GR; Coefield, S. (2020). Aerosol mass and optical properties, smoke influence on O-3, and high NO3 production rates in a western US city impacted by wildfires. J Geophys Res Atmos 125. http://dx.doi.org/10.1029/2020JD032791

Sha, T; Ma, X; Zhang, H; Janechek, N; Wang, Y; Wang, Y; Castro García, L; Jenerette, GD; Wang, J. (2021). Impacts of soil NOx emission on O3 air quality in rural California. Environ Sci Technol 55: 7113-7122. http://dx.doi.org/10.1021/acs.est.0c06834

Shah, V; Jacob, DJ; Dang, R; Lamsal, LN; Strode, SA; Steenrod, SD; Boersma, KF; Eastham, SD; Fritz, TM; Thompson, C; Peischl, J; Bourgeois, I; Pollack, IB; Nault, BA; Cohen, RC; Campuzano-Jost, P; Jimenez, JL; Andersen, ST; Carpenter, LJ; Evans, MJ. (2023). Nitrogen oxides in the free troposphere: Implications for tropospheric oxidants and the interpretation of satellite NO2 measurements. Atmos Chem Phys 23: 1227-1257. http://dx.doi.org/10.5194/acp-23-1227-2023

Shah, V; Jaeglé, L; Thornton, JA; Lopez-Hilfiker, FD; Lee, BH; Schroder, JC; Campuzano-Jost, P; Jimenez, JL; Guo, H; Sullivan, AP; Weber, RJ; Green, J. R.; Fiddler, MN; Bililign, S; Campos, TL; Stell, M; Weinheimer, AJ; Montzka, DD; Brown, SS. (2018). Chemical feedbacks weaken the wintertime response of particulate sulfate and nitrate to emissions reductions over the eastern United States. Proc Natl Acad Sci USA8110-8115. http://dx.doi.org/10.1073/pnas.1803295115

Sicard, P; Agathokleous, E; Anenberg, SC; De Marco, A; Paoletti, E; Calatayud, V. (2023). Trends in urban air pollution over the last two decades: A global perspective [Review]. Sci Total Environ 858: 160064. http://dx.doi.org/10.1016/j.scitotenv.2022.160064

Silvern, RF; Jacob, DJ; Mickley, LJ; Sulprizio, MP; Travis, KR; Marais, EA; Cohen, RC; Laughner, JL; Choi, S; Joiner, J; Lamsal, LN. (2019). Using satellite observations of tropospheric NO2 columns to infer long-term trends in US NOx emissions: The importance of accounting for the free tropospheric NO2 background. Atmos Chem Phys 19: 8863-8878. http://dx.doi.org/10.5194/acp-19-8863-2019

Simon, He; Hogrefe, Ch; Whitehill, An; Foley, KrM; Liljegren, Je; Possiel, No; Wells, Be; Henderson, BaH; Valin, LuC; Tonnesen, Ga; Appel, KW; Koplitz, Sh. (2024). Revisiting day-of-week ozone

patterns in an era of evolving US air quality. Atmos Chem Phys 24. http://dx.doi.org/10.5194/acp-24-1855-2024
Sobanski, N; Tuzson, B; Scheidegger, P; Looser, H; Kupferschmid, A; Iturrate, M; Pascale, C; Huglin, C; Emmenegger, L. (2021). Advances in High-Precision NO2 Measurement by Quantum Cascade Laser Absorption Spectroscopy. Appl Sci 11: 1222. http://dx.doi.org/10.3390/app11031222
Sokhi, RS; Singh, V; Querol, X; Finardi, S; Targino, AC; Andrade, MF; Pavlovic, R; Garland, RM; Massagué, J; Kong, S; Baklanov, A; Ren, L; Tarasova, O; Carmichael, G; Peuch, VH; Anand, V; Arbilla, G; Badali, K; Beig, G; Zavala, M. (2021). A global observational analysis to understand changes in air quality during exceptionally low anthropogenic emission conditions. Environ Int 157: 106818. http://dx.doi.org/10.1016/j.envint.2021.106818
Song, W; Liu, XY; Houlton, BZ; Liu, CQ. (2022). Isotopic constraints confirm the significant role of microbial nitrogen oxides emissions from the land and ocean environment. National Science Review 9: nwac106. http://dx.doi.org/10.1093/nsr/nwac106
Sonntag, DB; Gao, HO; Morse, P; O'Reilly, M. (2015). Energy consumption and emission rates of highway mowing activities. IEEE Trans Veh Tech 64: 4954-4964. http://dx.doi.org/10.1109/TVT.2014.2381597
Souri, AH; Choi, Y; Jeon, W; Li, X; Pan, S; Diao, L; Westenbarger, DA. (2016). Constraining NOx emissions using satellite NO2 measurements during 2013 DISCOVER-AQ Texas campaign. Atmos Environ 131: 371-381. http://dx.doi.org/10.1016/j.atmosenv.2016.02.020
Squizzato, S; Masiol, M; Rich, DQ; Hopke, PK. (2018). PM2.5 and gaseous pollutants in New York State during 2005-2016: Spatial variability, temporal trends, and economic influences. Atmos Environ 183: 209-224. http://dx.doi.org/10.1016/j.atmosenv.2018.03.045
Stavrakou, T; Müller, JF; Bauwens, M; Boersma, KF; van Geffen, J. (2020). Satellite evidence for changes in the NO2 weekly cycle over large cities. Sci Rep 10: 10066. http://dx.doi.org/10.1038/s41598-020-66891-0
Steinbacher, M; Zellweger, C; Schwarzenbach, B; Bugmann, S; Buchmann, B; Ordóñez, C; Prevot, ASH; Hueglin, C. (2007). Nitrogen oxides measurements at rural sites in Switzerland: Bias of conventional measurement techniques. J Geophys Res Atmos 112: D11307. http://dx.doi.org/10.1029/2006JD007971
Streets, DG; Canty, T; Carmichael, GR; de Foy, B; Dickerson, RR; Duncan, BN; Edwards, DP; Haynes, JA; Henze, DK; Houyoux, MR; Jacob, DJ; Krotkov, NA; Lamsal, L; Liu, Y; Lu, Z; Martin, RV; Pfister, GG; Pinder, RW; Salawitch, RJ; Wecht, KJ. (2013). Emissions estimation from satellite retrievals: A review of current capability [Review]. Atmos Environ 77: 1011-1042. http://dx.doi.org/10.1016/j.atmosenv.2013.05.051
Su, JG; Apte, JS; Lipsitt, J; Garcia-Gonzales, DA; Beckerman, BS; de Nazelle, A; Luis Texcalac-Sangrador, J; Jerrett, M. (2015). Populations potentially exposed to traffic-related air pollution in seven world cities. Environ Int 78: 82-89. http://dx.doi.org/10.1016/j.envint.2014.12.007
Suel, E; Sorek-Hamer, M; Moise, I; von Pohle, M; Sahasrabhojanee, A; Asanjan, AA; Arku, RE; Alli, AS; Barratt, B; Clark, SN; Middel, A; Deardorff, E; Lingenfelter, V; Oza, NC; Yadav, N; Ezzati, M; Brauer, M. (2022). What you see is what you breathe? Estimating air pollution spatial variation using street-level imagery. Remote Sensing 14: 3429. http://dx.doi.org/10.3390/rs14143429
Sugrue, RA; Preble, C; Tarplin, AG; Kirchstetter, TW. (2022). In-use passenger vessel emission rates of black carbon and nitrogen oxides. Environ Sci Technol 56: 7679-7686. http://dx.doi.org/10.1021/acs.est.2c00435
Sun, L; Chen, T; Jiang, Y; Zhou, Y; Sheng, L; Lin, J; Li, J; Dong, C; Wang, C; Wang, X; Zhang, Q; Wang, W; Xue, L. (2020). Ship emission of nitrous acid (HONO) and its impacts on the marine atmospheric oxidation chemistry. Sci Total Environ 735: 139355. http://dx.doi.org/10.1016/j.scitotenv.2020.139355
Theys, N; Volkamer, R; Müller, JF; Zarzana, KJ; Kille, N; Clarisse, L; De Smedt, I; Lerot, C; Finkenzeller, H; Hendrick, F; Koenig, TK; Lee, CF; Knote, C; Yu, H; Van Roozendael, M.

(2020). Global nitrous acid emissions and levels of regional oxidants enhanced by wildfires. Nat Geosci 13: 681-686. http://dx.doi.org/10.1038/s41561-020-0637-7

Thompson, GJ; Carder, DK; Besch, MC; Thiruvengadam, A; Kappanna, HK. (2014). In-use emissions testing of light-duty diesel vehicles in the United States. Morgantown, WV: Center for Alternative Fuels, Engines & Emissions, University of West Virginia. https://theicct.org/sites/default/files/publications/WVU_LDDV_in-use_ICCT_Report_Final_may2014.pdf

Thornton, JA; Kercher, JP; Riedel, TP; Wagner, NL; Cozic, J; Holloway, JS; Dube, WP; Wolfe, GM; Quinn, PK; Middlebrook, AM; Alexander, B; Brown, SS. (2010). A large atomic chlorine source inferred from mid-continental reactive nitrogen chemistry. Nature 464: 271-274. http://dx.doi.org/10.1038/nature08905

Tong, DQ; Lamsal, Lo; Pan, Li; Ding, C; Kim, H; Lee, P; Chai, T; Pickering, KE; Stajner, I. (2015). Long-term NOx trends over large cities in the United States during the great recession: Comparison of satellite retrievals, ground observations, and emission inventories. Atmos Environ 107: 70-84. http://dx.doi.org/10.1016/j.atmosenv.2015.01.035

Toro, C; Foley, K; Simon, H; Henderson, B; Baker, KR; Eyth, A; Timin, B; Appel, W; Luecken, D; Beardsley, M; Sonntag, D; Possiel, N; Roberts, S. (2021). Evaluation of 15 years of modeled atmospheric oxidized nitrogen compounds across the contiguous United States. Elementa Sci Anthropocene 9. http://dx.doi.org/10.1525/elementa.2020.00158

Travis, KR, Jacob, D. J.; Fisher, JA; Kim, PS; Marais, EA; Zhu, L; Yu, K; Miller, CC; Yantosca, RM; Sulprizio, MP; Thompson, AM; Wennberg, PO; Crounse, JD; St. Clair, JM; Cohen, RC; Laughner, JL; Dibb, JE; Hall, SR; Ullmann, K; Wolfe, GM; Neuman, JA; Zhou, X. (2016a). Why do models overestimate surface ozone in the Southeastern United States? Atmos Chem Phys Discuss 16: 13561-13577. http://dx.doi.org/10.5194/acp-2016-110

Travis, KRJDJ; Fisher, JA; Kim, PS; Marais, EA; Zhu, L; Yu, K; Miller, CC; Yantosca, RM; Sulprizio, MP; Thompson, AM; Wennberg, PO; Crounse, JD; St. Clair, JM; Cohen, RC; Laughner, JL; Dibb, JE; Hall, SR; Ullmann, K; Wolfe, GM; Neuman, JA; Zhou, X. (2016b). Why do models overestimate surface ozone in the Southeastern United States? Atmos Chem Phys Discuss 16: 13561-13577. http://dx.doi.org/10.5194/acp-2016-110

Tsai, C; Spolaor, Ma; Colosimo, SF; Pikelnaya, O; Cheung, R; Williams, E; Gilman, JB; Lerner, BM; Zamora, RJ; Warneke, C; Roberts, JM; Ahmadov, R; de Gouw, J; Bates, T; Quinn, PK; Stutz, J. (2018). Nitrous acid formation in a snow-free wintertime polluted rural area. Atmos Chem Phys 18: 1977-1996. http://dx.doi.org/10.5194/acp-18-1977-2018

Tumbleson, RH; Balachandran, S. (2022). Air Quality and Traffic Trends in Cincinnati, Ohio during the COVID-19 Pandemic. Atmosphere (Basel) 13: 1459. http://dx.doi.org/10.3390/atmos13091459

Turgut, ET; Usanmaz, O; Rosen, MA. (2013). Estimation of vertical and horizontal distribution of takeoff and climb NOx emission for commercial aircraft. Energ Convers Manag 76: 121-127. http://dx.doi.org/10.1016/j.enconman.2013.07.029

U.S. EPA (U.S. Environmental Protection Agency). (1971). Air quality criteria for nitrogen oxides [EPA Report]. (AP-84). Washington DC: U.S. Environmental Protection Agency, Air Pollution Control Office. http://nepis.epa.gov/Exe/ZyPURL.cgi?Dockey=20013K3B.txt

U.S. EPA (U.S. Environmental Protection Agency). (2004). Air quality criteria for particulate matter (Final report, 2004) [EPA Report]. (EPA 600/P-99/002aF-bF). Washington, DC. http://cfpub.epa.gov/ncea/cfm/recordisplay.cfm?deid=87903

U.S. EPA (U.S. Environmental Protection Agency). (2009). Integrated science assessment for particulate matter. (EPA/600/R-08/139F). Washington, DC. http://cfpub.epa.gov/ncea/cfm/recordisplay.cfm?deid=216546

U.S. EPA (U.S. Environmental Protection Agency). (2013a). 2011 National Emissions Inventory data and documentation. Available online at https://www.epa.gov/air-emissions-inventories (accessed December 1, 2014).

U.S. EPA (U.S. Environmental Protection Agency). (2013b). Integrated science assessment for ozone and related photochemical oxidants [EPA Report]. (EPA/600/R-10/076F). Research Triangle Park, NC: U.S. Environmental Protection Agency, Office of Research and Development, National Center for Environmental Assessment-RTP Division. http://cfpub.epa.gov/ncea/isa/recordisplay.cfm?deid=247492

U.S. EPA (U.S. Environmental Protection Agency). (2016). Integrated science assessment for oxides of nitrogen: Health criteria (Final report, Jan 2016) [EPA Report]. (EPA/600/R-15/068). Washington, DC. https://cfpub.epa.gov/ncea/isa/recordisplay.cfm?deid=310879

U.S. EPA (U.S. Environmental Protection Agency). (2017). Policy assessment for the review of the primary national ambient air quality standards for oxides of nitrogen [EPA Report]. (EPA-452/R-17-003). Washington, DC. https://www.epa.gov/sites/default/files/2017-04/documents/policy_assessment_for_the_review_of_the_no2_naaqs_-_final_report.pdf

U.S. EPA (U.S. Environmental Protection Agency). (2019). Integrated Science Assessment (ISA) for particulate matter (final report, Dec 2019). (EPA/600/R-19/188). Washington, DC. https://cfpub.epa.gov/ncea/isa/recordisplay.cfm?deid=347534

U.S. EPA (U.S. Environmental Protection Agency). (2020a). Integrated Science Assessment (ISA) for ozone and related photochemical oxidants (final report, Apr 2020) [EPA Report]. (EPA/600/R-20/012). Washington, DC. https://nepis.epa.gov/Exe/ZyPURL.cgi?Dockey=P10111KI.txt

U.S. EPA (U.S. Environmental Protection Agency). (2020b). Integrated science assessment for oxides of nitrogen, oxides of sulfur, and particulate matter—Ecological criteria (final report) [EPA Report]. (EPA/600/R-20/278). Research Triangle Park, NC: U.S. Environmental Protection Agency, Office of Research and Development. https://cfpub.epa.gov/ncea/isa/recordisplay.cfm?deid=349473

U.S. EPA. Method 7E— Determination of nitrogen oxides emissions from stationary sources (instrumental analyzer procedure), 40 CFR (2020c).

U.S. EPA (U.S. Environmental Protection Agency). (2021). Overview of progress and findings from the cross-EPA coordination effort for understanding and evaluating NOx emissions discrepancies. (EPA-454/R-21-008). Washington, DC. https://www.epa.gov/system/files/documents/2021-12/epa-454_r-21-008_final.pdf

U.S. EPA (U.S. Environmental Protection Agency). (2022). National emissions inventory (NEI). Available online at https://www.epa.gov/air-emissions-inventories/national-emissions-inventory (accessed August 31, 2022).

U.S. EPA (U.S. Environmental Protection Agency). (2023a). 2020 National Emissions Inventory (NEI) Data (August 2023 version) (Version August 2023). Washington, DC: US Environmental Protection Agency. Retrieved from https://www.epa.gov/air-emissions-inventories/2020-national-emissions-inventory-nei-data

U.S. EPA (U.S. Environmental Protection Agency). (2023b). 2020 National Emissions Inventory technical support document: Biogenics – vegetation and soil [EPA Report]. (EPA-454/R-23-001h). Washington, DC. https://www.epa.gov/system/files/documents/2023-03/NEI2020_TSD_Section8_Biogenics_0.pdf

U.S. EPA (U.S. Environmental Protection Agency). (2023c). List of designated reference and equivalent methods, December 2023 [EPA Report]. Washington, DC. https://www.epa.gov/system/files/documents/2023-12/list_of_frm_fem_-december_2023_final.pdf

U.S. EPA (U.S. Environmental Protection Agency). (2023d). NAAQS review analysis. Available online at https://www.epa.gov/air-quality-analysis/naaqs-review-analysis (accessed September 12, 2024).

U.S. EPA (U.S. Environmental Protection Agency). (2024a). List of designated reference and equivalence methods. Research Triangle Park, NC: U.S. Environmental Protection Agency :: U.S. EPA.

U.S. EPA (U.S. Environmental Protection Agency). (2024b). List of designated reference and equivalent methods, December 15, 2024. Research Triangle Park, NC: U.S. Environmental Protection

Agency :: U.S. EPA. https://www.epa.gov/system/files/documents/2024-12/amtic-list-december-2024_final.pdf
U.S. EPA (U.S. Environmental Protection Agency). (2024c). Nitrogen dioxide trends. Available online at https://www.epa.gov/air-trends/nitrogen-dioxide-trends
U.S. EPA (U.S. Environmental Protection Agency). (2024d). Technical support document (TSD) for adoption of the generic reaction set method (GRSM) as a regulatory non-default tier-3 NO2 screening option. (EPA-454/R-24-005).
U.S. EPA (U.S. Environmental Protection Agency). (2024e). Updates to air emissions trends methodology, 2002-2023: February 2024. Washington, D.C.: U.S. Environmental Protection Agency :: U.S. EPA. https://www.epa.gov/system/files/documents/2024-02/trends_feb2024.pdf
U.S. EPA RD (US EPA Office of Research and Development). (2022). CMAQ. Available online (accessed December 9, 2024).
Unal, A; Hu, Y; Chang, ME; Talat Odman, M; Russell, AG. (2005). Airport related emissions and impacts on air quality: Application to the Atlanta International Airport. Atmos Environ 39: 5787-5798. http://dx.doi.org/10.1016/j.atmosenv.2005.05.051
Urbanski, S. (2014). Wildland fire emissions, carbon, and climate: Emission factors. For Ecol Manage 317: 51-60. http://dx.doi.org/10.1016/j.foreco.2013.05.045
Valin, LC; Russell, AR; Cohen, RC. (2014). Chemical feedback effects on the spatial patterns of the NOx weekend effect: A sensitivity analysis. Atmos Chem Phys 14: 1-9. http://dx.doi.org/10.5194/acp-14-1-2014
van Geffen, J; Boersma, KF; Eskesl, H; Sneep, M; ter Linden, M; Zara, M; Veefkind, JP. (2020). S5P TROPOMI NO2 slant column retrieval: Method, stability, uncertainties and comparisons with OMI. Atmos Meas Tech 13: 1315-1335. http://dx.doi.org/10.5194/amt-13-1315-2020
VandenBoer, TC; Markovic, MZ; Sanders, JE; Ren, X; Pusede, SE; Browne, EC; Cohen, RC; Zhang, L; Thomas, J; Brune, WH; Murphy, JG. (2014). Evidence for a nitrous acid (HONO) reservoir at the ground surface in Bakersfield, CA, during CalNex 2010. J Geophys Res Atmos 119: 9093-9106. http://dx.doi.org/10.1002/2013JD020971
VandenBoer, TC; Young, CJ; Talukdar, RK; Markovic, MZ; Brown, SS; Roberts, JM; Murphy, JG. (2015). Nocturnal loss and daytime source of nitrous acid through reactive uptake and displacement. Nat Geosci 8: 55-60. http://dx.doi.org/10.1038/NGEO2298
Vette, A; Burke, J; Norris, G; Landis, M; Batterman, S; Breen, M; Isakov, V; Lewis, T; Gilmour, MI; Kamal, A; Hammond, D; Vedantham, R; Bereznicki, S; Tian, N; Croghan, C. (2013). The Near-Road Exposures and Effects of Urban Air Pollutants Study (NEXUS): Study design and methods. Sci Total Environ 448: 38-47. http://dx.doi.org/10.1016/j.scitotenv.2012.10.072
Villena, G; Bejan, I; Kurtenbach, R; Wiesen, P; Kleffmann, J. (2012). Interferences of commercial NO2 instruments in the urban atmosphere and in a smog chamber. Atmos Meas Tech 5: 149-159. http://dx.doi.org/10.5194/amt-5-149-2012
Vinken, GCM; Boersma, KF; Maasakkers, JD; Adon, M; Martin, RV. (2014). Worldwide biogenic soil NOx emissions inferred from OMI NO2 observations. Atmos Chem Phys 14: 10363-10381. http://dx.doi.org/10.5194/acp-14-10363-2014
Wagner, A; Blechschmidt, AM; Bouarar, I; Brunke, EG; Clerbaux, C; Cupeiro, M; Cristofanelli, P; Eskes, H; Flemming, J; Flentje, H; George, M; Gilge, S; Hilboll, A; Inness, A; Kapsomenakis, J; Richter, A; Ries, L; Spangl, W; Stein, O; Zerefos, C. (2015). Evaluation of the MACC operational forecast system - Potential and challenges of global near-real-time modelling with respect to reactive gases in the troposphere. Atmos Chem Phys 15: 14005-14030. http://dx.doi.org/10.5194/acp-15-14005-2015
Walker, JT; Beachley, G; Amos, HM; Baron, JS; Bash, J; Baumgardner, R; Bell, MD; Benedict, KB; Chen, X; Clow, DW; Cole, A; Coughlin, JG; Cruz, K; Daly, RW; Decina, SM; Elliott, EM; Fenn, ME; Ganzeveld, L; Gebhart, K; Isil, SS; Kerschner, BM; Larson, RS; Lavery, T; Lear, GG; Macy, T; Mast, MA; Mishoe, K; Morris, KH; Padgett, PE; Pouyat, RV; Puchalski, M; Pye, HOT; Rea, AW; Rhodes, MF; Rogers, CM; Saylor, R; Scheffe, R; Schichtel, BA; Schwede, DB;

Sexstone, GA; Sive, BC; Sosa Echeverría, R; Templer, PH; Thompson, T; Tong, D; Wetherbee, GA; Whitlow, TH; Wu, Z; Yu, Z; Zhang, L. (2019). Toward the improvement of total nitrogen deposition budgets in the United States. Sci Total Environ 691: 1328-1352. http://dx.doi.org/10.1016/j.scitotenv.2019.07.058

Walters, LJ; May, MS; Johnson, DE; MacMann, RS; Woodward, WA. (1999). Time-variability of NO x emissions from Portland cement kilns. Environ Sci Technol 33: 700-704. http://dx.doi.org/10.1021/es980203b

Wang, H; Gong, FY; Newman, S; Zeng, ZC. (2022). Consistent weekly cycles of atmospheric NO2, CO, and CO2 in a North American megacity from ground-based, mountaintop, and satellite measurements. Atmos Environ 268: 118809. http://dx.doi.org/10.1016/j.atmosenv.2021.118809

Wang, JM; Jeong, CH; Zimmerman, N; Healy, RM; Evans, GJ. (2018). Real world vehicle fleet emission factors: Seasonal and diurnal variations in traffic related air pollutants. Atmos Environ 184: 77-86. http://dx.doi.org/10.1016/j.atmosenv.2018.04.015

Wang, Y; Faloona, I, anC; Houlton, BZ. (2023a). Satellite NO2 trends reveal pervasive impacts of wildfire and soil emissions across California landscapes. Environ Res Lett 18: 094032. http://dx.doi.org/10.1088/1748-9326/acec5f

Wang, Y; Faloona, Ia; Houlton, BZ. (2023b). Satellite NO2 trends reveal pervasive impacts of wildfire and soil emissions across California landscapes. Environ Res Lett 18: 094032. http://dx.doi.org/10.1088/1748-9326/acec5f

Wang, Y; Ge, C; Castro Garcia, L; Jenerette, GD; Oikawa, PY; Wang, J. (2021). Improved modelling of soil NO (x) emissions in a high temperature agricultural region: Role of background emissions on NO2 trend over the US. Environ Res Lett 16: 084061. http://dx.doi.org/10.1088/1748-9326/ac16a3

Wang, Y; Ma, YF; Eskes, H; Inness, A; Flemming, J; Brasseur, GP. (2020). Evaluation of the CAMS global atmospheric trace gas reanalysis 2003-2016 using aircraft campaign observations. Atmos Chem Phys 20: 4493-4521. http://dx.doi.org/10.5194/acp-20-4493-2020

Watson, JG; Cao, J; Chen, LWA; Wang, Q; Tian, J; Wang, X; Gronstal, S; Ho, SSH; Watts, AC; Chow, JC. (2019). Gaseous, PM2.5 mass, and speciated emission factors from laboratory chamber peat combustion. Atmos Chem Phys 19: 14173-14193. http://dx.doi.org/10.5194/acp-19-14173-2019

Weinstock, L. (2012). Putting multipollutant monitoring into practice: EPA's NCore network. EM Magazine May 2012: 26-31.

Weiss, M; Bonnel, P; Kuehlwein, J; Provenza, A; Lambrecht, Ud; Alessandrini, S; Carriero, M; Colombo, R; Forni, F; Lanappe, G; Le Lijour, P; Manfredi, U; Montigny, F; Sculati, M. (2012). Will Euro 6 reduce the NOx emissions of new diesel cars? - Insights from on-road tests with Portable Emissions Measurement Systems (PEMS). Atmos Environ 62: 657-665. http://dx.doi.org/10.1016/j.atmosenv.2012.08.056

Weissert, L; Miles, E; Miskell, G; Alberti, K; Feenstra, B; Henshaw, GS; Papapostolou, V; Patel, H; Polidori, A; Salmond, JA; Williams, DE. (2020). Hierarchical network design for nitrogen dioxide measurement in urban environments. Atmos Environ 228: 117428. http://dx.doi.org/10.1016/j.atmosenv.2020.117428

Wild, RJ; Dubé, WP; Aikin, KC; Eilerman, SJ; Neuman, JA; Peischl, J; Ryerson, TB; Brown, SS. (2017). On-road measurements of vehicle NO2/NOx emission ratios in Denver, Colorado, USA. Atmos Environ 148: 182-189. http://dx.doi.org/10.1016/j.atmosenv.2016.10.039

Winer, AM; Peters, JW; Smith, JP; Pitts, JN, Jr. (1974). Response of commercial chemiluminescent NO-NO2 analyzers to other nitrogen-containing compounds. Environ Sci Technol 8: 1118-1121. http://dx.doi.org/10.1021/es60098a004

Xiang, J; Austin, E; Gould, T; Larson, T; Shirai, J; Liu, Y; Marshall, J; Seto, E. (2020). Impacts of the COVID-19 responses on traffic-related air pollution in a northwestern US city. Sci Total Environ 747: 141325. http://dx.doi.org/10.1016/j.scitotenv.2020.141325

Xiao, GNA; Wang, T; Chen, XQ; Zhou, LZ. (2022). Evaluation of ship pollutant emissions in the ports of Los Angeles and Long Beach. J Mar Sci Eng 10: 1206. http://dx.doi.org/10.3390/jmse10091206

Xie, Y; Zhao, B; Zhang, L; Luo, R. (2015). Spatiotemporal variations of PM2.5 and PM10 concentrations between 31 Chinese cities and their relationships with SO2, NO2, CO and O3. Particuology 20: 141-149. http://dx.doi.org/10.1016/j.partic.2015.01.003

Yan, XY; Ohara, T; Akimoto, I. (2005). Statistical modeling of global soil NOx emissions. Global Biogeochem Cycles 19: n/a-n/a. http://dx.doi.org/10.1029/2004GB002276

Yao, Y; Artigas, FJ; Fan, S; Gao, Y. (2022). Impact of the COVID-19 pandemic on air quality in metropolitan New Jersey. Water Air Soil Pollut 233: 289. http://dx.doi.org/10.1007/s11270-022-05764-w

Ye, C; Zhang, N; Gao, H; Zhou, X. (2017). Photolysis of particulate nitrate as a source of HONO and NOx. Environ Sci Technol 51: 6849-6856. http://dx.doi.org/10.1021/acs.est.7b00387

Ye, C; Zhou, X; Pu, D; Stutz, J; Festa, J; Spolaor, M; Tsai, C; Cantrell, C; Mauldin, RL; Campos, T; Weinheimer, A; Hornbrook, RS; Apel, EC; Guenther, A; Kaser, L; Yuan, B; Karl, T; Haggerty, J; Hall, S; Ullmann, K; Smith, JN; Ortega, J; Knote, C. (2016). Rapid cycling of reactive nitrogen in the marine boundary layer. Nature 532: 489-491. http://dx.doi.org/10.1038/nature17195

Ye, C; Zhou, X; Pu, D; Stutz, J; Festa, J; Spolaor, M; Tsai, C; Cantrell, C; Mauldin, RL, III; Weinheimer, A; Hornbrook, RS; Apel, EC; Guenther, A; Kaser, L; Yuan, B; Karl, T; Haggerty, J; Hall, S; Ullmann, K; Ortega, J. (2018). Tropospheric HONO distribution and chemistry in the southeastern US. Atmos Chem Phys 18: 9107-9120. http://dx.doi.org/10.5194/acp-18-9107-2018

Ye, L; Wang, Y. (2020). Long-term air quality study in Fairbanks, Alaska: Air pollutant temporal variations, correlations, and PM2.5 source apportionment. Atmosphere (Basel) 11: 1203. http://dx.doi.org/10.3390/atmos11111203

Yi, HM; Cazaunau, M; Gratien, A; Michoud, V; Pangui, E; Doussin, JF; Chen, W. (2021). Intercomparison of IBBCEAS, NitroMAC and FTIR analyses for HONO, NO2 and CH2O measurements during the reaction of NO2 with H2O vapour in the simulation chamber CESAM. Atmos Meas Tech 14: 5701-5715. http://dx.doi.org/10.5194/amt-14-5701-2021

Yu, CA; Huang, LB; Xue, LK; Shen, HQ; Li, ZY; Zhao, M; Yang, J; Zhang, YN; Li, HY; Mu, JS; Wang, WX. (2022). Photoenhanced heterogeneous uptake of NO2 and HONO formation on authentic winter time urban grime. ACS Earth Space Chem 6: 1960-1968. http://dx.doi.org/10.1021/acsearthspacechem.2c00054

Yu, H; Russell, A; Mulholland, J; Odman, T; Hu, Y; Chang, HH; Kumar, N. (2018). Cross-comparison and evaluation of air pollution field estimation methods. Atmos Environ 179: 49-60. http://dx.doi.org/10.1016/j.atmosenv.2018.01.045

Yu, KA; Li, M; Harkins, C; He, J; Zhu, Q; Verreyken, B; Schwantes, RH; Cohen, RC; McDonald, BC; Harley, RA. (2023). Improved Spatial Resolution in Modeling of Nitrogen Oxide Concentrations in the Los Angeles Basin. Environ Sci Technol 57: 20689-20698. http://dx.doi.org/10.1021/acs.est.3c06158

Zamora, ML; Buehler, C; Datta, A; Gentner, DR; Koehler, K. (2023). Identifying optimal co-location calibration periods for low-cost sensors. Atmos Meas Tech 16: 169-179. http://dx.doi.org/10.5194/amt-16-169-2023

Zare, A; Romer, PS; Nguyen, T; Keutsch, FN; Skog, K; Cohen, RC. (2018a). A comprehensive organic nitrate chemistry: Insights into the lifetime of atmospheric organic nitrates. Atmos Chem Phys 18: 15419-15436. http://dx.doi.org/10.5194/acp-18-15419-2018

Zare, A; Romer, PS; Tran, N; Keutsch, FN; Skog, K; Cohen, RC. (2018b). A comprehensive organic nitrate chemistry: Insights into the lifetime of atmospheric organic nitrates. Atmos Chem Phys 18: 15419-15436. http://dx.doi.org/10.5194/acp-18-15419-2018

Zhang, R; Wang, Y; Smeltzer, C; Qu, H; Koshak, W; Boersma, KF. (2018). Comparing OMI-based and EPA AQS in situ NO2 trends: Towards understanding surface NOx emission changes. Atmos Meas Tech 11: 3955-3967. http://dx.doi.org/10.5194/amt-11-3955-2018

Zhang, X; Yin, Y; van Der A, R; Lapierre, JL; Chen, Q; Kuang, X; Yan, S; Chen, J; He, C; Shi, R. (2020). Estimates of lightning NOx production based on high-resolution OMI NO2 retrievals

over the continental US. Atmos Meas Tech 13: 1709-1734. http://dx.doi.org/10.5194/amt-13-1709-2020

Zhao, X; Griffin, D; Fioletov, V; Mclinden, C; Cede, A; Tiefengraber, M; Mueller, M; Bognar, K; Strong, K; Boersma, F; Eskes, H; Davies, J; Ogyu, A; Lee, SC. (2020). Assessment of the quality of TROPOMI high-spatial-resolution NO2 data products in the Greater Toronto Area. Atmos Meas Tech 13: 2131-2159. http://dx.doi.org/10.5194/amt-13-2131-2020

Zhu, J; Chen, L; Liao, H; Dang, R. (2019a). Correlations between PM2.5 and ozone over China and associated underlying reasons. Atmosphere (Basel) 10: 352. http://dx.doi.org/10.3390/atmos10070352

Zhu, Q; Laughner, JL; Cohen, RC. (2019b). Lightning NO2 simulation over the contiguous US and its effects on satellite NO2 retrievals. Atmos Chem Phys 19: 13067-13078. http://dx.doi.org/10.5194/acp-19-13067-2019

Zoogman, P; Liu, X; Suleiman, RM; Pennington, WF; Flittner, DE; Al-Saadi, JA; Hilton, BB; Nicks, DK; Newchurch, MJ; Carr, JL; Janz, SJ; Andraschko, MR; Arola, A; Baker, BD; Canova, BP; Miller, CC; Cohen, RC; Davis, JE; Dussault, ME; Edwards, DP; Fishman, J; Ghulam, A; González Abad, G; Grutter, M; Herman, JR; Houck, J; Jacob, DJ; Joiner, J; Kerridge, BJ; Kim, J; Krotkov, NA; Lamsal, L; Li, C; Lindfors, A; Martin, RV; McElroy, CT; McLinden, C; Natraj, V; Neil, DO; Nowlan, CR; O'Sullivan, EJ; Palmer, PI; Pierce, RB; Pippin, MR; Saiz-Lopez, A; Spurr, RJD; Szykman, JJ; Torres, O; Veefkind, JP; Veihelmann, B; Wang, H; Wang, J; Chance, K. (2017). Tropospheric emissions: Monitoring of pollution (TEMPO). J Quant Spectrosc Radiat Transf 186: 17-39. http://dx.doi.org/10.1016/j.jqsrt.2016.05.008

Zuraski, K; Harkins, C; Peischl, J; Coggon, MM; Stockwell, CE; Robinson, MA; Gilman, J; Warneke, C; McDonald, BC; Brown, SS. (2025). On-road measurements of nitrogen oxides, co, co2, and voc emissions in two southwestern U.S. cities. ACS ES&T air 0. http://dx.doi.org/10.1021/acsestair.4c00316